Constraints on the magma source and rift evolution from geochemistry of the Stratoid flood basalts (Afar, Ethiopia)

G. Tortelli[1,2], A. Gioncada[1], C. Pagli[1], E. Braschi[3], E. F. Gebru[4,5], D. Keir[2,6]

[1] Dipartimento di Scienze della Terra, Università di Pisa, Via Santa Maria, 53, 56126 Pisa, Italy

[2] Dipartimento di Scienze della Terra, Università degli Studi di Firenze, Via G. La Pira, 4, 50121 Florence, Italy

[3] CNR, IGG, sezione di Firenze, Via G. La Pira, 4, 50121 Firenze, Italy

[4] Department of Geosciences, University of Fribourg, Chemin du Musée 6, 1700 Fribourg, Switzerland

[5] School of Earth Sciences, Addis Ababa University, P. O. Box, 1176, Addis Ababa, Ethiopia

[6] School of Ocean and Earth Science, University of Southampton, European Way, SO14 3ZH, Southampton, U.K.

Corresponding author: Gianmaria Tortelli (gianmaria.tortelli@unifi.it)

Key Points:

- Metasomatized, amphibole-bearing lithospheric component in the mantle sources of the 4.5-0.6 Ma basaltic magmatism in Afar
- Deeper partial melting column for the Upper Stratoid Series mantle source with respect to the Lower Stratoid and the Gulf Series
- Stratoid Series flood basalt volcanism related to rift jump of the Red Sea rift branch and not to a single magmatic event

This article has been accepted for publication and undergone full peer review but has not been through the copyediting, typesetting, pagination and proofreading process, which may lead to differences between this version and the Version of Record. Please cite this article as doi: 10.1029/2022GC010434.

Abstract

The relationship between rifting and continental flood basalt eruptions is debated, and a control by mantle plume is commonly invoked for flood basalts production. In this work we investigate the relationship between magmatism and rifting by studying the flood basalts erupted in Afar (4.5-0.6 Ma), known as the Stratoid and Gulf Series. We present new field observations and petrography, major and trace elements analyses and mineral chemistry of lavas collected during a regional campaign in Afar. The Series are characterised by E-MORB magmatism and residual amphibole in the mantle source, consistent with the contribution of metasomatized sub-continental lithospheric mantle during partial melting. Differences in garnet-compatible elements indicate a shallower melting column for the oldest and youngest products (4.5-2.6 Ma Lower Stratoid Series; 1.1-0.6 Ma Gulf Series), and deeper for the products erupted at 2.6-1.1 Ma (Upper Stratoid Series). Incompatible elements ratios (Th/Nb, Th/Zr) indicate a higher degree of partial melting for the Gulf with respect to the Upper Stratoid Series. Accordingly with independent geophysical and stratigraphic evidence, we explain our results with rift re-localization: the Pliocene rift caused thinning of the lithosphere and the Lower Stratoid eruptions in Southern Afar, then the Pleistocene rift jumped to Central Afar under a less-extended lithosphere, producing the Upper Stratoid and, subsequently, as stretching of the lithosphere localized, the Gulf Series formed. Our findings suggest that rift migration and localization can exert a fundamental control on the spatial variability and character of flood basalts without requiring variations on the activity of the mantle plume.

Plain Language Summary

Afar is a volcanically active low-lying area in Ethiopia, where the separation of the tectonic plates is breaking up the African continent and leading to the formation of new oceans (i.e., Red Sea, Gulf of Aden). It is therefore an excellent place to study the role of volcanism and related subsurface movements of magma during this transition from continent to ocean. In this work we studied the Stratoid Series, a huge succession of basaltic lava flows covering much of the Afar depression, and the younger Afar Gulf Series lava flows, which were jointly erupted from 4.5 to 0.6 Ma. This study allows us to identify different mantle sources producing the magmas erupted during the breaking-up process and to recognize two distinct episodes of “break-up” in Afar. We

interpret the process that guides the passage from one to the other and identify the "evolutionary stages" of the break-up process toward what is going to be a new ocean.

1 Introduction

Magmatism in rift systems plays a key role along with tectonics in breaking up the continental lithosphere and eventual initiation of oceanic spreading (Acocella, 2014; Bosworth et al., 2005; Corti et al., 2015; Hayward and Ebinger, 1996; Manighetti et al., 1997; Stab et al., 2016; Wolfenden et al., 2005). However, ambiguity remains about the origin of one of the largest magmatic provinces associated with continental rifting, the Stratoid flood basalts in Afar, and how rifting evolved in space and time during the magma production. Both in Afar and globally, it is debated whether flood basalts associated with continental breakup are driven by the activity of a thermally anomalous mantle plume, or by plate extension and related thinning causing decompression melting (Buck, 1991; Corti et al., 2003; Farnetani and Hofmann, 2011; Frizon de Lamotte et al., 2015; Griffiths and Campbell, 1991; Koptev et al., 2016; Schmeling, 2010; Turcotte and Emerman, 1983). Geochemical, petrological and volcanological studies are crucial to characterise the magmatism (e.g., magma source/s, magma productivity, magma storage and ascent) in order to understand the links with rift related processes.

In this work we target the spatial and temporal variations of the Stratoid Series erupted over Southern and Central Afar at 4.5-1.1 Ma (Barberi and Santacroce, 1980; Varet, 2018) and the following Gulf Series erupted at 2.8-0.3 Ma near the current rift axis (Kidane et al., 2003; Rooney, 2020a). These Series allow us to investigate the origin of the widespread basaltic volcanism and the transition to the formation of narrow magmatic segments at the Afar Rift-Rift-Rift triple junction. In this work, we present new results of petrographic, microanalytical and geochemical analyses as well as field observations from a regional campaign in Central and Southern Afar in February 2020. Furthermore, we complement this dataset with new analyses of samples collected during the French-Italian campaigns in 1967–1973 (https://repositories.dst.unipi.it/index.php/afar-repositories). This geochemical work is based on samples that are temporally and spatially distributed over the Stratoid and the Gulf Series and hence allow us to identify variations in the mantle source between these previously undistinguished Series. These observations have therefore been used to interpret the evolution

of the Afar rift magmatism from 4.5 to 0.6 Ma. Our results are also compared to independent stratigraphic reconstruction of the Afar basins and crustal thickness models derived from seismic imaging, to explore links between the shifts in volcanism and tectonics.

2 Geological background

At the northern end of the EARS (East African Rift System) the Red Sea, Gulf of Aden, and Main Ethiopian Rift (Figure 1) intersect at the Afar depression and represents a classic example of a rift-rift-rift triple junction at the transition from continental rifting to oceanic spreading (Bastow and Keir, 2011; Bastow et al., 2018; Makris and Ginzburg, 1987). Volcanism in EARS began around 45 Ma in central and southern Ethiopia with the emplacement of the Ethiopian flood basalts and kimberlite magmas along the margins of the Tanzanian craton. During the Oligocene the flood basalt volcanism mainly emplaced over only ~1 Myr, at about 30 Ma, associated with the onset of rifting and the effect of a mantle plume (Ebinger et al., 1993; Eid et al., 2021; Hofmann et al., 1997; Kieffer et al., 2004; Marty et al., 1996; Pik et al., 1999; Steiner et al., 2022; Zumbo et al., 1995).

Rifting in Afar is thought to have started ~29 Ma, with tectono-magmatic reconstructions suggesting that the locus of strain of the southern Red Sea rift migrated eastward, from the western Afar border fault system toward the rift centre (Wolfenden et al., 2005). This migration was associated with a progressive narrowing of the active zone of extension and magmatism until 7 Ma by which time strain was mainly accommodated through dike intrusion (Wolfenden et al., 2005). The migration of extension was not only caused by strain localisation, but also due to triple junction tectonics. Using regional structural analysis, Tesfaye et al. (2003) reconstruct a ~160 Km northeast migration of the triple junction, from southernmost Afar (10°N-40°E) to the current position near Lake Abbe (11.2°N-41.8°E) in central Afar. Supporting this hypothesis, detailed anthropological studies in the Woranso-Mille region and Awash valley (Figure 1) reveals a northeast migration of the paleo-depocenter formation across Southern Afar during ~10-3 Ma (Kalb, 1995) until the development of the Hadar Basin depocenter (ca. 3.8-2.9 Ma; DiMaggio et al., 2015; Wynn et al., 2008; Figure 1). The sedimentary succession of the Hadar basin is topped by an angular unconformity separating it from the overlying Busidima Formation (ca. 2.7-0.15 Ma) and marking an important change in fluvial sedimentary processes in Afar (Campisano, 2012;

Quade et al., 2008; Wynn et al., 2008). Wynn et al. (2008) and Campisano (2012) suggest that the changes following the Hadar Basin deposition were the response of a major tectonic reorganisation in Afar.

Volcanism in Afar started at ~31-29 Ma with the eruption of the Ethiopia-Yemen flood basalt province (Baker et al., 1996; Hofmann et al., 1997). From 20 to 10 Ma the Mabla Series was emplaced along with the Afar rift margins. The Mabla Series was dominated by the explosive silicic activity (Stab et al., 2016; Wolfenden et al., 2005). Then the Dalha Series succession (10-5.6 Ma) began with mainly silicic activity and was followed by the basaltic fissural activity of the Dalhoid Series (5.6-3.9 Ma; Rooney, 2020a). In the Pliocene starting at 4.5 Ma, the largest volcanic succession of Afar was erupted, the Stratoid Series covering an area of ~55.000 km^2 in Central and Southern Afar and reaching ~1000 m in thickness. The Stratoid are mostly made of flat lying fissural basalts, minor rhyolitic lavas and pyroclastics. The basaltic emission centres have not been identified in the field and the base of the lava succession is not exposed (Barberi and Santacroce, 1980; Varet, 2018). The Stratoid Series are dissected by graben-forming normal faults, striking NW-SE to NNW-SSE in Central Afar (Red Sea trend), while south of the Tendaho Goba'Ad Discontinuity (T.G.D., separating the E-W extension direction of the MER from the NE-SW one of the Red Sea) the faults mainly strike NNE-SSW (Main Ethiopian Rift trend) (Figure 1). The precise timing of the Stratoid Series emplacements is still not well established. Overall, the literature data indicate ages ranging from 4.5 ± 0.19 Ma to 1.25 ± 0.09 Ma (Barberi et al., 1975; Courtillot et al., 1984; Feyissa et al., 2019; Kidane et al., 2003; Kunz et al., 1975; Lahitte et al., 2003a; Zumbo et al., 1995). Acocella (2010) indicated a rejuvenation of the Stratoid Series along a direction perpendicular to the Dobi and the Tendaho graben, with ages getting younger toward the inner portions of the graben. Kidane et al. (2003) divided the Stratoid Series based on their age and morphology in Upper and Lower Stratoid Series, respectively younger and older than 2.6 Ma. Towards the end of the Stratoid Series, central silicic volcanoes produced effusive and pyroclastic products (Barberi and Santacroce, 1980; Lahitte et al., 2003b).

After the Stratoid Series, the Gulf Series are emplaced. These were previously identified as the Upper part of the Stratoid Series (Varet, 1978) and later distinguished based on their younger age (2.8-0.3 Ma) and the decrease in the volume of the flows with respect to the Stratoid Series

(Daoud et al., 2011; Kidane et al., 2003; Lahitte et al., 2003a; Le Gall et al., 2015; Rooney, 2020a). The Gulf Series volcanism is located along the faults of the main grabens in central Afar and in the Gulf of Tadjoura (Figure 1) (i.e., Tendaho-Manda Hararo, Tat'Ali, Manda Inakir). Gasse et al. (1983) and Stab et al. (2016) hypothesized that the Gulf Series are the first products associated with the progressive localization of the extension to the magmatic segments, starting at ~1.1 Ma in central Afar (Kidane et al., 2003; Lahitte et al., 2003a) and at ~3 Ma in the Gulf of Tadjoura (Daoud et al., 2011; Le Gall et al., 2015). The Gulf Series products cover a much smaller area than the Stratoid lavas (Figure 1).

The Stratoid and Gulf Series basalts are both originated from transitional to subalkaline magmas modified by fractional crystallisation processes with major and trace elements (e.g., REE, La_N/Sm_N and Zr/Nb) and isotopic composition ($^{143}Nd/^{144}Nd$, $^{87}Sr/^{86}Sr$, $^{206}Pb/^{204}Pb$, $^{207}Pb/^{204}Pb$ and $^{208}Pb/^{204}Pb$) that largely overlap (Barberi and Santacroce 1980; Feyissa et al., 2019; Rooney 2020a). Rooney (2020a) and Rooney et al. (2014, 2017), based on the observed geochemical patterns (Ba peak, U-Th trough, and Nb-Ta peak) and modelled patterns of primitive, depleted and lithospheric mantle partial melting, identified the Stratoid and Gulf Series lavas as a mix of plume, depleted mantle, and African lithosphere. Moreover, Feyissa et al. (2019) and Rooney (2020a, 2020b), based on isotopic compositions show that the source of the Stratoid and Gulf Series lavas is a mixture of Afar plume, depleted mantle and African lithosphere (Rooney et al., 2012a; type III magmas of Rooney 2020b). Furthermore, Rooney (2020a) recognized a group of Stratoid Series samples within the Woranso-Mille region (Figure 1) and the Hayyabley basalts (near Djibouti) of the Gulf Series as lavas originated from a source extremely depleted in the most incompatible element and enriched in LILE (type VI).

Seismic imaging studies sensitive to discontinuities struggle to image the lithosphere-asthenosphere boundary (LAB) beneath Afar. However, a weak discontinuity at ~65-70 km depth has been interpreted as potentially the LAB (Lavayssiere et al., 2018). Seismic tomography beneath Afar shows slow velocity lobes of ~100-150 km length scale in the uppermost asthenosphere that are interpreted as the melt zone (Chambers et al., 2022; Gallacher et al., 2016). The slow seismic velocities are explained by partial melt at ~60-110 km depth (Chambers et al., 2022), broadly consistent with expectations that the melt zone is directly beneath the

lithosphere. This current depth of melting is also consistent with a ~95 km depth of base of melt zone derived from modelling REE compositions of young basaltic rocks in Afar (Ferguson et al., 2013). The crust beneath most of central and southern Afar is ~25-30 km, but locally thins to ~20 km beneath the magmatic segments and beneath previous zone of strain such as the Woranso-Mille region (Ahmed et al., 2022; Hammond et al., 2011; Wang et al., 2021). Furthermore, tectonic and geophysical studies (Stab et al., 2016; Wang et al., 2021) suggest presence of lower crustal intrusions/magmatic underplating near the Moho in the Afar Depression, that could potentially play an important role in the magmatic evolution of the erupted products.

3 Data

We analysed 44 new samples of lava flows from the Lower and Upper Stratoid Series and the Gulf Series, plus 4 new lava samples from the current magmatic segments, collected during a campaign in February 2020. The rationale was to cover as much as possible of the Stratoid and the Gulf Series in Southern and Central Afar (Figure 1). To improve the sampling distribution, we also studied 9 Stratoid and Gulf Series samples (orange circles in Figure 1) from the Afar Repository of the University of Pisa (https://repositories.dst.unipi.it/index.php/home-afar). Furthermore, previous major element analyses of 46 samples of the Upper Stratoid Series from Santarnecchi (1978, unpublished thesis of the University of Pisa) were included in this work.

With respect to the Gulf Series, we took into consideration only the lavas outcropping in the Tendaho and Immino grabens (Figure 1) and not in the Tadjoura Gulf. Thus, in this work we name these Gulf Series lavas as Central Afar Gulf Series (hereafter CAG Series).

4 Methods

4.1 Petrography

Thin sections were prepared for all lava samples (Table S1). The samples have been described with regard to their phenocryst abundance, mineral assemblage and micro-texture. The phenocrysts and micro-phenocrysts have been identified based on their size, and relation with the groundmass. The phenocryst abundance has been evaluated qualitatively by comparison with volume % estimation diagrams. Rock samples with phenocrysts less than 2% have been considered aphyric.

4.2 Analytical methods for mineral chemistry

Six samples from the Upper, Lower and CAG Series at different sites have been selected for electron microscopy and microanalysis (Table S2). Polished thin sections were studied by scanning electron microscopy-back scattered electron imaging (SEM-BSEI) and energy dispersive X-ray spectroscopy (EDS) microanalysis with the field emission scanning electron microscope FEI Quanta 450 ESEM-FEG provided with a Bruker QUANTAX XFlash Detector 6/10 at the Centro per la Integrazione della Strumentazione della Università di Pisa (CISUP). The samples were then analysed using the JEOL JAX8600 - EMPA device of the CNR-IGG, hosted in the "Filippo Olmi" laboratories (Department of Earth Sciences of Florence). The analytical conditions were 15 kV of accelerating voltage with 20 nA of beam current and 3 µm beam size for olivine, pyroxene, and oxide and 10 nA beam current and 5 µm beam size for plagioclase. The counting time is 15 s on peak and 7 s in the background for major elements (except for the Na counting 10 s on peak and 5 s in the background). For the trace elements the counting time varies between 30-40 s on peak and between 15-20 s on the background. The primary standards used for calibration are albite Astimex for Si and Na, plagioclase Astimex for Al, olivine Astimex for Mg, diopside Asimex for Ca, sanidine Astimex for K, ilmenite Smithsonian for Ti and Fe, apatite Astimex for P, barite Astimex for Ba and celestite Astimex for Sr.

4.3 Analytical methods for geochemistry

A total of 42 samples (9 of the Lower Stratoid Series, 20 of the Upper Stratoid Series, 9 of the CAG and 4 of the axial samples) have been analysed for major and trace elements (Table S3). The pulp was prepared by crushing and milling the samples in agate jars. Major element analyses were carried out at Activation Laboratories Ltd. (Ontario, Canada) by means of inductively coupled plasma-optical emission spectroscopy (ICP-OES) whole rock analysis. Trace elements analyses were carried out at University of Pisa, Earth Sciences Department ICP-MS laboratories; 50–60 mg 50–60 mg of each powdered sample was dissolved by means of multiple steps in a mixture of HF and HNO_3 on a hot plate at ~ 170 °C in a screw-top perfluoroalkoxy (PFA) vessel and analysed using inductively coupled plasma mass spectrometry (ICP-MS) with a PerkinElmer NexION 300X. A procedural blank and one reference sample (WS-E, Whin Sill Dolerite; Govindaraju, 1994) underwent the same procedure. A solution containing ^{103}Rh, ^{187}Re and ^{209}Bi

has been added to our samples, to the blank and to the reference sample, to be used as an internal standard.

5 Results

5.1 Field observations

The Lower Stratoid Series lavas have been observed in outcrops along the road from Gewane to Mille (Figure 1). They consist of horizontally-jointed and massive blocky-jointed lava flows, reaching thickness of a few meters (Figure 2a). The thickness of the observed lava successions is moderate (~5 m), but to the east a lava succession of up to 400/500 m thick occurs (e.g., Karrayyu and Manda Eli Adda Do graben; satellite observations). The Upper Stratoid Series have been observed mainly along the Tendaho and Dobi graben escarpments with observed flow thickness on the order of ten meters (Figure 2b and 2c). The thick succession of sheet flows is cut by up to 1000-meter-high graben-bounding faults in the Tendaho graben. The thickness of the single flows and the total volume are, however, smaller with respect to the typical flood basalt volcanism, e.g., the Oligocene Ethiopian trap reaching pluri-decametric thick single flows for a total volume of ~720,000 km^3 (Krans et al., 2018; Mohr, 1983; Rooney, 2017). The Upper Stratoid lava flows are rather homogeneous, tabular, mainly massive, and predominantly blocky-jointed (Figure 2b and 2c). However, horizontal jointed and, to a small extent, well-formed columnar-jointed deposits have also been observed. Some flows show an increase in vesiculation toward the top. Subordinate pillow lavas have also been found, suggesting that water bodies may have existed during the Upper Stratoid emplacement and therefore an environment with episodic depressed areas and humid conditions. No evidence of long hiatuses, such as the ones marked by thick sedimentary deposit interbedded with basalt flows in the Awash valley (Alemseged et al., 2020; DiMaggio et al., 2015), has been recognised on the observed outcrops. This suggests an overall high eruption rate, which potentially also contributed to forming a relatively flat surface morphology. The CAG Series lava flows are overall less thick with respect to the Stratoid Series flows and show inner variations regarding structure and vesiculation. In central Tendaho, north-east of Aysaita, and in the Immino area (Figure 1) meter-thick (up to 2 m) massive and blocky-jointed flows interlayered with thin vesiculated facies were observed (Figure 2d). In Tendaho, a

subaqueous lava forming hummocky-like flows (e.g., Self et al., 1998) shows clinker, tilted block and pressure ridges suggesting flow inflation (Duraiswami et al., 2001; Rossi and Gudmundsson, 1996; Walker, 1991). Near Eli Dar (Figure 1) a reworked volcaniclastic deposit has been observed at the base of the meter-thick massive flow, suggesting a period of stasis in the magmatic activity. In the same area, Varet (2018) observed an erosive boundary and clastic sedimentation between the Stratoid Series and the CAG Series.

Overall, the Stratoid Series, have the characteristics of flood basalt volcanism, such as the thick, massive, and jointed sheet flows, but they are less voluminous with respect to the typical flood basalt province (e.g., Deccan Traps, Columbia River Basalt province). Sporadic pillow lavas indicate episodes of subaqueous activity while the absence of hiatuses is consistent with continuous volcanic activity. A stasis can be instead suggested between the Stratoid and the CAG Series. The CAG Series shows an important decrease in total and single flow thickness with respect to the Stratoid Series, and more variable features with respect to the more homogeneous lavas of the Stratoid Series.

5.2 Petrography and mineral chemistry

The Lower Stratoid Series are mainly aphyric or micro-porphyritic, with some scarcely porphyritic samples (Table S1). The populations of phenocrysts and microphenocrysts are dominated by plagioclase with minor olivine and clinopyroxene. The plagioclase phenocrysts are often sieve-textured and external resorption features are common (Figure 3a). Fe-Ti oxides and apatite are accessory minerals. The groundmass is mostly intergranular with subordinate hyalopilitic samples, and it is composed of plagioclase, olivine, clinopyroxene and Fe-Ti oxides.

The lavas of the Upper Stratoid Series, similarly to the Lower Stratoid Series, are mainly aphyric and micro-porphyritic (Table S1). Four Upper Stratoid samples are scarcely porphyritic and only one sample (AF20-12) reaches 35% of phenocryst abundance with phenocrysts of plagioclase and olivine. The most abundant phase is plagioclase, with minor olivine and clinopyroxene (Figure 3b). In some samples, plagioclase phenocrysts show internal and external resorption features. With regard to accessory minerals, Fe-Ti oxides have been observed in most of the samples, apatite in the more evolved samples, while sulfides (pyrrhotite and Cu-rich sulfide) have been found in two mafic samples (AF20-04 and AF20-19). The groundmass is mostly intergranular with

subordinate intersertal samples and composed of plagioclase, olivine, clinopyroxene and Fe-Ti oxides. The five more evolved lava samples are porphyritic and dominated by plagioclase with minor clinopyroxene and olivine, also found as glomerocrysts. Fe-Ti oxides and apatite are accessory phases. The groundmass is mostly intersertal and, subordinately, intergranular and is composed of plagioclase, olivine, clinopyroxene and Fe-Ti oxides.

The CAG Series lavas are instead generally porphyritic and micro-porphyritic, with only two aphyric samples (Table S1). One sample has an ophitic texture with plagioclase enclosed in clinopyroxene. As for the Stratoid Series, plagioclase is the most abundant phenocryst mineral, but olivine and clinopyroxene phenocrysts are also common (Figure 3c). In some samples, plagioclase phenocrysts have sieve textures and/or show external resorption features, together with olivine and clinopyroxene they form glomerocrysts. Quartz xenocrysts with pyroxene corona have been found in one sample. Fe-Ti oxides have been observed as accessory minerals. The groundmass is mostly intergranular and subordinately intersertal and composed of plagioclase, olivine, clinopyroxene and Fe-Ti oxides.

Six samples have been analysed for mineral chemistry, two lava flows of the Upper Stratoid Series (AF20-04 and AF20-19, respectively MgO 4.76 wt% and 4.54 wt%), one flow of the Lower Stratoid Series (H436, MgO 5.44 wt%) and three lava flows of the CAG Series (AF20-46, AF20-66 and AF20-25, respectively MgO 5.17 wt%, 4.69 wt% and 5.84 wt%) (Table S2). They have been selected based on composition (most of the mafic lavas range between MgO 4.5 wt% and 6.5 wt%) and on the presence of phenocrysts and micro-phenocryst (Figure 4).

Both in the Upper and the Lower Stratoid Series, plagioclase crystals are normally zoned with a compositional gap between the bytownite and the labradorite fields (Figure 4a). The cores are mainly bytownite ranging from An 75 to An 85 and the rims are mainly andesine-labradorite (An 43-58) with some bytownitic composition (An 76-85) (Figure 4a). The CAG Series plagioclase crystals are mostly normally zoned, with mainly bytownitic cores and some reaching more evolved compositions (An 50-65). Rims are mainly labradoritic (An 50-70) and no compositional gap has been observed (Figure 4a). The groundmass plagioclase has overall similar compositions for the three Series (Figure 4a). The olivine crystals of the Upper Stratoid Series are normally zoned, with cores Fo 54-63 and rims Fo 29-44 (Figure 4b). The olivine crystals in the Lower

Stratoid Series are normally zoned, and cores reach more Fo-rich composition with respect to the Upper Stratoid Series (up to Fo 76). The olivine crystals in the CAG Series are normally zoned with overlapping compositional ranges for cores (Fo 62-79) and rims (Fo 54-69). The groundmass compositions are overall similar between Lower and Upper Stratoid Series, while they are more mafic for the CAG Series (Figure 4b). The clinopyroxene is mainly augite for all the Series, with the exception of pigeonite in the Upper Stratoid Series groundmass and rim (Figure 4c). The CAG Series and the Lower Stratoid Series reach more diopsidic composition with respect to the Upper Stratoid Series (Figure 4c). The presence of only few clinopyroxene and olivine phenocrysts in the Lower Stratoid Series does not allow a robust comparison with the other Series. Lower and Upper Stratoid Series have both ilmenite and titanomagnetite and in sample AF20-04 the titanomagnetite forms preferentially the rims around an ilmenite core. For the CAG Series, AF20-46 have titanomagnetite only while in AF20-66 and AF20-25 both ilmenite and titanomagnetite are present (Table S2).

5.3 Major and trace element data

The Stratoid and CAG Series analysed samples are subalkaline, with transitional to tholeiitic affinity, and in the Total Alkali-Silica (TAS) classification diagram are mainly basalt-basaltic andesite, with two andesite, one trachyte and one rhyolite (Figure S1; Table S3). The CAG Series is on average more mafic (Table 1; Table S3) and includes the most primitive samples (up to MgO 8.38 wt%, 345 ppm of Cr and 168 ppm of Ni) compared to the Lower and Upper Stratoid Series (respectively up to MgO 6.47 wt% and 6.60 wt%; Figure 5; Table 1; Table S3). The Lower and Upper Stratoid Series basalts are mainly Qz-normative and subordinately Hy-Ol normative, while the CAG Series is mainly Hy-Ol normative.

The major element distributions of the three Series in variation diagrams are rather scattered, particularly for TiO_2, FeO P_2O_5 and Al_2O_3, and no single trend for each Series is recognized (Figure 5; Figure S2; Table S3). CaO, Na_2O and K_2O have overall similar trends for the three Series with CaO showing a more scattered behaviour for the CAG Series (Figure 5; Figure S2).

A group of samples, formed by two CAG Series samples from the Tendaho graben (AF20-22 and AF20-29) and two Lower Stratoid Series samples from the Woranso-Mille region (AF20-61 and AF20-62a) can be distinguished outside of the overall trend. The group is remarkably depleted in

TiO_2 and FeO_t and enriched in SiO_2, Al_2O_3, K_2O with respect to the rest of the samples for the same MgO wt%, (Figure 5; Figure S2) and is hereafter called the low Ti-Fe samples group.

Concerning trace elements, a marked discrimination among the three Series is provided by the Sr content, which is higher in the CAG and Upper Stratoid Series with respect to the Lower Stratoid Series (Figure 5). Incompatible trace elements are positively correlated with Zr showing overall overlapping trends for the three Series, except for Y and HREE (Figure S3; Table S3). Furthermore, the low Ti-Fe samples show definitely different incompatible trace elements contents and ratios (i.e., higher Th, U and Rb for the same Zr) with respect to their respective Series (Figure S3).

The incompatible trace elements and REE patterns, normalised to primitive mantle and chondrite concentrations respectively (McDonough and Sun, 1995), are presented in Figure 6. The Lower and Upper Stratoid Series basalts have E-MORB type REE patterns and are characterised by a slight U-Th trough and a Nb-Ta peak. The CAG Series also shows E-MORB-type REE patterns, but the Nb-Ta peak and U-Th though are more pronounced with respect to the Stratoid Series (Figure 6). The four low Ti-Fe samples have a positive peak in Th-U, high K and Rb, high La/Sm and low and scarcely fractionated MREE and HREE (Figure 6; Table S3). Moreover, two of the low Ti-Fe samples have positive anomalies in Pb (for the other two samples Pb is below the detection limit; Figure 6; Table S3).

Overall, the analysed samples exhibit characteristics of Enriched-MORB and correspond to the type III and IV magmatism of Rooney (2020a, 2020b) (Figure 6). The three Series have similar trends and ratios of many incompatible elements but show notable differences in HREE and Y (Figure S3). The samples belong overall to the HT1 group (High-Ti group 1 of Pik et al., 1998) with lower Ti content for the Lower Stratoid Series (Figure 5g). Overall, the three Series broadly overlap with the OIB, MORB and intracontinental basalt fields (Figure 5h). However, part of the Upper Stratoid have higher Nb/Ta and Zr/Hf indicating, according to their partition coefficient during partial melting (Hart and Dunn, 1993; McDade et al., 2003; van Westrenen et al., 2001), a slightly more intracontinental affinity with respect to the Lower Stratoid, possibly suggesting two different stages of the rift evolution (Figure 5h). Nevertheless, not all the CAG show a more MORB affinity with respect to the Upper Stratoid. Despite the rather scattered behaviour of the three

Series, the major and trace elements suggest an evolution dominated by fractional crystallisation of the minerals observed in thin sections, starting from the most primitive basalts (Figure 5; Figure S2). The trend is well constrained by the evolved and intermediate samples of Santarnecchi (1978), that studied the silicic central volcanoes intercalated in the upper part of the Stratoid Series (e.g., Gad Elu, Ado Ale, Oyma, Katahelu; Table S3), partially covering the Daly gap commonly observed in the Afar and Main Ethiopian Rift volcanism (Peccerillo et al., 2003, 2007). The constant decrease of Ni and Cr suggests fractionation of olivine from the most mafic terms. At 6% MgO a decrease in CaO and Al_2O_3 is observed suggesting fractionation of plagioclase and clinopyroxene, without a decrease in Sr. The decrease of TiO_2 and FeO at 5% MgO and of P_2O_5 at 4% MgO respectively indicate fractionation of Fe-Ti oxides and apatite.

6 Discussion

The geochemical study of the Lower and Upper Stratoid Series and CAG Series volcanic products erupted in Southern-Central Afar allows us to investigate differences of the magma source and melt evolution throughout the 4.5-0.6 Ma magmatism. Together with geophysical and stratigraphic evidence, we use our results to interpret the evolution of rifting in Afar in the last 4.5 Ma.

6.1 Mantle sources of the Stratoid Series and CAG Series magmatism

The Lower, Upper and CAG Series have similar characteristics in terms of lava composition. The lavas are mainly mafic, covering a similar differentiation range between 4.5 and 6.5 wt% MgO with few more primitive compositions (MgO up to 8 wt%). All basalts are subalkaline, Hy-Ol or Qz normative. The three Series also display overall similar trends of major and trace elements (excepting the four low Ti-Fe lavas). The mafic lavas, according to the Ba and Nb-Ta peaks, the negative K anomaly and to the U-Th trough (Figure 6), are classified as type III and IV of Rooney (2020a, 2020b), representative of lavas erupted under conditions of lithospheric thinning by a mixing of plume, depleted mantle, and African lithosphere.
Despite the samples not being primitive, crustal contamination did not have an important effect on magma evolution during its possible stationing at the base of the crust (i.e., magma underplating) nor in the shallower magma chambers during its ascent (Figure 7a; Figure S4). Most

of the samples fall in the MORB-OIB range (Nb/U 37-57, and Ce/Pb 20-30; Hofmann et al., 1986). The only exceptions are the two evolved Upper Stratoid samples having low Ce/Pb and high Nb/Rb, and the four Low Ti-Fe lavas having low Nb/U, Ce/Pb and high La/Nb, Rb/Nb. All the Series, in agreement with the literature data and with Nb/U and Ce/Pb ratios (Figure 7a), fall in between the MORB and OIB fields (Figure 7b; Figure S4). In Figure 7b the Lower Stratoid has higher Zr/Nb and lower La_N/Sm_N indicating a more MORB-like mantle source with respect to the Upper Stratoid and therefore possibly suggesting two different stages of the rift evolution. Overall the CAG has a more scattered distribution. However, considering only the samples collected at the Tendaho graben and excluding therefore the two samples of the Immino graben (Zr/Nb < 6; Figure 1; Figure 7b) and the two Low Ti-Fe samples (affected by crustal contamination), the CAG also has a more MORB-like affinity with respect to the Upper Stratoid. At the same time, all the Series have a marked negative anomaly in K and the positive peak in Ba and Nb-Ta, interpreted as indicative of amphibole and/or phlogopite in the mantle source (Furman and Graham, 1999; Rooney et al., 2017; Späth et al., 2001). The ratios Na_2O/K_2O and Ba/Rb can be used to discriminate between melting of phlogopite- and amphibole-bearing mantle sources, respectively lower and higher than 1 (Foley et al., 1999; Green, 1973; Rosenthal et al., 2009) and 11 (primitive mantle value from Sun and McDonough, 1989; Furman and Graham, 1999). The $Na_2O/K_2O > 1$, the Ba/Rb > 11 and the K/Th variation obtained by modelling a partial melting process of a mantle source with and without amphibole (Shaw, 1970, eq. 15; Figure 7c) indicate an amphibole-bearing SCLM involved in partial melting. The amphibole is stable in the mantle up to 3 GPa and 1050-1150 °C (Class and Goldstein, 1997; Green et al., 2010; Niida and Green, 1999), therefore indicating a contribution of a relatively cold SCLM source during the partial melting for all three Series. We therefore suggest that the presence of the anomalously hot Afar mantle (1350-1500 °C; Ferguson et al., 2013; Feyissa et al., 2019; Rooney et al., 2012b) induced amphibole metasomatism (Furman et al., 2016; Rooney et al., 2017) of the SCLM in Afar. Consequently, melting of the Afar plume and depleted mantle (Ferguson et al., 2013; Feyissa et al., 2019; Rooney 2020a, 2020b) together with the upper, easily-fusible (Pilet et al., 2008), amphibole-bearing SCLM produced the observed type III and IV magmatism of Rooney 2020a, 2020b.

The four low Ti-Fe samples, instead, lack the diagnostic positive anomalies in Nb-Ta and negative in K of type III and IV mantle source, but show positive anomalies in Th-U and Rb and high La/Sm (Figure 6). Two low Ti-Fe samples of the Woranso-Mille region, together with another sample of that region (AF20-60b), have low Zr and Nb for the same MgO wt% with respect to the other Lower Stratoid samples and low and scarcely fractionated MREE-HREE (Figure 6; Table S3). These characteristics resemble a group of samples of the Woranso-Mille region described by Rooney (2020a) as a rare occurrence of a depleted component "intrinsic" to the Afar plume (type VI). On the other hand, our low Ti-Fe lavas require the involvement of a crustal component (Figure 7c; Figure S4). Our data seem, therefore, to enhance the geochemical complexity of lavas in the Woranso-Mille area.

Considering the three Series, marked differences in garnet-compatible elements (e.g., Tb_N/Yb_N, Zr/Y; Figure 7d and 7e) and small but systematic differences in highly incompatible elements ratios (e.g., Th/Nb, Th/Zr; Figure 7f) have been observed in the lavas with MgO> 4 wt%. Yb (as the other HREE and Y) is highly compatible in garnet (Salters and Longhi, 1999) and, thus, partial melting of a garnet-bearing mantle source, with residual garnet, translates in the increase of Tb_N/Yb_N ratio with respect to a spinel-bearing source. Variation to the Tb_N/Yb_N ratio due to melting of a garnet-bearing lower crust or to fractionation of garnet or amphibole in water-saturated conditions (Alonso-Perez et al., 2009) can be ruled out for Central-Southern Afar due to the low crustal thickness (Hammond et al., 2011). Furthermore, no garnet nor amphibole have been observed in the thin sections. The influence of high pressure clinopyroxene fractionation, behaving similarly to the garnet, could also be ruled out due to its lower efficiency in fractionating MREE-HREE. Lastly, we suggest that the effect on Tb_N/Yb_N of amphibole variations during partial melting could be ruled out, as no variation is observed in other amphibole-compatible elements (e.g., K in Figure 6 and Figure 7c). Similarly, the effect of clinopyroxene fractionation on La/Sm could be ruled out as no variations between the Series has been observed in other clinopyroxene-compatible elements, such as V.

We therefore used the Tb/Yb ratio as a diagnostic parameter to discriminate the different depths of the magma-source melting column. In Figure 7d and 7e a marked distinction is evident within our samples at Tb_N/Yb_N ~1.7, with the Upper Stratoid Series having overall higher values and the

Lower Stratoid Series and the CAG Series having clear lower values. We model the batch melting process (Shaw, 1970, eq. 15) of the spinel and garnet-bearing mantle sources for various degrees of partial melting and mixing between the two source types using the mass balance equation (Figure 7d and 7e). The Upper Stratoid Series are well encompassed by the model with 3.5-4.5% of a prevalently garnet-bearing mantle source (70-50% garnet-bearing), while most of the Lower Stratoid Series and CAG Series basalt require a degree of partial melting higher than 4.5% of a mantle source primarily out of the garnet stability field (50-80% spinel-bearing source). According to the experimental studies of Klemme and O'Neill (2000) and to the Afar mantle temperature ranging between 1050-1150 °C (residual amphibole) and 1500°C (Ferguson et al., 2013; Feyissa et al., 2019; Rooney et al., 2012b), we identify the spinel-garnet transition between 16-27 Kbar (60-100 Km). Therefore, the Upper Stratoid Series basalts were mainly generated at relatively larger depths (greater than (>) 60-100 km-deep), while the Lower Stratoid Series and CAG Series are derived from shallower (less than (<) 60-100 km-deep) partial melting, and broadly consistent with the ~100 km-deep, base of melt zone constrained using seismology and geochemical modelling for the present day (Chambers et al., 2022; Ferguson et al., 2013). Notably, some samples of the Upper Stratoid Series, with ages around 1.1 Ma (Feyissa et al., 2019; Kidane et al., 2003) have Tb_N/Yb_N values intermediate between CAG Series and Upper Stratoid Series, suggesting a gradual shallowing of the melting column at the transition between the two Series (samples collected between the cities of Serdo and Silsa; Figure 1; Table S3).

We remark that only the two CAG lava flows analysed from the Immino graben show Tb_N/Yb_N of 1.99 and 2.03, indicating a deeper melting column than the rest of the CAG. This suggests less lithosphere extension and thinning in the Immino graben compared to Tendaho graben, the historically active zone (e.g., Keir et al., 2009). Further studies on samples from the CAG Series and Stratoid Series in the Immino and neighbouring grabens are however necessary to validate this hypothesis.

Highly incompatible element ratios, such as Th/Nb and Th/Zr, show a clear distinction between Upper Stratoid and CAG Series, suggesting variations in the relative primitive melts (Figure 7f). According to the partition coefficient of McKenzie and O'Nions (1991), Th is slightly more incompatible than Zr and Nb during partial melting. The lower values in Th/Nb and Th/Zr of the

CAG Series basalts with respect to the Upper Stratoid Series, coupled with the lower values in La_N/Sm_N, indicate an increase of the degree of melting after the eruption of the Upper Stratoid Series.

In summary, the 4.5-0.6 Ma mafic magmatism of Central and Southern Afar is related to partial melting of a metasomatized SCLM that melted (or dripped into the asthenosphere; Furman et al., 2016) together with depleted mantle and the rising Afar plume, originating the three components observed in the lavas (Figure 6 and 7). Despite the sustained stretching and thinning of the lithosphere preceding the Stratoid volcanism in Afar (e.g., Armitage et al., 2015) and the similarity of the involved mantle reservoirs (Figure 5; Figure 7), the Lower and Upper Stratoid Series are produced by two distinct mantle sources, respectively with a shallower and deeper melting column (Figure 7). The CAG Series basalts were generated from a shallower partial melting column and a higher degree of partial melting with respect to the Upper Stratoid Series, suggesting more rift focusing and lithosphere thinning for the Lower Stratoid Series and CAG (Figure 7).

6.2 Melt evolution of the Stratoid Series and CAG Series magmatism

The mafic and intermediate samples of the three Series overlap in most of the major and trace elements variations diagrams (figure 5) and no clear distinct trend between the Series has been recognized except for Sr. At the same time, different primitive magmas have been revealed by the trace element composition of the mafic lavas, and multiple evolutionary paths are suggested by the compositional spread of the samples with intermediate degree of evolution. Since the samples are aphyric or scarcely porphyritic, this variable composition cannot be attributed to mechanisms of phenocryst accumulation, except for one sample with high Al_2O_3 and CaO and 35% of plagioclase phenocrysts. A significant interaction with the crust can be excluded based on the element's ratios Nb/U, Rb/Nb, Ce/Pb (Table 1), except the four low Ti-Fe samples.

We use rhyolite-MELTS algorithm (Asimow et al., 2004; Ghiorso and Sack, 1995) to model the liquid line of descent for a range of pressures (0.5-3.5 Kbar), water content (0.5-2 wt%) and oxygen fugacity (QFM+1-QFM-2), starting from the most mafic sample for each Series, to investigate fractional crystallisation conditions for mafic-intermediate products. Except for the four low Fe-Ti samples, the range of conditions that best fit each individual Series are similar,

with pressure varying between 1.5 and 2.5 Kbar, the oxygen fugacity between QFM and QFM-1 and H_2O from 0.5 to 1 wt% (Figure S5a, S5b and S5c). These models suggest that there is no variation in time between the Series regarding the hydration state of the mantle nor regarding the oxygen fugacity. According to MELTS simulations, the variation of TiO_2 and FeO at 4-5 MgO wt% within the Upper Stratoid could be explained by an increase of the water content (up to 1 H_2O wt%) that, however, fails to fit the Al_2O_3 content (Figure S5b). Moreover, it is difficult to explain the variation in Sr between the Series with different conditions of fractional crystallisation considering the similarities of the other elements (i.e., Al_2O_3). Based on the MELTS modelling results (at 2 Kbar, QFM-0.5 and H_2O 0.5 wt%) olivine precipitates only for the CAG Series at ~8.3 MgO wt%. Clinopyroxene starts fractionating at ~7.14 MgO wt% for the CAG Series and at ~6.4-6.6 MgO wt% for the Stratoid Series. Plagioclase precipitates at ~6.9 MgO wt% for the CAG Series and at ~5.9-6.1 MgO wt% for the Stratoid Series. Spinel precipitates at ~5 MgO wt% for the CAG Series and the Upper Stratoid Series and at ~4.4 MgO wt% for the Lower Stratoid Series.

Despite the presence of only few phenocrysts of plagioclase, clinopyroxene and olivine in the samples (particularly for the Lower Stratoid Series), the mineral chemistry indicates possible differences in the plumbing system between the Series. Our data reveal that the CAG Series and the Lower Stratoid Series lavas host mafic mineral phases (Fo-rich olivine and Mg#-rich clinopyroxene) suggesting an early differentiation stage not observed instead in the Upper Stratoid (Figure 4). However, given the scarcity of the clinopyroxene phase (Table S2) and the lack of equilibrium with the bulk rock for the Stratoid Series, we only use the plagioclase phenocrysts analyses of the six samples to calculate the pressure of crystallisation by means of mineral-melt geothermobarometer (Putirka, 2008, Eq. 25a). For the modelling we used the whole rock analyses as melt composition (Putirka 2008) and a water concentration of 0.5 wt%. The equilibrium was checked based on the distribution coefficient $KD_{(An\text{-}Ab)}^{pl-liq}$ = 0.10 ± 0.05 at T < 1050 °C and 0.27 ± 0.11 at T ≥ 1050 °C (Putirka, 2008). Plagioclase-melt equilibrium is never observed for the Upper Stratoid suggesting a fast magma ascent leading to low phenocrysts content and plagioclase-liquid disequilibrium (La Spina et al., 2016). Plagioclase-melt equilibrium is instead observed for the Lower Stratoid Series ranging from 1.3 to 1.9 ± 3.8 kbar, and for the CAG Series ranging from 2.3 to 4.2 ± 3.8 kbar. Therefore, we suggest that during its ascent magma

possibly ponded at first at the base of the crust and then, rising toward the surface, at ~ 5-7 Km depth for the Lower Stratoid Series and at 9-16 Km depth for the CAG Series. The two-plagioclase populations could be related to an abrupt release of water driven by a decompression-induced crystallisation from a H_2O-rich melt. This scenario will induce a rapid transition toward the crystallisation of more Na-rich plagioclase (Lange et al., 2009).

6.3 Rift evolution in Southern and Central Afar

The results presented in this work and the above discussion about the mantle sources inferred for the Lower and Upper Stratoid and the CAG Series can be used, together with evidence from crustal structure and depocenter locations, to interpret the evolution of rifting activity from ~4.5 Ma ago (Figure 8).

Our geochemical results show that the Lower Stratoid (~4.5-2.6 Ma), were generated by a shallower melting column (< 60-100 km) with respect to the Upper Stratoid, suggesting a more stretched and thinned lithosphere (Figure 7 and 8). The Lower Stratoid Series outcrop only in Southern Afar (Figure 1) and are temporary coeval with the development of the Hadar Basin depocenter in Southern Afar (3.8-2.9 Ma; DiMaggio et al., 2015; Rooney, 2020a; Wynn et al., 2008; Figure 1), which spatially correspond to an area of thinned crust (~22 km; Hammond et al., 2011; Wang et al., 2021). We interpret these independent observations as evidence that the Lower Stratoid were produced during a phase of localised extension in Southern Afar with sufficient lithosphere thinning to allow for a shallow melting column (Figure 8). This interpretation is consistent with a number of geological and geophysical studies that interpret Red Sea related extension localised to the rift valley floor in South Afar during the Miocene (Hammond et al., 2011; Tesfaye et al., 2003; Wolfenden et al., 2005).

After the Lower Stratoid emplacement, the locus of Stratoid volcanism shifted dramatically from Southern to Central Afar to form the Upper Stratoid during 2.6 to 1.1 Ma. Our data indicate that the Upper Stratoid magmas were associated with a deeper melting column (> 60-100 km) with respect to the earlier Lower Stratoid Series and hence consistent with melting below a thicker lithosphere (Figure 7 and 8). These results are consistent with the locus of melting shifted NE to a new zone of extension in central Afar where the lithosphere had been thinned less. We interpret the NE shift in volcanism, the deepening of the melting column, and the geological

evidence for a co-eval, and pronounced change in fluvial depositional systems and locus of strain (Campisano, 2012; Di Maggio et al., 2015; Quade et al., 2008; Wynn et al., 2008), as indicative of a rift jump from the Pliocene rift in Southern Afar to the Pleistocene rift in Central Afar around the end of the Pliocene (Figure 8). We propose that the dramatic shift in strain and volcanism may have been triggered by tectonic reorganisation caused by the triple junction moving north-eastward from the Hadar Basin to central Afar, possibly due to the on land spreading of the Gulf of Aden in the Tadjoura gulf at ca. 3 Ma (Daoud et al., 2011; Le Gall et al., 2015). Our observation are in agreement with the regional reconstruction of the northeast migration of the Red Sea rift during ~29-7 Ma (Wolfenden et al., 2005), the inferred northeast migration of the triple junction (Tesfaye et al., 2003) and to the more local observations of the northeast migration of the depocenter during ~10-3 Ma along the Awash valley (Kalb, 1995). Around 1 Ma, after the eruptions of the Upper Stratoid Series over a wide area in Afar, the rift activity changed again with the emplacement of the CAG Series, the first recognized magmatic activity localised along the axial faults of the depression and associated with thinned crust in the Tendaho graben (Hammond et al., 2011). The CAG Series has been associated with the localization of strain (Rooney 2020a; Stab et al., 2016; Tesfaye et al., 2003). Our results are consistent with this interpretation since our analysis indicates a shallower melting column and a higher degree of melting for the CAG Series mantle source compared to the Upper Stratoid (Figure 7 and 8). We therefore interpret the CAG Series products as the first volcanic activity associated with the progressive focusing of rifting in Central Afar (i.e., Pleistocene rifting). Some Upper Stratoid lavas testify the progressive shallowing of the melting column and therefore the gradual focalization of the Pleistocene rifting from the Upper Stratoid Series to the CAG Series along the Tendaho Graben at ~1 Ma.

7 Conclusion

The geochemical constraints obtained by the study of mafic lavas in this work provide indication on mantle source depths of the Stratoid Series and Central Afar Gulf Series (4.5-0.6 Ma) in Central and Southern Afar. These data allow us to correlate the nature of the voluminous volcanism to the geodynamic evolution of the Red Sea rift branch in the last 4.5 Ma.

In agreement with previous studies, our data indicate that the Stratoid and Central Afar Gulf Series were both generated by partial melting of three mantle reservoirs, the Afar plume, the depleted mantle and the SCLM. Moreover, amphibole-compatible elements indicate the involvement of amphibole-bearing metasomatized SCLM. A deeper, garnet-bearing, partial melting column is required for the Upper Stratoid (2.6-1.1 Ma) with respect to the shallower, spinel-bearing, partial melting column of the Lower Stratoid (4.5-2.6 Ma) and Central Afar Gulf (1.1-0.6 Ma). This variations in the depth of melting reveals different mantle sources for the three Series. Moreover, the Central Afar Gulf have a higher degree of partial melting with respect to the Upper Stratoid. Similar differentiation paths dominated by fractional crystallisation explain the compositional range observed for the three Series. Mineral chemistry, and mineral-melt geobarometer indicate differences in the depth of the magma chambers, and in the magma ascending path between the three Series.

We associated the Afar flood basalt volcanism to two episodes of rifting. The Pliocene rift stretched the lithosphere and produced the Lower Stratoid Series in South Afar suggesting, together with geophysical and stratigraphical evidence, the area was the main locus of strain during this period. Then, around the end of the Pliocene, a rift jump relocated the Pleistocene rift in Central Afar and produced the Upper Stratoid Series under a thicker, less stretched, lithosphere indicating, together with stratigraphical evidence, less focused strain during their emplacement. A progressive shallowing of the mantle source has been then inferred passing from the Upper Stratoid Series to the focused activity of the Central Afar Gulf Series.

We conclude therefore that the break-up process migrated north-eastward from South to Central Afar through time in response to the Red Sea branch evolution. Accordingly, extensional processes can exert a fundamental control on the spatial and chemical variations of the recent flood basalt volcanism in Afar by inducing decompression melting without requiring variations on the activity of the mantle plume.

Acknowledgments

The research is part of the PhD of G.Tortelli and is funded by 2017 PRIN project-protocol MIUR: 2017P9AT72 PE10. G.Tortelli acknowledges support by the Pegasus. We thank R. Ishak and M. Gemelli (CISIM, University of Pisa), A. Orlando (EPMA lab., CNR-IGG of Firenze) and L. Ghezzi (ICP-MS lab., University of Pisa) for their support during analytical acquisition. We thank R. Santacroce (University of Pisa) for discussions and support. We thank the colleagues of the Addis Ababa University and the Ethiopian and Afar Regional governments for their support and help in organising the February 2020 campaign. We also thank the drivers of the rental agency Ethioder, and the local policeman and guides of the different woredas for their logistic support during the campaign. Open access funding provided by Università di Pisa within the CRUI-CARE Agreement. We also like to thank Tanya Furman and one anonymous reviewer for their valuable comments and suggestions, which help to improve the quality of our manuscript.

Open Research

Data presented in this work are contained within the supplementary files.

Data presented in this work are available on EarthChem Library (https://doi.org/10.26022/IEDA/112504).

No financial conflicts of interests for any author.

References

Acocella, V. (2010). Coupling volcanism and tectonics along divergent plate boundaries: Collapsed rifts from central Afar, Ethiopia. Bulletin, 122(9-10), 1717-1728. https://doi.org/10.1130/B30105.1

Acocella, V. (2014). Structural control on magmatism along divergent and convergent plate boundaries: Overview, model, problems. Earth-Science Reviews, 136, 226-288. https://doi.org/10.1016/j.earscirev.2014.05.006

Ahmed, A., Doubre, C., Leroy, S., Keir, D., Pagli, C., Hammond, J. O., et al. (2022). Across and along-strike crustal structure variations of the western Afar margin and adjacent plateau: Insights from receiver functions analysis. Journal of African Earth Sciences, 192, 104570. https://doi.org/10.1016/j.jafrearsci.2022.104570

Alemseged, Z., Wynn, J. G., Geraads, D., Reed, D., Andrew Barr, W., Bobe, R., et al. (2020). Fossils from Mille-Logya, Afar, Ethiopia, elucidate the link between Pliocene environmental changes and Homo origins. Nature communications, 11(1), 1-12. https://doi.org/10.1038/s41467-020-16060-8

Alonso-Perez, R., Müntener, O., & Ulmer, P. (2009). Igneous garnet and amphibole fractionation in the roots of island arcs: experimental constraints on andesitic liquids. Contributions to Mineralogy and Petrology, 157(4), 541-558. https://doi.org/10.1007/s00410-008-0351-8

Armitage, J. J., Ferguson, D. J., Goes, S., Hammond, J. O., Calais, E., Rychert, C. A., & Harmon, N. (2015). Upper mantle temperature and the onset of extension and break-up in Afar, Africa. Earth and Planetary Science Letters, 418, 78-90. https://doi.org/10.1016/j.epsl.2015.02.039

Asimow, P. D., Dixon, J. E., & Langmuir, C. H. (2004). A hydrous melting and fractionation model for mid-ocean ridge basalts: Application to the Mid-Atlantic Ridge near the Azores. Geochemistry, Geophysics, Geosystems, 5(1). https://doi.org/10.1029/2003GC000568

Baker, J., Snee, L., & Menzies, M. (1996). A brief Oligocene period of flood volcanism in Yemen: implications for the duration and rate of continental flood volcanism at the Afro-Arabian triple junction. Earth and Planetary Science Letters, 138(1-4), 39-55. https://doi.org/10.1016/0012-821X(95)00229-6

Barberi, F., & Santacroce, R. (1980). The Afar Stratoid Series and the magmatic evolution of East African rift system. *Bull. Soc. Geol. Fr*, *22*, 891-899.

Barberi, F., Ferrara, G., Santacroce, R., & Varet, J. (1975). Structural evolution of the Afar triple junction.

Barrat, J. A., Joron, J. L., Taylor, R. N., Fourcade, S., Nesbitt, R. W., & Jahn, B. M. (2003). Geochemistry of basalts from Manda Hararo, Ethiopia: LREE-depleted basalts in Central Afar. Lithos, 69(1-2), 1-13. https://doi.org/10.1016/S0024-4937(03)00044-6

Bastow, I. D., & Keir, D. (2011). The protracted development of the continent–ocean transition in Afar. Nature Geoscience, 4(4), 248-250. https://doi.org/10.1038/ngeo1095

Bastow, I. D., Booth, A. D., Corti, G., Keir, D., Magee, C., Jackson, C. A. L., et al. (2018). The Development of Late-Stage Continental Breakup: Seismic Reflection and Borehole Evidence from the Danakil Depression, Ethiopia. Tectonics, 37(9), 2848-2862. https://doi.org/10.1029/2017TC004798

Bosworth, W., Huchon, P., & McClay, K. (2005). The red sea and gulf of aden basins. *Journal of African Earth Sciences*, *43*(1-3), 334-378. https://doi.org/10.1016/j.jafrearsci.2005.07.020

Buck, W. R. (1991). Modes of continental lithospheric extension. Journal of Geophysical Research: Solid Earth, 96(B12), 20161-20178. https://doi.org/10.1029/91JB01485

Campisano, C. J. (2012). Geological summary of the Busidima formation (Plio-Pleistocene) at the Hadar paleoanthropological site, Afar Depression, Ethiopia. Journal of human evolution, 62(3), 338-352. https://doi.org/10.1016/j.jhevol.2011.05.002

Chambers, E. L., Harmon, N., Rychert, C. A., Gallacher, R. J., & Keir, D. (2022). Imaging the seismic velocity structure of the crust and upper mantle in the northern East African Rift using Rayleigh wave tomography. Geophysical Journal International, 230(3), 2036-2055. https://doi.org/10.1093/gji/ggac156

Class, C., & Goldstein, S. L. (1997). Plume-lithosphere interactions in the ocean basins: constraints from the source mineralogy. Earth and Planetary Science Letters, 150(3-4), 245-260. https://doi.org/10.1016/S0012-821X(97)00089-7

Corti, G., Agostini, A., Keir, D., Van Wijk, J., Bastow, I. D., & Ranalli, G. (2015). Magma-induced axial subsidence during final-stage rifting: Implications for the development of seaward-dipping reflectors. Geosphere, 11(3), 563-571. https://doi.org/10.1130/GES01076.1

Corti, G., Bonini, M., Conticelli, S., Innocenti, F., Manetti, P., & Sokoutis, D. (2003). Analogue modelling of continental extension: a review focused on the relations between the patterns of deformation and the presence of magma. Earth-Science Reviews, 63(3-4), 169-247. https://doi.org/10.1002/2017TC004799

Courtillot, V., Achache, J., Landre, F., Bonhommet, N., Montigny, R., & Féraud, G. (1984). Episodic spreading and rift propagation: new paleomagnetic and geochronologic data from the Afar nascent passive margin. Journal of Geophysical Research: Solid Earth, 89(B5), 3315-3333. https://doi.org/10.1029/JB089iB05p03315

Daoud, M. A., Le Gall, B., Maury, R. C., Rolet, J., Huchon, P., & Guillou, H. (2011). Young rift kinematics in the Tadjoura rift, western Gulf of Aden, Republic of Djibouti. Tectonics, 30(1). https://doi.org/10.1029/2009TC002614

Deniel, C., Vidal, P., Coulon, C., Vellutini, P. J., & Piguet, P. (1994). Temporal evolution of mantle sources during continental rifting: the volcanism of Djibouti (Afar). Journal of Geophysical Research: Solid Earth, 99(B2), 2853-2869. https://doi.org/10.1029/93JB02576

DiMaggio, E. N., Campisano, C. J., Rowan, J., Dupont-Nivet, G., Deino, A. L., Bibi, F., et al. (2015). Late Pliocene fossiliferous sedimentary record and the environmental context of early Homo from Afar, Ethiopia. Science, 347(6228), 1355-1359. https://doi.org/10.1126/science.aaa1415

Duraiswami, R. A., Bondre, N. R., Dole, G., Phadnis, V. M., & Kale, V. S. (2001). Tumuli and associated features from the western Deccan Volcanic Province, India. Bulletin of Volcanology, 63(7), 435-442. https://doi.org/10.1007/s004450100160

Ebinger, C. J., Yemane, T., Woldegabriel, G., Aronson, J. L., & Walter, R. C. (1993). Late Eocene–Recent volcanism and faulting in the southern main Ethiopian rift. Journal of the Geological Society, 150(1), 99-108. https://doi.org/10.1144/gsjgs.150.1.0099

Eid, B., Lhuillier, F., Gilder, S. A., Pfänder, J. A., Gebru, E. F., & Aßbichler, D. (2021). Exceptionally high emplacement rate of the afar mantle plume head. Geophysical Research Letters, 48(23), e2021GL094755. https://doi.org/10.1029/2021GL094755

Farnetani, C. G., Hofmann, A. W., & Gupta, H. (2011). Mantle plumes. Encyclopedia of solid Earth geophysics. Springer, Dordrecht, 857-869. https://doi.org/10.1007/978-90-481-8702-7_132

Ferguson, D. J., Maclennan, J., Bastow, I. D., Pyle, D. M., Jones, S. M., Keir, D., et al. (2013). Melting during late-stage rifting in Afar is hot and deep. *Nature*, *499*(7456), 70-73. https://doi.org/10.1038/nature12292

Feyissa, D. H., Kitagawa, H., Bizuneh, T. D., Tanaka, R., Kabeto, K., & Nakamura, E. (2019). Transition from Plume-driven to Plate-driven Magmatism in the Evolution of the Main Ethiopian Rift. Journal of Petrology, 60(8), 1681-1715. https://doi.org/10.1093/petrology/egz043

Foley, S., Musselwhite, D., & Van der Laan, S. R. (1999). Melt compositions from ultramafic vein assemblages in the lithospheric mantle: a comparison of cratonic and non-cratonic settings. In International Kimberlite Conference (7th: 1998) (pp. 238-246). Red Roof Design.

Frizon de Lamotte, D., Fourdan, B., Leleu, S., Leparmentier, F., & de Clarens, P. (2015). Style of rifting and the stages of Pangea breakup. Tectonics, 34(5), 1009-1029. https://doi.org/10.1002/2014TC003760

Furman, T., & Graham, D. (1999). Erosion of lithospheric mantle beneath the East African Rift system: geochemical evidence from the Kivu volcanic province. In Developments in Geotectonics (Vol. 24, pp. 237-262). Elsevier. https://doi.org/10.1016/S0419-0254(99)80014-7

Furman, T., Nelson, W. R., & Elkins-Tanton, L. T. (2016). Evolution of the East African rift: Drip magmatism, lithospheric thinning and mafic volcanism. Geochimica et Cosmochimica Acta, 185, 418-434. https://doi.org/10.1016/j.gca.2016.03.024

Furman, T., Nelson, W. R., & Elkins-Tanton, L. T. (2016). Evolution of the East African rift: Drip magmatism, lithospheric thinning and mafic volcanism. Geochimica et Cosmochimica Acta, 185, 418-434. https://doi.org/10.1016/j.gca.2016.03.024

Gallacher, R., Keir, D., Harmon, N., Stuart, G., Leroy, S., Hammond, J. O. S., Kendall, J-M., Ayele, A., Goitom, B., Ogubazghi, G., & Ahmed, A. (2016). The initiation of segmented buoyancy-driven melting during continental breakup. Nature Communications, 7, [13110]. https://doi.org/10.1038/ncomms13110

Gasse, F., Fournier, M., Richard, O., & Ruegg, J. C. (1983). Notice explicative: carte géologique de la République de Djibouti à 1/100 000: Djibouti.

Ghiorso, M. S., & Sack, R. O. (1995). Chemical mass transfer in magmatic processes IV. A revised and internally consistent thermodynamic model for the interpolation and extrapolation of liquid-solid equilibria in magmatic systems at elevated temperatures and pressures. Contributions to Mineralogy and Petrology, 119(2), 197-212. https://doi.org/10.1007/BF00307281

Govindaraju, K. (1994). 1994 compilation of working values and sample description for 383 geostandards. Geostandards newsletter, 18, 1-158. https://doi.org/10.1046/j.1365-2494.1998.53202081.x-i1

Green, D. H. (1973). Experimental melting studies on a model upper mantle composition at high pressure under water-saturated and water-undersaturated conditions. Earth and Planetary Science Letters, 19(1), 37-53. https://doi.org/10.1016/0012-821X(73)90176-3

Green, D. H., Hibberson, W. O., Kovács, I., & Rosenthal, A. (2010). Water and its influence on the lithosphere–asthenosphere boundary. Nature, 467(7314), 448-451. https://doi.org/10.1038/nature09369

Griffiths, R. W., & Campbell, I. H. (1991). Interaction of mantle plume heads with the Earth's surface and onset of small-scale convection. Journal of Geophysical Research: Solid Earth, 96(B11), 18295-18310. https://doi.org/10.1029/91JB01897

Hammond, J. O., Kendall, J. M., Stuart, G. W., Keir, D., Ebinger, C., Ayele, A., & Belachew, M. (2011). The nature of the crust beneath the Afar triple junction: Evidence from receiver functions. *Geochemistry, Geophysics, Geosystems*, *12*(12). https://doi.org/10.1029/2011GC003738

Hart, S. R., & Dunn, T. (1993). Experimental cpx/melt partitioning of 24 trace elements. Contributions to Mineralogy and Petrology, 113(1), 1-8. https://doi.org/10.1007/BF00320827

Hayward, N. J., & Ebinger, C. J. (1996). Variations in the along-axis segmentation of the Afar Rift System. *Tectonics*, *15*(2), 244-257. https://doi.org/10.1029/95TC02292

Hofmann, A. W., Jochum, K. P., Seufert, M., & White, W. M. (1986). Nb and Pb in oceanic basalts: new constraints on mantle evolution. Earth and Planetary science letters, 79(1-2), 33-45. https://doi.org/10.1016/0012-821X(86)90038-5

Hofmann, C., Courtillot, V., Feraud, G., Rochette, P., Yirgu, G., Ketefo, E., & Pik, R. (1997). Timing of the Ethiopian flood basalt event and implications for plume birth and global change. Nature, 389(6653), 838-841. https://doi.org/10.1038/39853

Hofmann, C., Courtillot, V., Feraud, G., Rochette, P., Yirgu, G., Ketefo, E., & Pik, R. (1997). Timing of the Ethiopian flood basalt event and implications for plume birth and global change. Nature, 389(6653), 838-841. https://doi.org/10.1038/39853

Irvine, T. N., & Baragar, W. R. A. (1971). A guide to the chemical classification of the common volcanic rocks. Canadian journal of earth sciences, 8(5), 523-548. https://doi.org/10.1139/e71-055

Kalb, J. E. (1995). Fossil elephantoids, Awash paleolake basins, and the Afar triple junction, Ethiopia. Palaeogeography, Palaeoclimatology, Palaeoecology, 114(2-4), 357-368. https://doi.org/10.1016/0031-0182(94)00088-P

Kebede, T., Koeberl, C., & Koller, F. (1999). Geology, geochemistry and petrogenesis of intrusive rocks of the Wallagga area, western Ethiopia. Journal of African Earth Sciences, 29(4), 715-734. https://doi.org/10.1016/S0899-5362(99)00126-8

Keir, D., Hamling, I. J., Ayele, A., Calais, E., Ebinger, C., Wright, T. J., et al. (2009). Evidence for focused magmatic accretion at segment centers from lateral dike injections captured beneath the Red Sea rift in Afar. Geology, 37(1), 59-62. https://doi.org/10.1130/G25147A.1

Kidane, T., Courtillot, V., Manighetti, I., Audin, L., Lahitte, P., Quidelleur, X., et al. (2003). New paleomagnetic and geochronologic results from Ethiopian Afar: Block rotations linked to rift overlap and propagation and determination of a∼ 2 Ma reference pole for stable Africa. *Journal of Geophysical Research: Solid Earth*, *108*(B2). https://doi.org/10.1029/2001JB000645

Kieffer, B., Arndt, N., Lapierre, H., Bastien, F., Bosch, D., Pecher, A., et al. (2004). Flood and shield basalts from Ethiopia: magmas from the African superswell. Journal of Petrology, 45(4), 793-834. https://doi.org/10.1093/petrology/egg112

Klemme, S., & O'Neill, H. S. (2000). The near-solidus transition from garnet lherzolite to spinel lherzolite. Contributions to Mineralogy and Petrology, 138(3), 237-248. https://doi.org/10.1007/s004100050560

Koptev, A., Burov, E., Calais, E., Leroy, S., Gerya, T., Guillou-Frottier, L., & Cloetingh, S. (2016). Contrasted continental rifting via plume-craton interaction: Applications to Central East African Rift. Geoscience Frontiers, 7(2), 221-236. https://doi.org/10.1016/j.gsf.2015.11.002

Krans, S. R., Rooney, T. O., Kappelman, J., Yirgu, G., & Ayalew, D. (2018). From initiation to termination: a petrostratigraphic tour of the Ethiopian Low-Ti Flood Basalt Province. Contributions to Mineralogy and Petrology, 173(5), 1-22. https://doi.org/10.1007/s00410-018-1460-7

Kunz, K., Kreuzer, H., & Müller, P. (1975). Potassium-Argon age determinations of the Trap basalt of the south-eastern part of the Afar Rift. Afar depression of Ethiopia, 1, 370-374.

La Spina, G., Burton, M., Vitturi, M. D. M., & Arzilli, F. (2016). Role of syn-eruptive plagioclase disequilibrium crystallization in basaltic magma ascent dynamics. Nature communications, 7(1), 1-10. https://doi.org/10.1038/ncomms13402

Lahitte, P., Gillot, P. Y., & Courtillot, V. (2003b). Silicic central volcanoes as precursors to rift propagation: the Afar case. Earth and Planetary Science Letters, 207(1-4), 103-116. https://doi.org/10.1016/S0012-821X(02)01130-5

Lahitte, P., Gillot, P. Y., Kidane, T., Courtillot, V., & Bekele, A. (2003a). New age constraints on the timing of volcanism in central Afar, in the presence of propagating rifts. Journal of Geophysical Research: Solid Earth, 108(B2). https://doi.org/10.1029/2001JB001689

Lange, R. A., Frey, H. M., & Hector, J. (2009). A thermodynamic model for the plagioclase-liquid hygrometer/thermometer. American Mineralogist, 94(4), 494-506. https://doi.org/10.2138/am.2009.3011

Lavayssiere, A., Rychert, C., Harmon, N., Keir, D., Hammond, J. O. S., Kendall, J-M., Doubre, C., & Leroy, S. (2018). Imaging lithospheric discontinuities beneath the northern East African Rift using S-to-P receiver functions. Geochemistry, Geophysics, Geosystems, 19(10), 4048-4062. https://doi.org/10.1029/2018GC007463

Le Gall, B., Daoud, M.A., Maury, R., Gasse, F., Rolet, J., Jalludin, M., Caminiti, A.-M., Moussa, N., (2015). Geological Map of the Republic of Djibouti. Centre d'Etude et de Recherche de Djibouti (CERD) and CCGM

Makris, J., & Ginzburg, A. (1987). The Afar Depression: transition between continental rifting and sea-floor spreading. Tectonophysics, 141(1-3), 199-214. https://doi.org/10.1016/0040-1951(87)90186-7

Manighetti, I., Tapponnier, P., Courtillot, V., Gruszow, S., & Gillot, P. Y. (1997). Propagation of rifting along the Arabia-Somalia plate boundary: The gulfs of Aden and Tadjoura. Journal of Geophysical Research: Solid Earth, 102(B2), 2681-2710. https://doi.org/10.1029/96JB01185

Marty, B., Pik, R., & Yirgu, G. (1996). Helium isotopic variations in Ethiopian plume lavas: nature of magmatic sources and limit on lower mantle contribution. Earth and Planetary Science Letters, 144(1-2), 223-237. https://doi.org/10.1016/0012-821X(96)00158-6

McDade, P., Blundy, J. D., & Wood, B. J. (2003). Trace element partitioning on the Tinaquillo Lherzolite solidus at 1.5 GPa. Physics of the Earth and Planetary Interiors, 139(1-2), 129-147. https://doi.org/10.1016/S0031-9201(03)00149-3

McDonough, W. F., & Sun, S. S. (1995). The composition of the Earth. Chemical geology, 120(3-4), 223-253. https://doi.org/10.1016/0009-2541(94)00140-4

McKenzie, D. A. N., & O'nions, R. K. (1991). Partial melt distributions from inversion of rare earth element concentrations. *Journal of Petrology*, *32*(5), 1021-1091. https://doi.org/10.1093/petrology/32.5.1021

Mohr, P. (1983). Ethiopian flood basalt province. *Nature*, *303*(5918), 577-584. https://doi.org/10.1038/303577a0

Niida, K., & Green, D. H. (1999). Stability and chemical composition of pargasitic amphibole in MORB pyrolite under upper mantle conditions. Contributions to Mineralogy and Petrology, 135(1), 18-40. https://doi.org/10.1007/s004100050495

Peccerillo, A., Barberio, M. R., Yirgu, G., Ayalew, D., Barbieri, M., & Wu, T. W. (2003). Relationships between mafic and peralkaline silicic magmatism in continental rift settings: a petrological, geochemical, and isotopic study of the Gedemsa volcano, central Ethiopian rift. Journal of Petrology, 44(11), 2003-2032. https://doi.org/10.1093/petrology/egg068

Peccerillo, A., Donati, C., Santo, A. P., Orlando, A., Yirgu, G., & Ayalew, D. (2007). Petrogenesis of silicic peralkaline rocks in the Ethiopian rift: geochemical evidence and volcanological implications. Journal of African Earth Sciences, 48(2-3), 161-173. https://doi.org/10.1016/j.jafrearsci.2006.06.010

Peccerillo, A., Mandefro, B., Solomon, G., Bedru, H., & Tesfaye, K. (1998). The Precambrian rocks from Southern Ethiopia: petrology, geochemistry and their interaction with the recent volcanism from the Ethiopian Rift Valley. Neues Jahrbuch Für Mineralogie-Abhandlungen, 237-262. https://doi.org/10.1127/njma/173/1998/237

Pfänder, J. A., Jung, S., Münker, C., Stracke, A., & Mezger, K. (2012). A possible high Nb/Ta reservoir in the continental lithospheric mantle and consequences on the global Nb budget–Evidence from continental basalts from Central Germany. Geochimica et Cosmochimica Acta, 77, 232-251. https://doi.org/10.1016/j.gca.2011.11.017

Pik, R., Deniel, C., Coulon, C., Yirgu, G., & Marty, B. (1999). Isotopic and trace element signatures of Ethiopian flood basalts: evidence for plume–lithosphere interactions. Geochimica et Cosmochimica Acta, 63(15), 2263-2279. https://doi.org/10.1016/S0016-7037(99)00141-6

Pik, R., Deniel, C., Coulon, C., Yirgu, G., Hofmann, C., & Ayalew, D. (1998). The northwestern Ethiopian Plateau flood basalts: classification and spatial distribution of magma types. Journal of Volcanology and Geothermal Research, 81(1-2), 91-111. https://doi.org/10.1016/S0377-0273(97)00073-5

Pilet, S., Baker, M. B., & Stolper, E. M. (2008). Metasomatized lithosphere and the origin of alkaline lavas. Science, 320(5878), 916-919. https://doi.org/10.1126/science.1156563

Putirka, K. D. (2008). Thermometers and barometers for volcanic systems. Reviews in mineralogy and geochemistry, 69(1), 61-120. https://doi.org/10.2138/rmg.2008.69.3

Quade, J., Levin, N. E., Simpson, S. W., Butler, R., McIntosh, W. C., Semaw, S., et al. (2008). The geology of Gona, Afar, Ethiopia. Geol. Soc. Am. Bull, 446, 1-31. https://doi.org/10.1130/2008.2446(01)

Rooney, T. O. (2017). The Cenozoic magmatism of East-Africa: Part I—Flood basalts and pulsed magmatism. Lithos, 286, 264-301. https://doi.org/10.1016/j.lithos.2017.05.014

Rooney, T. O. (2020a). The Cenozoic magmatism of East Africa: Part IV–The terminal stages of rifting preserved in the Northern East African Rift System. Lithos, 360, 105381. https://doi.org/10.1016/j.lithos.2020.105381

Rooney, T. O. (2020b). The Cenozoic magmatism of East Africa: part V–magma sources and processes in the East African Rift. Lithos, 360, 105296. https://doi.org/10.1016/j.lithos.2019.105296

Rooney, T. O., Bastow, I. D., Keir, D., Mazzarini, F., Movsesian, E., Grosfils, E. B., et al. (2014). The protracted development of focused magmatic intrusion during continental rifting. Tectonics, 33(6), 875-897. https://doi.org/10.1002/2013TC003514

Rooney, T. O., Hanan, B. B., Graham, D. W., Furman, T., Blichert-Toft, J., & Schilling, J. G. (2012a). Upper mantle pollution during Afar plume–continental rift interaction. Journal of Petrology, 53(2), 365-389. https://doi.org/10.1093/petrology/egr065

Rooney, T. O., Herzberg, C., & Bastow, I. D. (2012b). Elevated mantle temperature beneath East Africa. Geology, 40(1), 27-30. https://doi.org/10.1130/G32382.1

Rooney, T. O., Nelson, W. R., Ayalew, D., Hanan, B., Yirgu, G., & Kappelman, J. (2017). Melting the lithosphere: Metasomes as a source for mantle-derived magmas. Earth and Planetary Science Letters, 461, 105-118. https://doi.org/10.1016/j.epsl.2016.12.010

Rosenthal, A., Foley, S. F., Pearson, D. G., Nowell, G. M., & Tappe, S. (2009). Petrogenesis of strongly alkaline primitive volcanic rocks at the propagating tip of the western branch of the East African Rift. Earth and Planetary Science Letters, 284(1-2), 236-248. https://doi.org/10.1016/j.epsl.2009.04.036

Rossi, M. J., & Gudmundsson, A. (1996). The morphology and formation of flow-lobe tumuli on Icelandic shield volcanoes. Journal of Volcanology and Geothermal Research, 72(3-4), 291-308. https://doi.org/10.1016/0377-0273(96)00014-5

Rudnick, R. & Gao, S. (2003). Composition of the Continental Crust. Treatise Geochem 3:1-64. https://doi.org/10.1016/B0-08-043751-6/03016-4

Salters, V. J., & Longhi, J. (1999). Trace element partitioning during the initial stages of melting beneath mid-ocean ridges. Earth and Planetary Science Letters, 166(1-2), 15-30. https://doi.org/10.1016/S0012-821X(98)00271-4

Santarnecchi, E. (1978). Studio chimico e petrografico dei massicci riolitici intercalati nella parte superiore della serie Stratoide (depressione dell'Afar, Etiopia) (single cycle master's degree unpublished thesis). Location: University of Pisa.

Schmeling, H. (2010). Dynamic models of continental rifting with melt generation. Tectonophysics, 480(1-4), 33-47. https://doi.org/10.1016/j.tecto.2009.09.005

Self, S., Keszthelyi, L., & Thordarson, T. (1998). The importance of pahoehoe. Annual Review of Earth and Planetary Sciences, 26(1), 81-110. https://doi.org/10.1146/annurev.earth.26.1.81

Shaw, D. M. (1970). Trace element fractionation during anatexis. Geochimica et Cosmochimica Acta, 34(2), 237-243. http://dx.doi.org/10.1016/0016-7037(70)90009-8

Sifeta, K., Roser, B. P., & Kimura, J. I. (2005). Geochemistry, provenance, and tectonic setting of Neoproterozoic metavolcanic and metasedimentary units, Werri area, Northern Ethiopia. Journal of African Earth Sciences, 41(3), 212-234. https://doi.org/10.1016/j.jafrearsci.2005.04.004

Späth, A., Le Roex, A. P., & Opiyo-Akech, N. (2001). Plume–lithosphere interaction and the origin of continental rift-related alkaline volcanism—the Chyulu Hills volcanic province, southern Kenya. Journal of Petrology, 42(4), 765-787. https://doi.org/10.1093/petrology/42.4.765

Spencer, K. J., & Lindsley, D. H. (1981). A solution model for coexisting iron–titanium oxides. American mineralogist, 66(11-12), 1189-1201.

Stab, M., Bellahsen, N., Pik, R., Quidelleur, X., Ayalew, D., & Leroy, S. (2016). Modes of rifting in magma-rich settings: Tectono-magmatic evolution of Central Afar. Tectonics, 35(1), 2-38. https://doi.org/10.1002/2015TC003893

Steiner, R. A., Rooney, T. O., Girard, G., Rogers, N., Ebinger, C. J., Peterson, L., & Phillips, R. K. (2022). Initial Cenozoic magmatic activity in East Africa: new geochemical constraints on magma distribution within the Eocene continental flood basalt province. Geological Society, London, Special Publications, 518(1), 435-465. https://doi.org/10.1144/SP518-2020-262

Sun, S. S., & McDonough, W. F. (1989). Chemical and isotopic systematics of oceanic basalts: implications for mantle composition and processes. Geological Society, London, Special Publications, 42(1), 313-345. https://doi.org/10.1144/GSL.SP.1989.042.01.19

Tadesse, G., & Allen, A. (2005). Geology and geochemistry of the Neoproterozoic Tuludimtu Ophiolite suite, western Ethiopia. Journal of African Earth Sciences, 41(3), 192-211. https://doi.org/10.1016/j.jafrearsci.2005.04.001

Tesfaye, S., Harding, D. J., & Kusky, T. M. (2003). Early continental breakup boundary and migration of the Afar triple junction, Ethiopia. Geological Society of America Bulletin, 115(9), 1053-1067. https://doi.org/10.1130/B25149.1

Turcotte, D. L., & Emerman, S. H. (1983). Mechanisms of active and passive rifting. In Developments in geotectonics (Vol. 19, pp. 39-50). Elsevier. https://doi.org/10.1016/B978-0-444-42198-2.50010-9

Van Westrenen, W., Blundy, J. D., & Wood, B. J. (2001). High field strength element/rare earth element fractionation during partial melting in the presence of garnet: Implications for identification of mantle heterogeneities. Geochemistry, Geophysics, Geosystems, 2(7). https://doi.org/10.1029/2000GC000133

Varet, J. (1978). Geology of central and southern Afar (Ethiopia and Djibouti Republic) (map and 124 pp. report). Centre Natl. de la Rec. Sci., Paris.

Varet, J. (2018). Geology of Afar (East Africa). Springer. https://doi.org/10.1007/978-3-319-60865-5

Walker, G. P. (1991). Structure, and origin by injection of lava under surface crust, of tumuli,"lava rises","lava-rise pits", and "lava-inflation clefts" in Hawaii. Bulletin of Volcanology, 53(7), 546-558. https://doi.org/10.1007/BF00298155

Wang, T., Gao, S. S., Yang, Q., & Liu, K. H. (2021). Crustal structure beneath the Ethiopian Plateau and adjacent areas from receiver functions: Implications for partial melting and magmatic underplating. Tectonophysics, 809, 228857. https://doi.org/10.1016/j.tecto.2021.228857

Wolfenden, E., Ebinger, C., Yirgu, G., Renne, P. R., & Kelley, S. P. (2005). Evolution of a volcanic rifted margin: Southern Red Sea, Ethiopia. Geological Society of America Bulletin, 117(7-8), 846-864. https://doi.org/10.1130/B25516.1

Wolfenden, E., Ebinger, C., Yirgu, G., Renne, P. R., & Kelley, S. P. (2005). Evolution of a volcanic rifted margin: Southern Red Sea, Ethiopia. Geological Society of America Bulletin, 117(7-8), 846-864. https://doi.org/10.1130/B25516.1

Wynn, J. G., Roman, D. C., Alemseged, Z., Reed, D., Geraads, D., & Munro, S. (2008). Stratigraphy, depositional environments, and basin structure of the Hadar and Busidima Formations at Dikika, Ethiopia. Geological Society of America Special paper, 446, 87-118. https://doi.org/10.1130/2008.2446(04)

Yihunie, T., Adachi, M., & Yamamoto, K. (2006). Geochemistry of the Neoproterozoic metabasic rocks from the Negele area, southern Ethiopia: tectonomagmatic implications. Journal of African Earth Sciences, 44(3), 255-269. https://doi.org/10.1016/j.jafrearsci.2005.12.004

Zumbo, V., Féraud, G., Bertrand, H., & Chazot, G. (1995). 40Ar39Ar chronology of Tertiary magmatic activity in southern Yemen during the early Red Sea-Aden rifting. Journal of volcanology and geothermal research, 65(3-4), 265-279. https://doi.org/10.1016/0377-0273(94)00106-Q

Caption

Figure 1. (a) Topographic map of the East African Rift System with plate boundary, name and spreading vector with respect to Nubia fixed plate. The black box encloses the Afar depression represented in picture (b). (b) Geological map of the Afar depression modified from Varet (1978), Kidane et al. (2003) and Stab et al. (2016). Lava samples are from the 2020 campaign (white circles) and the Afar repository of the University of Pisa (orange circles). The dashed box represents the approximate location of the Woranso-Mille region. Dotted line indicates the Tendaho Goba Ad Discontinuity (T.G.D.). Datum WGS1984, background Multi-Directional Hillshade.

Figure 2. Field photographs of the three Series. (a) Lower Stratoid Series massive blocky-jointed lava flows. (b) Upper Stratoid Series typical blocky-jointed flows escarpment. (c) Closer look of the top flow of panel (b). (d) CAG Series lava flows alternating vesiculated and massive portions, less voluminous with respect to the Stratoid Series.

Figure 3. Transmitted light petrographic (PPL and XPL) and SEM images (from top to the bottom) of the three Series respectively. (a) Lower Stratoid Series sieved and resorbed plagioclase in hyalopilitic groundmass. Note that the SEM image is not from the same sample of the petrographic images. (b) Upper Stratoid Series sample with phenocryst and micro-phenocryst in intergranular groundmass. (c) CAG Series porphyritic lava. Pl, plagioclase; Cpx, clinopyroxene; Ol olivine; Fe-Ti ox, Fe-Ti oxides.

Figure 4. (a) Feldspar (An-Ab-Or), (b) olivine (Fo-Fa-Tep) and (c) clinopyroxene (En-Fs-Hd-Di) classification diagrams of the three Series: Lower Stratoid Series (green), Upper Stratoid Series (red) and CAG Series (blue). Different symbols identify phenocrysts core (full symbols), rim (empty symbols) and groundmass (crosses).

Figure 5. (a-f) Major and compatible trace elements binary diagrams of Stratoid, CAG and Axial Series. Data of silicic central volcanoes intercalated in the upper part of the Upper Stratoid Series are from Santarnecchi (1978) and reported in Table S3. LT and HT1 fields are from Kieffer et al. (2004); Pik et al. (1998).(g) Classification diagram Nb/Y vs. Ti/Y from Pik et al., 1998 (LT, low-Ti type; HT1, high-Ti1 type; HT2, high-Ti2 type) for mafic rock (MgO > 4 wt%) of Stratoid, CAG and Axial Series. (h) Nb/Ta vs. Zr/Hf diagram for mafic rock (MgO > 4 wt%) of Stratoid Series, CAG Series and Axial Series. Fields for MORBs, OIBs and intracontinental basalts are from Pfänder et al. (2012). CC is continental crust (Rudnick and Gao, 2003), and BSE is the Bulk Silicate Earth. Stratoid Series literature data of Central and Southern Afar (solid line) are from Barberi and Santacroce (1980); Deniel et al. (1994); Feyissa et al. (2019). Axial literature data of Manda Hararo and Manda Inakir (dashed line) are from Barrat et al. (2003); Deniel et al. (1994); Feyissa et al. (2019).

Figure 6. Chondrite-normalised REE patterns and primitive mantle-normalised trace element spider diagrams of Lower and Upper Stratoid Series and CAG Series. Grey lines are from Feyissa et al. (2019) and the distinction between Upper and Lower Stratoid Series has been made based on their location and the

map of Kidane et al. (2003). Magma types III, IV and VI of Rooney (2020b) are shown for comparison. Normalising values after McDonough and Sun (1995).

Figure 7. (a) Nb/U vs. Rb/Nb indicating a minor role of crustal contamination on magma evolution for Stratoid, CAG and Axial Series. The MORB and OIB field (Nb/U 37-57) is from Hofmann et al. (1986). The Southern Ethiopian Precambrian basement (Rb/Nb >1) is from Peccerillo et al. (1998). UCC and LCC are respectively the upper continental crust and the lower continental crust (Rudnick and Gao, 2003). (b) Zr/Nb vs. La_N/Sm_N show variation in the degree of enrichment of lavas from the Stratoid, CAG and Axial Series mafic rock (MgO > 4 wt%). OIB, N-MORB and E-MORB values from Sun and McDonough (1989). Normalising values after McDonough and Sun (1995). (c) K/Th vs. Th for Stratoid, CAG and Axial Series mafic rock (MgO > 4 wt%) in order to distinguish between a spinel lherzolite and spinel-amphibole lherzolite source. Partial melting of primitive mantle (McDonough and Sun, 1995) is calculated using the non-modal batch melting model of Shaw (1970), the partition coefficients from McKenzie and O'Nions (1991), and the following amphibole-garnet and -spinel lherzolites source mineral modes: garnet lherzolite: 0.58 Ol, 0.15 Opx, 0.20 Cpx, 0.02 Gt, 0.05 amp that melts in the proportion 0.10 Ol, 0.20 Opx, 0.40 Cpx, 0.10 Gt, 0.20 amp; spinel lherzolite: 0.58 Ol, 0.15 Opx, 0.20 Cpx, 0.02 sp., 0.05 amp that melts in the proportion 0.10 Ol, 0.20 Opx, 0.40 Cpx, 0.10 sp., 0.20 amp. Solid lines show the variation of the degree of partial melting from 1% to 20%. Literature data are from Feyissa et al. (2019) and the distinction between Upper and Lower Stratoid Series has been made based on their location and the map of Kidane et al. (2003). (d-e) Tb_N/Yb_N vs. La_N/Sm_N mafic rock (MgO > 4 wt%) show variation in the depth of the melting column and in the degree of partial melting between the Series. (e) Enlargement of panel (d). Solid lines show the variation of the degree of partial melting from 1% to 15% while dashed lines identify the mixing trend from 100% amphibole-garnet lherzolite to 100% amphibole-spinel lherzolite. Primitive mantle, melting model, partition coefficient, mineral modes and literature data are the same as panel (c). Normalising values after McDonough and Sun (1995). (f) Th/Nb vs. Th/Zr diagram shows the distinction between the CAG Series and the Lower and Upper Stratoid Series mafic rock (MgO > 4 wt%) due to the Th being slightly more incompatible than Zr and Nb during partial melting (McKenzie and O'Nions, 1991). One of the Lower Stratoid Series low Ti-Fe samples is out of the graph range (AF20-62a, Th/Zr 0.05 and Th/Nb 0.47). Literature data as in panel (c).

Figure 8. Schematic cartoon depicting the partial melting of the three mantle reservoirs (Afar plume, depleted mantle, and amphibole-bearing SCLM) during rifting evolution in Afar last 4.5 Ma. (a) The Pliocene rift produced the Lower Stratoid Series from a shallow melting column associated with a thinned lithosphere. (b) The jump of the rift relocates the Pleistocene rift north-east in Central Afar and led to the formation of the Upper Stratoid Series from a deeper melting column associated with a thicker, less stretched lithosphere. (c) The focalization of the Pleistocene rift led to a shallow melting column and a thinned lithosphere for the CAG Series mantle source. The sketch is not to scale, and the partial melting area is approximative. Spl, spinel; gt, garnet. See text for more details.

Table 1. Summary table of the main petrographic and chemical characteristics of the Lower Stratoid, Upper Stratoid and CAG Series. The complete datasets are presented in Table S1 and Table S3.

Note. *Due to Pb being below the detection limit, Ce/Pb values are the means of 5 Lower Stratoid samples, 6 Upper Stratoid samples and 3 CAG samples.

Table S1. Petrographic and mineralogical analysis of the studied Lower Stratoids, Upper Stratoids and CAG Series samples. Pl, plagioclase; Cpx, clinopyroxene; Ol olivine; Ilm, ilmenite; Mag, magnetite; Ap, apatite; opq, opaque minerals.
Note. Number in brackets refer to samples AF20-12. Sulfide accessories have been observed in samples AF20-04 and AF20-19.

			Phenocrysts abundance	**Phenocrysts**			**Micro-Phenocrysts**			**Accessories**			**Groundmass**	
Texture	Sample	Mg# range	Vol%	Pl	Cpx	Ol	Pl	Cpx	Ol	Ilm	Mag	Ap	Mineral	Texture
	Lower Stratoids													
Aphiric microcrystalline	AF20-3 - AF20-79 - AF20-80	35-37	<2%	-	-	-	-	-	-	x	x	x	pl, cpx, ol, opq	intergranular - intersertal
Porphyritic	AF20-61 - H436 - H449	42-48	2-10%	1-4 mm	-	-	x	-	x	-	x	-	pl, cpx, ol, opq	intergranular - hyalopilitic
Micro-Porphyritic	H323 - H332 - AF20-60a,b -AF20-62a,	34-48	<2%	-	-	-	x	x	-	-	x	-	pl, cpx, opq	intergranular - hyalopilitic
	Upper Stratoids													
Aphiric-microcrystalline	AF20-57 - AF20-6 - AF20-7 - AF20-9 - A	31-46	<2%	-	-	-	-	-	-	x	x	x	pl, cpx, ol, opq	intergranular/intersertal
Porphyritic	AF20-16 - AF20-19 - AF20-4 - AF20-54	37-48	2-10% (35%)	1-2 mm (8 mm)	-	- (1-2 mm)	x	x	x	x	x	-	pl, cpx, ol, opq	intergranular
Porphyritic (felsic)	AF20-14a,b,c - AF20-69a,b	19-29	15-30%	1-3 mm	0.5-1 mm	0.5 mm	-	-	-	-	x	x	pl, opq	intergranular - intersertal
Micro-Porphyritic	AF20-56 - AF20-59 - AF20-20 - Z137 -	39-42	<2%	-	-	-	x	x	x	x	x	-	pl, cpx, ol, opq	intergranular - intersertal
Aphyric coarse-grained	AF20-15 (dyke)	35	-	-	-	-	-	-	-	-	x	-	pl, ol, opq	intersertal
	CAG													
Aphiric	AF20-64 - AF20-65	38	<2%	-	-	-	-	-	-	x	x	-	pl, cpx, ol, opq	intergranular
Porphyritic	AF20-22 - AF20-29 - AF20-25 - AF20-4	40-52	2-20%	2-7 mm	0.5-1 mm	0.5-1.5 mm	x	x	x	x	x	-	pl, cpx, ol, opq	intergranular - intersertal
Micro-Porphyritic	AF20-23 - H307	43	<2%	-	-	-	x	-	x	x	x	-	pl, cpx, ol, opq	intergranular - intersertal
Ophitic	H216	55	-	1-2 mm	1-2 mm	0.5-1.5 mm	-	-	-	x	x	-	pl, cpx, ol, opq	-

Table S2. Electron Probe Microanalysis. Point and profile analysis.
Note. Fe-Ti oxides end-members following Spencer and Lindsley (1981). Microanalysis were performed using the Electron Probe MicroAnalyzer (EPMA) JEOL JXA8230 device of the joined CNR-IGG-DST laboratory at the Department of Earth Sciences of Florence.

Sample	Crystal	Type	Size	Zone	SiO_2 (wt%)	TiO_2	Al_2O_3	Fe_2O_3	MgO	CaO	Na_2O	K_2O	SrO	BaO	sum	Ab	An	Or
Lower Stratoids																		
H436		Phenocryst		Core	47.64	0.08	32.85	0.58	0.15	15.94	2.19	0.06	0.02	0.05	99.57	19.85	79.68	0.37
H436		Phenocryst		Intermediate	49.15	0.07	31.11	0.79	0.16	14.79	2.99	0.11	0.13	0.05	99.34	26.59	72.71	0.61
H436		Phenocryst		Rim	53.85	0.14	28.14	0.87	0.12	11.12	5.07	0.29	0.09	0.06	99.74	44.40	53.85	1.64
H436		Groundmass			52.42	0.10	28.84	0.79	0.12	12.14	4.37	0.24	0.08	0.08	99.17	38.83	59.61	1.42
H436		Groundmass			52.07	0.16	29.08	0.96	0.09	12.24	4.33	0.22	0.06	0.05	99.26	38.48	60.15	1.28
H436		Groundmass			52.34	0.13	28.90	0.82	0.14	12.23	4.34	0.21	0.08	0.05	99.23	38.60	60.08	1.24
H436		Phenocryst		Core	47.38	0.06	32.04	0.74	0.15	15.87	2.24	0.07	0.08	0.05	98.67	20.21	79.28	0.42
H436		Phenocryst		Rim	52.64	0.13	28.90	0.84	0.10	12.22	4.39	0.24	0.07	0.07	99.59	38.77	59.69	1.42
H436		Phenocryst		Core	48.09	0.08	31.83	0.59	0.17	15.50	2.46	0.06	0.05	0.05	98.89	22.21	77.32	0.37
H436		Phenocryst		Rim	53.58	0.12	28.11	0.71	0.12	11.34	4.83	0.26	0.07	0.07	99.21	42.80	55.58	1.50
H436		Micro-Phenocryst		Core	48.28	0.09	31.74	0.79	0.12	15.06	2.57	0.11	0.02	0.04	98.81	23.41	75.88	0.64
H436		Micro-Phenocryst		Rim	53.56	0.15	28.22	0.88	0.12	11.01	4.82	0.31	0.08	0.06	99.20	43.36	54.73	1.80
H436		Groundmass			52.61	0.13	29.02	0.80	0.10	11.82	4.52	0.24	0.04	0.04	99.32	40.27	58.27	1.39
H436		Phenocryst		Core	48.62	0.08	31.91	0.66	0.16	15.17	2.61	0.10	0.06	0.06	99.42	23.55	75.75	0.59
H436		Phenocryst		Rim	52.81	0.13	29.15	0.81	0.13	12.07	4.41	0.24	0.06	0.08	99.87	39.18	59.26	1.42
H436		Micro-Phenocryst		Core	53.48	0.16	27.97	0.92	0.18	11.18	4.98	0.25	0.06	0.05	99.23	43.95	54.49	1.47
H436		Micro-Phenocryst		Rim	53.67	0.11	28.08	0.75	0.10	10.82	5.13	0.31	0.08	0.08	99.13	45.31	52.77	1.79
H436		Groundmass			52.80	0.13	28.95	0.76	0.13	11.95	4.55	0.23	0.09	0.06	99.64	40.20	58.36	1.34
H436		Phenocryst		Core	48.58	0.08	32.66	0.73	0.14	15.76	2.19	0.07	0.03	0.01	100.26	20.03	79.50	0.44
H436		Phenocryst		Core	49.16	0.04	32.18	0.60	0.19	15.24	2.55	0.08	0.08	0.04	100.14	23.09	76.38	0.47
H436		Phenocryst		Rim	53.93	0.12	28.60	0.71	0.13	11.15	4.73	0.28	0.05	0.07	99.77	42.63	55.58	1.67
H436		Micro-Phenocryst		Core	49.86	0.10	31.34	0.82	0.14	14.34	2.85	0.14	0.06	0.05	99.68	26.18	72.90	0.84
H436		Micro-Phenocryst		Rim	53.10	0.11	29.26	0.70	0.13	11.84	4.40	0.24	0.07	0.05	99.90	39.61	58.88	1.42
H436		Micro-Phenocryst		Core	48.15	0.09	32.57	0.67	0.12	15.86	2.16	0.08	0.03	0.06	99.79	19.65	79.74	0.50
H436		Micro-Phenocryst		Rim	57.18	0.11	26.52	0.57	0.07	8.86	5.97	0.46	0.09	0.09	99.92	53.37	43.76	2.72
H436		Micro-Phenocryst		Core	49.85	0.08	31.39	0.78	0.16	14.74	2.87	0.11	0.11	0.09	100.18	25.87	73.34	0.62
H436		Micro-Phenocryst		Intermediate	53.23	0.13	29.05	0.77	0.17	12.25	4.41	0.22	0.09	0.08	100.40	38.88	59.70	1.29
H436		Micro-Phenocryst		Rim	54.25	0.14	28.55	0.71	0.11	11.39	4.91	0.25	0.05	0.05	100.41	43.13	55.31	1.46
H436		Groundmass		Core	55.73	0.12	27.82	0.79	0.10	10.19	5.47	0.34	0.03	0.08	100.66	48.21	49.69	1.95
H436		Groundmass		Rim	53.72	0.11	28.95	0.86	0.10	11.66	4.73	0.27	0.02	0.04	100.45	41.62	56.75	1.56
H436		Groundmass			52.78	0.12	29.44	0.92	0.19	12.43	4.17	0.19	0.06	0.06	100.35	37.29	61.46	1.14
H436		Phenocryst		Core	49.06	0.07	32.13	0.84	0.14	15.23	2.71	0.09	0.10	0.06	100.43	24.23	75.13	0.53
H436		Phenocryst		Intermediate	49.50	0.10	31.91	0.89	0.16	14.96	2.75	0.11	0.01	0.01	100.40	24.80	74.52	0.66
H436		Phenocryst		Intermediate	49.10	0.08	32.00	1.03	0.13	15.16	2.67	0.11	0.13	0.08	100.48	24.00	75.22	0.64
H436		Phenocryst		Intermediate	49.63	0.08	31.70	0.89	0.12	14.92	2.86	0.11	0.00	0.03	100.35	25.59	73.70	0.65
H436		Phenocryst		Intermediate	49.57	0.08	31.62	0.79	0.15	14.93	2.83	0.10	0.04	0.05	100.15	25.38	73.94	0.60
H436		Phenocryst		Intermediate	49.27	0.11	31.97	0.86	0.13	15.34	2.69	0.08	0.03	0.08	100.56	23.94	75.43	0.48
H436		Phenocryst		Intermediate	50.15	0.08	31.45	0.81	0.14	14.76	3.04	0.10	0.07	0.09	100.69	26.96	72.31	0.57
H436		Phenocryst		Intermediate	50.40	0.09	31.15	0.80	0.16	14.38	3.10	0.13	0.07	0.06	100.34	27.84	71.29	0.76
H436		Phenocryst		Intermediate	49.26	0.08	31.70	0.74	0.12	14.94	2.76	0.10	0.04	0.06	99.80	24.87	74.43	0.59
H436		Phenocryst		Intermediate	49.33	0.07	31.98	0.76	0.14	15.17	2.74	0.10	0.13	0.03	100.44	24.48	74.89	0.57
H436		Phenocryst		Intermediate	49.28	0.08	31.88	0.75	0.15	15.24	2.73	0.09	0.07	0.05	100.30	24.33	75.09	0.50
H436		Phenocryst		Intermediate	49.45	0.09	31.80	0.72	0.15	15.11	2.74	0.09	0.08	0.03	100.23	24.57	74.84	0.53
H436		Phenocryst		Intermediate	50.38	0.11	30.77	0.77	0.15	14.20	3.21	0.11	0.08	0.09	99.87	28.77	70.41	0.66
H436		Phenocryst		Intermediate	49.66	0.10	31.50	0.82	0.16	14.75	2.86	0.10	0.04	0.05	100.04	25.79	73.53	0.59
H436		Phenocryst		Intermediate	48.68	0.09	32.19	0.80	0.16	15.45	2.52	0.09	0.02	0.07	100.06	22.63	76.74	0.51
H436		Phenocryst		Intermediate	49.22	0.07	31.82	0.77	0.15	15.18	2.69	0.09	0.09	0.03	100.11	24.13	75.31	0.51
H436		Phenocryst		Intermediate	48.84	0.09	32.10	0.88	0.15	15.34	2.57	0.09	0.12	0.05	100.21	23.15	76.25	0.52
H436		Phenocryst		Intermediate	50.85	0.09	30.95	0.74	0.16	14.27	3.23	0.12	0.06	0.06	100.53	28.81	70.38	0.71
H436		Phenocryst		Intermediate	50.55	0.06	30.97	0.77	0.15	14.34	3.18	0.12	0.03	0.07	100.24	28.37	70.80	0.71
H436		Phenocryst		Intermediate	50.17	0.07	31.18	0.75	0.15	14.60	2.98	0.10	0.01	0.07	100.07	26.75	72.52	0.61

H436		Phenocryst		Intermediate	55.40	0.16	27.87	0.77	0.10	10.48	5.37	0.34	0.08	0.08	100.65	47.13	50.77	1.96
H436		Phenocryst		Intermediate	53.14	0.16	29.14	1.08	0.07	12.08	4.48	0.26	0.01	0.08	100.49	39.52	58.83	1.51
H436		Phenocryst		Intermediate	62.32	0.24	21.75	0.74	0.06	5.04	6.21	2.07	0.10	0.11	98.63	59.83	26.83	13.13
H436		Phenocryst		Rim	53.19	0.13	29.12	0.88	0.12	12.36	4.29	0.23	0.07	0.08	100.45	38.00	60.52	1.35
Upper Stratoids																		
AF20-04	1	Groundmass	<100µ	Core	55.46	0.16	27.73	0.95	0.11	10.61	5.22	0.36	-	-	100.60	46.15	51.78	2.07
AF20-04	2	Groundmass	<250µ	Core	54.86	0.11	28.51	0.75	0.20	11.20	4.97	0.28	-	-	100.87	43.81	54.58	1.61
AF20-04	4	Groundmass	<250µ	Core	54.56	0.15	28.24	0.80	0.15	11.24	4.90	0.30	-	-	100.32	43.36	54.91	1.73
AF20-04	5	Groundmass	<250µ	Core	54.36	0.13	28.24	0.76	0.15	11.34	4.79	0.30	-	-	100.07	42.56	55.71	1.74
AF20-04	6	Groundmass	<250µ	Core	57.31	0.09	26.27	0.93	0.08	8.99	6.15	0.50	-	-	100.33	53.70	43.42	2.87
AF20-04	8	Groundmass	<250µ	Core	54.53	0.14	28.10	0.82	0.13	11.26	5.09	0.33	-	-	100.39	44.15	53.97	1.87
AF20-04	9	Phenocryst	<2000µ	Core	47.71	0.06	33.20	0.76	0.09	16.74	1.79	0.05	-	-	100.39	16.15	83.56	0.29
AF20-04	9	Phenocryst	<2000µ	Intermediate	47.30	0.06	33.25	0.60	0.15	16.81	1.90	0.05	-	-	100.12	16.90	82.79	0.32
AF20-04	9	Phenocryst	<2000µ	Rim	54.26	0.12	28.56	0.78	0.14	11.45	4.96	0.26	-	-	100.53	43.25	55.24	1.51
AF20-04	10	Groundmass	<250µ	Core	56.20	0.17	27.41	1.02	0.06	10.11	5.63	0.37	-	-	100.97	49.15	48.73	2.12
AF20-04	11	Groundmass	<250µ	Core	54.39	0.12	28.65	0.69	0.13	11.61	4.81	0.26	-	-	100.66	42.21	56.29	1.51
AF20-04	12	Micro-Phenocryst		Core	48.23	0.07	32.93	0.60	0.19	16.40	2.03	0.05	-	-	100.49	18.25	81.47	0.28
AF20-04	12	Micro-Phenocryst		Rim	47.13	0.06	33.60	0.65	0.15	16.99	1.79	0.03	-	-	100.41	15.99	83.82	0.19
AF20-04	13	Groundmass		Core	55.49	0.13	27.42	0.77	0.11	10.43	5.38	0.34	-	-	100.06	47.33	50.71	1.96
AF20-04	14	Groundmass	<250µ	Core	56.50	0.13	27.13	0.74	0.08	9.94	5.60	0.37	-	-	100.48	49.40	48.48	2.13
AF20-04	15	Groundmass	<250µ	Core	53.68	0.10	29.01	0.77	0.11	12.06	4.66	0.27	-	-	100.66	40.50	57.95	1.55
AF20-04	18	Groundmass	<250µ	Core	55.59	0.12	27.96	0.67	0.12	10.79	5.31	0.33	-	-	100.89	46.22	51.92	1.86
AF20-04	20	Groundmass	<100µ	Core	54.88	0.13	27.63	0.96	0.10	10.91	5.30	0.32	0.12	0.06	100.41	45.88	52.17	1.85
AF20-04	21	Groundmass	<250µ	Core	54.51	0.13	28.04	0.85	0.10	11.33	4.86	0.31	0.08	0.03	100.22	42.91	55.24	1.79
AF20-04	22	Groundmass	<100µ	Core	55.52	0.13	27.20	0.81	0.13	10.42	5.32	0.34	0.07	0.07	99.99	47.02	50.89	1.97
AF20-04	23	Phenocryst	<1000µ	Core	47.84	0.08	32.82	0.64	0.16	16.70	1.99	0.06	0.06	0.05	100.41	17.68	81.87	0.35
AF20-04	23	Phenocryst	<1000µ	Rim	54.44	0.14	28.58	0.65	0.13	11.63	4.83	0.27	0.12	0.08	100.87	42.18	56.13	1.55
AF20-04	24	Micro-Phenocryst	~500µ	Core	48.88	0.06	32.30	0.66	0.18	16.07	2.41	0.06	0.10	0.04	100.74	21.24	78.34	0.35
AF20-04	24	Micro-Phenocryst	~500µ	Rim	55.81	0.13	26.83	0.98	0.15	9.95	5.48	0.41	0.11	0.05	99.89	48.67	48.87	2.38
AF20-04	24	Micro-Phenocryst	~500µ	Core	47.26	0.06	32.60	0.80	0.15	16.50	1.88	0.08	0.01	0.04	99.37	17.00	82.47	0.46
AF20-04	24	Micro-Phenocryst	~500µ	Rim	54.58	0.18	28.41	0.78	0.12	11.52	4.81	0.28	0.13	0.06	100.88	42.30	55.97	1.62
AF20-04	36	Groundmass	<250µ	Core	54.03	0.12	28.50	0.80	0.11	11.87	4.70	0.27	0.11	0.06	100.56	41.03	57.32	1.54
AF20-04	42	Groundmass		Core	53.75	0.13	28.79	0.81	0.08	11.98	4.49	0.27	0.08	0.05	100.43	39.74	58.63	1.54
AF20-04	42	Groundmass		Rim	61.22	0.14	23.68	0.66	0.03	5.88	7.44	1.00	0.13	0.17	100.35	65.37	28.56	5.75
AF20-04	37	Groundmass	<250µ	Core	55.88	0.14	27.28	0.85	0.10	10.32	5.48	0.37	0.06	0.08	100.56	47.90	49.83	2.12
AF20-04	38	Groundmass	<250µ	Core	53.94	0.14	28.32	0.88	0.11	11.70	4.55	0.28	0.06	0.07	100.06	40.54	57.68	1.65
AF20-04	39	Groundmass	<100µ		58.44	0.09	25.25	0.84	0.09	7.89	6.54	0.61	0.15	0.08	99.97	57.78	38.51	3.56
AF20-04	40	Groundmass	<100µ		60.62	0.13	23.74	0.73	0.03	6.14	7.42	0.84	0.14	0.14	99.93	65.11	29.81	4.83
AF20-04	41	Groundmass	<100µ	Core	52.86	0.13	28.67	0.83	0.13	12.06	4.37	0.24	0.12	0.06	99.46	38.99	59.53	1.38
AF20-04	25	Groundmass	<250µ	Core	54.12	0.15	28.01	0.97	0.10	11.54	4.66	0.30	0.09	0.08	100.02	41.40	56.69	1.76
AF20-04	26	Phenocryst	<2000µ	Core	46.65	0.06	32.67	0.59	0.14	16.91	1.68	0.04	0.13	0.04	98.89	15.16	84.51	0.26
AF20-04	26	Phenocryst	<2000µ	Core	47.38	0.06	32.68	0.54	0.15	16.82	1.77	0.05	0.09	0.05	99.58	15.92	83.69	0.30
AF20-04	26	Phenocryst	<2000µ	Rim	53.85	0.13	27.91	0.82	0.06	11.28	4.82	0.30	0.08	0.07	99.32	42.79	55.33	1.75
AF20-04	26	Phenocryst	<2000µ	Rim	53.50	0.12	28.48	0.98	0.06	11.82	4.58	0.27	0.07	0.09	99.96	40.49	57.80	1.56
AF20-04	27	Phenocryst	<1000µ	Core	49.26	0.08	31.29	0.60	0.22	15.36	2.73	0.10	0.12	0.07	99.83	24.18	75.14	0.55
AF20-04	27	Phenocryst	<1000µ	Rim	53.95	0.12	27.71	0.65	0.14	11.20	4.84	0.26	0.10	0.04	99.01	43.18	55.21	1.55
AF20-04	28	Groundmass	<250µ	Core	56.76	0.12	25.90	0.80	0.08	9.22	6.00	0.46	0.13	0.06	99.55	52.58	44.66	2.65
AF20-04	29	Micro-Phenocryst	<500µ	Core	54.21	0.15	27.62	0.82	0.11	11.01	4.98	0.29	0.11	0.09	99.40	44.15	53.98	1.72
AF20-04	30	Groundmass	<250µ	Core	53.43	0.15	28.24	0.85	0.10	12.03	4.59	0.27	0.06	0.05	99.76	40.17	58.19	1.56
AF20-04	33	Phenocryst	<1000µ	Core	47.26	0.05	31.99	0.58	0.15	16.46	2.07	0.07	0.03	0.06	98.72	18.43	81.08	0.38
AF20-04	34	Micro-Phenocryst	<500µ	Rim	54.45	0.13	27.28	0.70	0.12	10.91	5.22	0.31	0.09	0.07	99.27	45.51	52.59	1.77
AF20-04	34	Groundmass	<500µ	Core	53.68	0.11	27.89	0.86	0.09	11.36	4.72	0.28	0.07	0.06	99.12	42.18	56.08	1.64
AF20-04	34	Groundmass	<500µ	Rim	60.49	0.10	23.46	0.80	0.04	5.95	7.31	0.99	0.16	0.19	99.51	64.76	29.11	5.78
AF20-04	35	Phenocryst	<2000µ	Core	48.08	0.06	31.61	0.61	0.16	15.69	2.30	0.06	0.12	0.05	98.74	20.86	78.66	0.38
AF20-04	35	Phenocryst	<2000µ	Rim	46.65	0.04	32.90	0.66	0.12	17.10	1.61	0.05	0.06	0.03	99.22	14.51	85.14	0.30
AF20-04	35	Phenocryst	<2000µ	Intermediate	52.58	0.11	28.71	0.76	0.15	12.57	4.25	0.23	0.06	0.08	99.49	37.42	61.14	1.30

AF20-04	43	Groundmass		Core	54.28	0.15	27.82	0.85	0.10	11.04	4.79	0.30	0.10	0.06	99.49	43.12	55.00	1.77
AF20-04	44	Groundmass		Core	54.03	0.14	27.84	0.86	0.15	11.32	4.66	0.30	0.03	0.06	99.40	41.91	56.21	1.76
AF20-04	45	Groundmass		Core	53.40	0.14	27.74	0.67	0.13	11.68	4.67	0.26	0.12	0.04	98.85	41.33	57.10	1.50
AF20-04	31	Groundmass	<100µ	Core	54.18	0.14	27.70	0.73	0.11	11.18	4.79	0.31	0.05	0.07	99.26	42.81	55.24	1.82
AF20-04	32	Groundmass	<100µ	Core	56.97	0.12	26.03	0.74	0.08	9.08	5.93	0.46	0.09	0.08	99.57	52.62	44.57	2.67
AF20-04	47	Groundmass	<250µ	Rim	64.24	0.09	21.63	0.95	0.04	3.88	8.07	1.54	0.13	0.27	100.84	71.56	18.98	8.97
AF20-04	48	Groundmass	<250µ	Core	54.89	0.14	28.16	0.93	0.10	10.97	5.15	0.33	0.07	0.07	100.80	45.01	52.95	1.92
AF20-04	49	Groundmass	<250µ		54.46	0.15	28.39	1.14	0.11	11.40	4.85	0.31	0.09	0.05	100.96	42.70	55.43	1.77
AF20-04	50	Groundmass	<100µ	Core	54.12	0.14	28.63	0.79	0.12	11.35	4.90	0.28	0.10	0.08	100.51	43.05	55.17	1.64
AF20-04	51	Groundmass	<250µ	Core	54.13	0.15	28.24	0.81	0.11	11.50	5.11	0.30	0.12	0.05	100.52	43.80	54.43	1.69
AF20-04	52	Groundmass	<250µ	Rim	56.76	0.14	26.73	0.80	0.10	9.52	5.90	0.46	0.12	0.09	100.62	51.38	45.83	2.62
AF20-04	52	Groundmass	<250µ	Core	56.87	0.10	26.53	0.72	0.09	9.19	6.02	0.50	0.12	0.08	100.22	52.64	44.37	2.85
AF20-04	53	Micro-Phenocryst	<500µ	Core	59.36	0.10	25.00	0.76	0.05	7.45	6.91	0.67	0.11	0.09	100.49	60.14	35.85	3.85
AF20-04	55	Micro-Phenocryst	<250µ	Core	56.19	0.15	27.39	0.86	0.08	10.07	5.54	0.41	0.08	0.09	100.86	48.64	48.85	2.35
AF20-04	56	Groundmass	<250µ	Core	53.95	0.13	28.51	0.73	0.11	11.42	4.92	0.29	0.09	0.06	100.22	43.05	55.17	1.67
AF20-04	57	Groundmass	<250µ	Rim	59.41	0.10	25.17	0.83	0.02	7.39	6.93	0.64	0.13	0.11	100.73	60.50	35.66	3.65
AF20-04	59	Groundmass	<250µ	Core	54.49	0.13	28.13	0.83	0.09	11.28	4.91	0.32	0.07	0.08	100.32	43.18	54.85	1.82
AF20-04	60	Groundmass	<250µ	Rim	60.48	0.12	24.01	0.75	0.04	6.37	7.38	0.84	0.15	0.15	100.29	64.25	30.65	4.84
AF20-04	61	Phenocryst	<1000µ	Core	46.44	0.05	32.78	0.59	0.17	16.92	1.69	0.04	0.05	0.04	98.75	15.25	84.45	0.24
AF20-04	61	Phenocryst	<1000µ	Intermediate	46.86	0.07	33.02	0.58	0.16	16.92	1.71	0.04	0.07	0.05	99.47	15.37	84.28	0.26
AF20-04	61	Phenocryst	<1000µ	Intermediate	47.06	0.06	33.38	0.58	0.15	16.90	1.71	0.04	0.07	0.06	100.01	15.38	84.25	0.26
AF20-04	61	Phenocryst	<1000µ	Intermediate	47.01	0.07	33.28	0.55	0.16	16.86	1.79	0.04	0.07	0.03	99.85	16.03	83.66	0.25
AF20-04	61	Phenocryst	<1000µ	Intermediate	47.01	0.06	33.51	0.54	0.15	16.96	1.62	0.04	0.03	0.08	100.02	14.70	84.89	0.26
AF20-04	61	Phenocryst	<1000µ	Intermediate	47.53	0.05	33.05	0.58	0.16	16.65	1.85	0.05	0.11	0.07	100.08	16.70	82.89	0.29
AF20-04	61	Phenocryst	<1000µ	Intermediate	47.68	0.05	32.95	0.58	0.17	16.55	1.98	0.05	0.13	0.07	100.21	17.75	81.85	0.27
AF20-04	61	Phenocryst	<1000µ	Intermediate	46.57	0.07	33.31	0.61	0.15	16.94	1.62	0.04	0.08	0.07	99.46	14.72	84.93	0.23
AF20-04	61	Phenocryst	<1000µ	Intermediate	46.92	0.04	33.39	0.58	0.15	17.11	1.73	0.05	0.05	0.04	100.08	15.39	84.23	0.30
AF20-04	61	Phenocryst	<1000µ	Intermediate	46.89	0.05	33.60	0.59	0.15	17.22	1.68	0.04	0.06	0.06	100.33	14.92	84.72	0.25
AF20-04	61	Phenocryst	<1000µ	Intermediate	46.74	0.06	33.32	0.60	0.14	17.05	1.61	0.04	0.09	0.04	99.68	14.53	85.15	0.24
AF20-04	61	Phenocryst	<1000µ	Intermediate	46.74	0.05	33.51	0.63	0.13	17.26	1.64	0.05	0.06	0.04	100.10	14.59	85.07	0.28
AF20-04	61	Phenocryst	<1000µ	Intermediate	46.79	0.06	33.72	0.66	0.11	17.15	1.59	0.06	0.12	0.04	100.28	14.28	85.33	0.33
AF20-04	61	Phenocryst	<1000µ	Intermediate	46.63	0.04	33.75	0.65	0.11	17.14	1.50	0.05	0.06	0.04	99.97	13.64	86.00	0.28
AF20-04	61	Phenocryst	<1000µ	Intermediate	47.63	0.08	32.77	0.91	0.19	16.43	1.89	0.07	0.08	0.03	100.06	17.14	82.41	0.40
AF20-04	61	Phenocryst	<1000µ	Intermediate	53.85	0.13	28.31	0.74	0.15	11.67	4.66	0.26	0.11	0.07	99.94	41.25	57.11	1.53
AF20-04	61	Phenocryst	<1000µ	Intermediate	55.69	0.12	27.37	0.74	0.11	10.27	5.27	0.36	0.06	0.07	100.04	47.09	50.70	2.09
AF20-04	61	Phenocryst	<1000µ	Intermediate	55.92	0.15	27.50	0.67	0.13	10.39	5.30	0.36	0.13	0.07	100.61	46.95	50.85	2.07
AF20-04	61	Phenocryst	<1000µ	Rim	57.21	0.11	26.36	0.76	0.07	8.75	6.13	0.48	0.10	0.09	100.05	54.28	42.80	2.77
AF20-04	62	Groundmass	<50µ		57.12	0.14	26.36	0.86	0.05	8.81	5.97	0.48	0.10	0.07	99.96	53.47	43.57	2.83
AF20-04	63	Groundmass	<50µ		53.83	0.14	28.66	0.85	0.06	11.47	4.70	0.28	0.12	0.08	100.18	41.80	56.41	1.65
Af20-19	1	Groundmass		Core	56.07	0.22	26.99	1.09	0.07	10.11	5.60	0.48	0.09	0.07	100.77	48.63	48.54	2.72
Af20-19	2	Groundmass		Core	56.19	0.15	27.04	0.81	0.05	10.31	5.49	0.47	0.13	0.03	100.67	47.73	49.54	2.68
Af20-19	3	Groundmass		Core	54.92	0.13	27.80	0.90	0.06	10.71	5.16	0.40	0.09	0.06	100.22	45.41	52.15	2.34
Af20-19	4	Groundmass		Core	54.44	0.13	28.26	0.94	0.10	11.43	4.84	0.32	0.08	0.05	100.59	42.56	55.53	1.82
Af20-19	5	Groundmass		Core	55.45	0.10	27.42	1.07	0.04	10.12	5.67	0.42	0.12	0.06	100.45	49.07	48.43	2.40
Af20-19	6	Groundmass		Core	56.34	0.16	26.83	1.02	0.05	9.47	5.80	0.51	0.08	0.06	100.31	50.95	46.01	2.93
Af20-19	7	Groundmass		Core	54.59	0.14	28.03	0.95	0.05	10.98	5.14	0.37	0.05	0.07	100.38	44.82	52.91	2.15
Af20-19	8	Groundmass		Core	54.84	0.19	27.65	1.38	0.06	10.97	5.01	0.35	0.08	0.06	100.58	44.28	53.58	2.02
Af20-19	9	Groundmass		Core	55.34	0.20	27.33	1.23	0.07	10.50	5.24	0.40	0.12	0.06	100.48	46.30	51.26	2.33
Af20-19	10	Groundmass		Core	54.72	0.16	28.11	0.91	0.11	11.28	4.78	0.32	0.10	0.07	100.57	42.51	55.46	1.90
Af20-19	10	Groundmass		Intermediate	54.90	0.16	27.96	0.86	0.07	10.88	5.00	0.37	0.09	0.05	100.33	44.35	53.39	2.17
Af20-19	10	Groundmass		Rim	55.73	0.14	27.50	0.86	0.05	10.25	5.38	0.40	0.11	0.07	100.49	47.53	50.02	2.32
Af20-19	11	phenocryst		Intermediate	48.97	0.12	32.19	0.89	0.09	15.85	2.36	0.08	0.13	0.02	100.61	21.15	78.34	0.47
Af20-19	11	phenocryst		Intermediate	48.90	0.11	32.23	0.78	0.12	15.92	2.42	0.07	0.03	0.03	100.55	21.46	78.06	0.43
Af20-19	11	phenocryst		Core	48.80	0.06	32.15	0.68	0.15	15.73	2.26	0.05	0.02	0.04	99.87	20.58	79.03	0.32
Af20-19	11	phenocryst		Intermediate	48.57	0.09	32.33	0.83	0.14	16.27	2.28	0.08	0.02	0.06	100.59	20.09	79.33	0.47
Af20-19	11	phenocryst		Intermediate	48.78	0.07	32.05	0.77	0.12	15.56	2.40	0.07	0.09	0.07	99.90	21.74	77.74	0.39
Af20-19	12	phenocryst		Core	48.45	0.11	32.23	0.71	0.15	16.07	2.31	0.07	0.05	0.04	100.12	20.56	79.00	0.38

Af20-19	12	phenocryst		Intermediate	49.03	0.06	31.64	0.72	0.16	15.37	2.78	0.10	0.07	0.06	99.91	24.47	74.87	0.56
Af20-19	12	phenocryst		Intermediate	47.99	0.07	32.57	0.71	0.13	16.42	2.24	0.05	0.13	0.03	100.26	19.73	79.95	0.28
Af20-19	12	phenocryst		Intermediate	47.79	0.05	32.83	0.76	0.15	16.49	2.17	0.04	0.05	0.10	100.35	19.12	80.46	0.24
Af20-19	12	phenocryst		Intermediate	49.13	0.06	32.14	0.73	0.17	15.51	2.57	0.07	0.08	0.05	100.46	22.97	76.52	0.42
Af20-19	12	phenocryst		Intermediate	48.74	0.06	31.90	0.72	0.18	15.63	2.73	0.07	0.12	0.05	100.11	23.88	75.63	0.40
Af20-19	12	phenocryst		Rim	48.57	0.09	32.03	0.77	0.14	15.66	2.50	0.07	0.05	0.07	99.87	22.30	77.16	0.41
Central Afar Gulf																		
AF20-46	1	Phenocryst	<1500µ	Core	51.97	0.12	30.26	0.79	0.20	13.84	3.48	0.11	0.10	0.05	100.91	31.03	68.23	0.65
AF20-46	1	Phenocryst	<1500µ	Rim	50.26	0.10	31.30	0.92	0.18	14.93	2.97	0.11	0.04	0.06	100.86	26.25	73.03	0.61
AF20-46	2	Micro-Phenocryst	<500µ	Core	55.04	0.14	27.95	0.93	0.13	11.36	5.00	0.25	0.09	0.08	100.96	43.66	54.75	1.45
AF20-46	3	Micro-Phenocryst	<500µ	Core	51.07	0.12	30.64	0.96	0.18	14.16	3.31	0.11	0.10	0.05	100.69	29.52	69.76	0.64
AF20-46	5	Groundmass	?		54.44	0.15	27.86	1.07	0.11	11.16	4.91	0.28	0.09	0.04	100.10	43.55	54.73	1.65
AF20-46	6	Micro-Phenocryst	<250µ	Core	54.75	0.14	27.90	0.91	0.13	11.10	5.01	0.25	0.06	0.05	100.29	44.29	54.18	1.45
AF20-46	6	Micro-Phenocryst	<250µ	Rim	54.91	0.19	28.18	0.96	0.12	11.29	4.84	0.28	0.03	0.06	100.86	42.91	55.34	1.63
AF20-46	9	Groundmass	<50µ		54.20	0.16	28.21	1.23	0.12	11.81	4.79	0.25	0.09	0.07	100.92	41.70	56.75	1.42
AF20-46	11	Groundmass	<50µ		54.12	0.16	28.25	1.23	0.12	11.94	4.67	0.28	0.07	0.08	100.90	40.70	57.56	1.60
AF20-46	12	Groundmass	<150µ		54.95	0.15	27.76	1.02	0.16	10.80	5.17	0.29	0.12	0.09	100.49	45.55	52.64	1.66
AF20-46	13	Groundmass	<150µ		54.45	0.14	28.17	1.15	0.11	11.25	4.84	0.30	0.08	0.06	100.54	42.97	55.16	1.77
AF20-46	14	Groundmass	<150µ		53.79	0.16	28.42	1.06	0.12	11.89	4.38	0.24	0.07	0.07	100.19	39.38	59.11	1.39
AF20-46	15	Groundmass	<50µ		54.29	0.20	27.36	1.61	0.15	10.79	5.00	0.32	0.11	0.06	99.88	44.70	53.33	1.85
AF20-46	16	Groundmass	<50µ		54.94	0.17	27.90	0.99	0.12	10.98	5.22	0.30	0.09	0.08	100.80	45.40	52.76	1.69
AF20-46	17	Groundmass	<50µ		55.57	0.15	27.15	1.05	0.12	10.50	5.15	0.29	0.03	0.04	100.07	46.20	52.01	1.72
AF20-46	18	Groundmass	<50µ		53.19	0.13	28.98	0.86	0.17	12.58	4.27	0.16	0.09	0.04	100.47	37.65	61.37	0.91
AF20-46	19	Groundmass	<150µ		54.55	0.16	28.19	1.06	0.10	11.19	4.83	0.31	0.06	0.08	100.52	42.99	55.06	1.82
AF20-46	20	Groundmass	<150µ		54.99	0.17	27.22	1.09	0.14	10.66	5.38	0.34	0.09	0.06	100.13	46.77	51.21	1.92
AF20-46	21	Groundmass	<150µ		53.84	0.13	28.09	1.16	0.16	11.73	4.50	0.23	0.13	0.08	100.05	40.36	58.12	1.38
AF20-46	22	Groundmass	<150µ		53.91	0.17	28.23	1.11	0.15	11.61	4.55	0.30	0.07	0.10	100.21	40.70	57.35	1.76
AF20-46	23	Groundmass	<50µ		53.45	0.14	28.63	1.04	0.09	11.88	4.64	0.24	0.10	0.03	100.24	40.84	57.76	1.36
AF20-46	24	Groundmass	<50µ		56.26	0.19	26.86	1.22	0.08	9.87	5.52	0.42	0.09	0.08	100.58	49.01	48.41	2.44
AF20-46	25	Groundmass	<50µ		53.95	0.17	27.98	1.23	0.14	11.26	4.84	0.27	0.07	0.05	99.97	43.00	55.31	1.60
AF20-46	26	Groundmass	<50µ		56.09	0.17	26.80	1.13	0.12	9.75	5.80	0.39	0.09	0.07	100.41	50.62	47.04	2.21
AF20-46	27	Phenocryst	<1500µ	Core	47.91	0.07	32.24	0.78	0.19	15.98	2.09	0.06	0.06	0.04	99.40	19.03	80.54	0.37
AF20-46	27	Phenocryst	<1500µ	Intermediate	48.16	0.07	32.37	0.74	0.16	16.07	2.17	0.08	0.10	0.05	99.95	19.50	79.95	0.47
AF20-46	27	Phenocryst	<1500µ	Intermediate	48.12	0.08	32.21	0.78	0.17	16.09	2.21	0.06	0.04	0.07	99.83	19.83	79.67	0.37
AF20-46	27	Phenocryst	<1500µ	Intermediate	48.54	0.08	32.22	0.76	0.17	16.05	2.32	0.07	0.10	0.05	100.36	20.64	78.88	0.39
AF20-46	27	Phenocryst	<1500µ	Intermediate	48.68	0.05	32.33	0.70	0.17	15.99	2.28	0.06	0.09	0.06	100.41	20.42	79.12	0.36
AF20-46	27	Phenocryst	<1500µ	Intermediate	48.34	0.06	32.32	0.73	0.16	16.04	2.24	0.06	0.03	0.07	100.04	20.10	79.45	0.32
AF20-46	27	Phenocryst	<1500µ	Intermediate	48.20	0.06	32.25	0.73	0.17	15.97	2.20	0.05	0.05	0.03	99.71	19.91	79.74	0.30
AF20-46	27	Phenocryst	<1500µ	Intermediate	51.51	0.08	30.18	0.75	0.20	13.71	3.64	0.12	0.07	0.07	100.32	32.17	67.01	0.69
AF20-46	27	Phenocryst	<1500µ	Intermediate	50.89	0.09	30.33	0.73	0.19	13.99	3.44	0.11	0.11	0.07	99.94	30.52	68.69	0.66
AF20-46	27	Phenocryst	<1500µ	Intermediate	50.06	0.08	31.07	0.73	0.17	14.92	2.95	0.09	0.05	0.04	100.18	26.21	73.18	0.53
AF20-46	27	Phenocryst	<1500µ	Intermediate	48.41	0.05	32.13	0.82	0.17	15.65	2.29	0.08	0.09	0.03	99.71	20.83	78.65	0.45
AF20-46	27	Phenocryst	<1500µ	Intermediate	48.70	0.05	32.23	0.79	0.18	15.99	2.43	0.08	0.10	0.07	100.63	21.46	77.97	0.44
AF20-46	27	Phenocryst	<1500µ	Intermediate	49.36	0.08	31.41	0.73	0.14	15.19	2.73	0.08	0.13	0.06	99.92	24.41	75.03	0.45
AF20-46	27	Phenocryst	<1500µ	Intermediate	49.14	0.09	31.60	0.72	0.17	15.51	2.64	0.07	0.00	0.08	100.01	23.42	76.05	0.39
AF20-46	27	Phenocryst	<1500µ	Intermediate	48.92	0.07	31.88	0.75	0.17	15.53	2.52	0.07	0.05	0.09	100.03	22.54	76.89	0.41
AF20-46	27	Phenocryst	<1500µ	Intermediate	48.63	0.07	31.96	0.81	0.17	15.67	2.50	0.07	0.09	0.06	100.02	22.30	77.18	0.41
AF20-46	27	Phenocryst	<1500µ	Intermediate	50.99	0.10	30.36	0.78	0.19	13.93	3.59	0.12	0.11	0.05	100.21	31.52	67.68	0.72
AF20-46	27	Phenocryst	<1500µ	Intermediate	50.81	0.09	30.53	0.87	0.21	14.06	3.44	0.12	0.06	0.05	100.24	30.47	68.75	0.70
AF20-46	27	Phenocryst	<1500µ	Rim	51.13	0.10	30.28	0.90	0.18	13.88	3.59	0.12	0.08	0.05	100.31	31.64	67.57	0.70
AF20-46	28	Phenocryst	<1000µ ?	Core	48.61	0.07	32.42	0.74	0.15	16.07	2.27	0.05	0.12	0.07	100.57	20.27	79.29	0.31
AF20-46	28	Phenocryst	<1000µ ?	Intermediate	48.80	0.09	32.47	0.77	0.15	15.96	2.33	0.07	0.08	0.03	100.75	20.79	78.75	0.41
AF20-46	28	Phenocryst	<1000µ ?	Intermediate	48.57	0.06	32.14	0.77	0.15	15.82	2.36	0.08	0.05	0.07	100.08	21.14	78.27	0.47
AF20-46	28	Phenocryst	<1000µ ?	Intermediate	49.03	0.08	31.89	0.76	0.17	15.69	2.59	0.08	0.09	0.06	100.42	22.89	76.55	0.46
AF20-46	28	Phenocryst	<1000µ ?	Intermediate	48.45	0.06	32.24	0.79	0.14	16.12	2.25	0.07	0.09	0.07	100.25	20.03	79.46	0.39
AF20-46	28	Phenocryst	<1000µ ?	Intermediate	48.79	0.05	32.07	0.78	0.19	15.75	2.38	0.07	0.05	0.06	100.18	21.38	78.13	0.38

AF20-46	28	Phenocryst	<1000µ ?	Intermediate	48.65	0.08	32.26	0.72	0.13	15.65	2.43	0.08	0.10	0.03	100.12	21.84	77.64	0.46
AF20-46	28	Phenocryst	<1000µ ?	Intermediate	48.82	0.06	32.09	0.76	0.18	15.79	2.41	0.07	0.09	0.07	100.34	21.52	77.96	0.39
AF20-46	28	Phenocryst	<1000µ ?	Intermediate	48.56	0.10	31.97	0.78	0.14	15.64	2.54	0.08	0.05	0.07	99.93	22.61	76.83	0.44
AF20-46	28	Phenocryst	<1000µ ?	Intermediate	50.90	0.10	30.60	0.85	0.17	13.99	3.35	0.16	0.04	0.07	100.23	29.92	68.99	0.96
AF20-46	28	Phenocryst	<1000µ ?	Intermediate	49.40	0.08	32.06	0.79	0.19	15.42	2.52	0.07	0.07	0.02	100.61	22.71	76.86	0.39
AF20-46	28	Phenocryst	<1000µ ?	Intermediate	48.58	0.07	32.13	0.80	0.15	15.82	2.42	0.05	0.11	0.02	100.15	21.61	78.06	0.29
AF20-46	28	Phenocryst	<1000µ ?	Intermediate	52.03	0.12	29.74	0.80	0.23	13.30	3.84	0.14	0.03	0.05	100.28	34.04	65.09	0.79
AF20-46	28	Phenocryst	<1000µ ?	Intermediate	50.87	0.10	30.75	0.79	0.23	14.29	3.22	0.11	0.13	0.07	100.54	28.76	70.47	0.65
AF20-46	28	Phenocryst	<1000µ ?	Intermediate	50.35	0.08	30.97	0.82	0.16	14.50	3.10	0.12	0.10	0.05	100.25	27.70	71.52	0.70
AF20-46	28	Phenocryst	<1000µ ?	Intermediate	51.39	0.14	30.22	0.81	0.19	13.61	3.60	0.13	0.05	0.05	100.18	32.09	67.08	0.74
AF20-46	28	Phenocryst	<1000µ ?	Rim	51.25	0.12	30.06	0.90	0.18	13.71	3.81	0.15	0.09	0.04	100.31	33.18	65.90	0.85
AF20-46	30	Phenocryst	<2000µ	Core	47.57	0.05	33.19	0.64	0.14	16.92	1.98	0.05	0.13	0.08	100.75	17.42	82.16	0.28
AF20-46	30	Phenocryst	<2000µ	Intermediate	47.14	0.05	33.04	0.60	0.14	16.92	1.83	0.05	0.08	0.09	99.95	16.25	83.27	0.31
AF20-46	30	Phenocryst	<2000µ	Intermediate	47.65	0.06	32.98	0.61	0.14	16.81	1.80	0.05	0.05	0.05	100.20	16.17	83.44	0.30
AF20-46	30	Phenocryst	<2000µ	Intermediate	47.41	0.09	33.05	0.64	0.15	16.88	1.95	0.05	0.11	0.06	100.39	17.25	82.36	0.28
AF20-46	30	Phenocryst	<2000µ	Intermediate	47.40	0.07	32.86	0.71	0.15	16.56	1.99	0.05	0.09	0.02	99.89	17.81	81.87	0.27
AF20-46	30	Phenocryst	<2000µ	Intermediate	47.24	0.04	33.08	0.64	0.14	16.79	1.82	0.05	0.09	0.09	99.97	16.34	83.22	0.28
AF20-46	30	Phenocryst	<2000µ	Intermediate	48.27	0.07	32.65	0.67	0.15	16.36	2.05	0.05	0.04	0.09	100.39	18.42	81.13	0.28
AF20-46	30	Phenocryst	<2000µ	Intermediate	48.10	0.06	32.51	0.66	0.15	15.87	2.14	0.04	0.06	0.06	99.64	19.55	80.08	0.26
AF20-46	30	Phenocryst	<2000µ	Intermediate	48.26	0.04	32.57	0.63	0.14	16.09	2.11	0.06	0.05	0.06	100.00	19.06	80.48	0.35
AF20-46	30	Phenocryst	<2000µ	Intermediate	48.29	0.06	32.46	0.66	0.14	16.16	2.19	0.06	0.08	0.05	100.15	19.60	79.95	0.35
AF20-46	30	Phenocryst	<2000µ	Intermediate	48.29	0.11	32.61	0.66	0.18	16.34	2.24	0.05	0.13	0.06	100.66	19.76	79.84	0.29
AF20-46	30	Phenocryst	<2000µ	Intermediate	48.31	0.02	32.53	0.65	0.13	16.19	2.21	0.05	0.03	0.03	100.15	19.75	79.89	0.32
AF20-46	30	Phenocryst	<2000µ	Intermediate	48.16	0.05	31.06	0.68	1.43	15.73	1.91	0.09	0.10	0.05	99.25	17.89	81.48	0.53
AF20-46	30	Phenocryst	<2000µ	Intermediate	47.85	0.08	32.67	0.64	0.16	16.64	2.09	0.04	0.00	0.05	100.22	18.45	81.22	0.24
AF20-46	30	Phenocryst	<2000µ	Intermediate	47.55	0.05	33.08	0.63	0.17	16.75	1.93	0.06	0.07	0.04	100.32	17.21	82.39	0.32
AF20-46	30	Phenocryst	<2000µ	Intermediate	47.42	0.06	33.07	0.64	0.13	16.95	1.89	0.04	0.12	0.03	100.34	16.76	82.94	0.24
AF20-46	30	Phenocryst	<2000µ	Intermediate	48.10	0.05	32.58	0.66	0.18	16.27	2.04	0.04	0.08	0.09	100.08	18.42	81.17	0.26
AF20-46	30	Phenocryst	<2000µ	Intermediate	48.84	0.07	32.12	0.67	0.18	15.88	2.41	0.07	0.11	0.07	100.40	21.44	78.04	0.39
AF20-46	30	Phenocryst	<2000µ	Intermediate	48.41	0.04	32.52	0.70	0.14	16.08	2.23	0.07	0.12	0.04	100.35	19.99	79.54	0.41
AF20-46	30	Phenocryst	<2000µ	Intermediate	48.82	0.07	32.20	0.65	0.17	15.96	2.30	0.04	0.09	0.08	100.39	20.63	78.99	0.25
AF20-46	30	Phenocryst	<2000µ	Intermediate	48.82	0.09	32.13	0.68	0.17	15.94	2.41	0.07	0.11	0.06	100.47	21.34	78.12	0.43
AF20-46	30	Phenocryst	<2000µ	Intermediate	48.64	0.06	32.14	0.63	0.15	16.04	2.41	0.05	0.04	0.03	100.19	21.32	78.35	0.27
AF20-46	30	Phenocryst	<2000µ	Intermediate	48.44	0.09	32.32	0.66	0.19	15.95	2.34	0.05	0.09	0.05	100.17	20.89	78.70	0.31
AF20-46	30	Phenocryst	<2000µ	Intermediate	48.87	0.04	32.20	0.68	0.15	15.79	2.38	0.05	0.08	0.04	100.28	21.31	78.29	0.31
AF20-46	30	Phenocryst	<2000µ	Intermediate	49.16	0.05	31.98	0.67	0.16	15.67	2.50	0.07	0.09	0.05	100.40	22.31	77.20	0.40
AF20-46	30	Phenocryst	<2000µ	Intermediate	47.92	0.05	32.58	0.73	0.18	16.25	2.08	0.06	0.06	0.06	99.97	18.74	80.80	0.35
AF20-46	30	Phenocryst	<2000µ	Intermediate	48.47	0.05	32.28	0.64	0.17	15.83	2.25	0.05	0.09	0.07	99.89	20.35	79.24	0.29
AF20-46	30	Phenocryst	<2000µ	Intermediate	48.66	0.07	32.24	0.62	0.17	15.91	2.24	0.06	0.09	0.04	100.10	20.21	79.34	0.37
AF20-46	30	Phenocryst	<2000µ	Intermediate	48.12	0.05	32.55	0.66	0.15	16.34	2.22	0.05	0.09	0.05	100.29	19.65	79.99	0.27
AF20-46	30	Phenocryst	<2000µ	Intermediate	48.47	0.05	32.55	0.71	0.17	15.91	2.27	0.05	0.05	0.06	100.29	20.47	79.15	0.28
AF20-46	30	Phenocryst	<2000µ	Intermediate	48.36	0.07	32.19	0.70	0.17	15.91	2.23	0.07	0.10	0.08	99.86	20.13	79.33	0.40
AF20-46	30	Phenocryst	<2000µ	Intermediate	48.33	0.06	32.39	0.70	0.16	16.14	2.25	0.05	0.07	0.05	100.19	20.06	79.56	0.28
AF20-46	30	Phenocryst	<2000µ	Intermediate	50.53	0.07	31.33	0.66	0.19	14.93	2.97	0.07	0.06	0.07	100.88	26.30	73.16	0.41
AF20-46	30	Phenocryst	<2000µ	Intermediate	49.95	0.10	31.10	0.71	0.18	14.91	2.91	0.09	0.08	0.05	100.07	25.96	73.45	0.50
AF20-46	30	Phenocryst	<2000µ	Intermediate	48.50	0.09	32.31	0.69	0.16	16.02	2.36	0.07	0.07	0.06	100.34	20.95	78.54	0.40
AF20-46	30	Phenocryst	<2000µ	Intermediate	48.83	0.06	32.12	0.65	0.17	16.06	2.35	0.08	0.07	0.07	100.46	20.79	78.59	0.49
AF20-46	30	Phenocryst	<2000µ	Intermediate	48.42	0.07	30.80	0.65	0.18	16.18	2.75	0.08	0.11	0.03	99.28	23.40	76.07	0.47
AF20-46	30	Phenocryst	<2000µ	Intermediate	48.84	0.05	31.87	0.68	0.20	15.58	2.52	0.08	0.07	0.03	99.93	22.54	76.96	0.44
AF20-46	30	Phenocryst	<2000µ	Intermediate	48.36	0.06	32.18	0.68	0.13	16.09	2.19	0.07	0.08	0.03	99.87	19.67	79.87	0.40
AF20-46	30	Phenocryst	<2000µ	Intermediate	48.39	0.07	32.13	0.71	0.16	15.97	2.32	0.06	0.04	0.07	99.92	20.69	78.82	0.37
AF20-46	30	Phenocryst	<2000µ	Intermediate	50.95	0.08	30.54	0.75	0.21	14.07	3.26	0.11	0.06	0.07	100.09	29.33	69.88	0.65
AF20-46	30	Phenocryst	<2000µ	Intermediate	51.30	0.10	30.28	0.82	0.17	13.85	3.51	0.11	0.06	0.03	100.24	31.25	68.08	0.62
AF20-46	30	Phenocryst	<2000µ	Intermediate	51.30	0.08	30.01	0.81	0.21	13.65	3.29	0.11	0.03	0.06	99.54	30.12	69.13	0.64
AF20-46	30	Phenocryst	<2000µ	Rim	51.34	0.08	30.18	0.87	0.18	13.72	3.75	0.15	0.05	0.09	100.41	32.77	66.19	0.88
AF20-46	31	Groundmass			57.44	0.20	25.69	1.09	0.09	8.76	5.66	0.70	0.11	0.11	99.86	51.53	44.08	4.19
AF20-46	32	Phenocryst	<2000µ	Core	48.97	0.10	32.04	0.75	0.17	15.74	2.53	0.07	0.08	0.05	100.50	22.39	77.09	0.43

AF20-46	32	Phenocryst	<2000µ	Intermediate	49.40	0.08	31.53	0.71	0.17	15.54	2.60	0.07	0.09	0.07	100.25	23.12	76.34	0.41
AF20-46	32	Phenocryst	<2000µ	Intermediate	49.67	0.06	31.55	0.78	0.19	15.07	2.89	0.08	0.05	0.09	100.40	25.57	73.80	0.47
AF20-46	32	Phenocryst	<2000µ	Intermediate	48.43	0.08	31.89	0.75	0.16	16.16	2.45	0.07	0.08	0.02	100.09	21.42	78.14	0.40
AF20-46	32	Phenocryst	<2000µ	Intermediate	48.28	0.09	32.03	0.79	0.14	16.42	2.26	0.06	0.07	0.10	100.25	19.87	79.62	0.33
AF20-46	32	Phenocryst	<2000µ	Intermediate	49.83	0.06	31.30	0.72	0.23	15.17	2.81	0.08	0.08	0.06	100.33	24.95	74.50	0.44
AF20-46	32	Phenocryst	<2000µ	Intermediate	47.34	0.03	32.76	0.70	0.16	16.78	1.76	0.05	0.05	0.06	99.68	15.85	83.76	0.29
AF20-46	32	Phenocryst	<2000µ	Intermediate	47.30	0.02	33.25	0.70	0.13	17.17	1.76	0.04	0.02	0.09	100.46	15.57	84.04	0.23
AF20-46	32	Phenocryst	<2000µ	Intermediate	47.02	0.05	33.47	0.65	0.10	17.27	1.60	0.04	0.06	0.07	100.32	14.29	85.38	0.21
AF20-46	32	Phenocryst	<2000µ	Intermediate	47.20	0.07	33.56	0.64	0.10	17.22	1.57	0.05	0.05	0.08	100.53	14.12	85.46	0.28
AF20-46	32	Phenocryst	<2000µ	Intermediate	47.06	0.03	33.42	0.67	0.15	17.23	1.68	0.03	0.08	0.03	100.38	14.97	84.80	0.18
AF20-46	32	Phenocryst	<2000µ	Intermediate	47.19	0.05	33.24	0.66	0.16	17.16	1.63	0.05	0.06	0.03	100.22	14.61	85.07	0.27
AF20-46	32	Phenocryst	<2000µ	Intermediate	47.42	0.05	33.30	0.67	0.15	17.08	1.79	0.04	0.01	0.06	100.58	15.90	83.76	0.22
AF20-46	32	Phenocryst	<2000µ	Intermediate	47.44	0.06	33.30	0.70	0.13	17.13	1.90	0.04	0.04	0.04	100.76	16.65	83.04	0.25
AF20-46	32	Phenocryst	<2000µ	Intermediate	48.24	0.08	32.72	0.66	0.13	16.42	1.98	0.05	0.11	0.04	100.43	17.83	81.77	0.32
AF20-46	32	Phenocryst	<2000µ	Intermediate	48.42	0.05	32.45	0.75	0.16	16.33	2.14	0.06	0.07	0.07	100.50	19.11	80.44	0.33
AF20-46	32	Phenocryst	<2000µ	Intermediate	48.20	0.05	32.52	0.73	0.12	16.39	2.13	0.06	0.05	0.04	100.29	18.97	80.62	0.33
AF20-46	32	Phenocryst	<2000µ	Rim	48.45	0.07	31.97	0.73	0.16	15.86	2.24	0.05	0.09	0.08	99.69	20.29	79.28	0.29
AF20-46	33	Phenocryst	<500µ	Core	48.79	0.04	32.02	0.76	0.17	15.36	2.47	0.07	0.10	0.07	99.85	22.40	77.05	0.43
AF20-46	33	Phenocryst	<500µ	Intermediate	49.01	0.08	31.42	0.80	0.17	15.38	2.62	0.08	0.02	0.06	99.64	23.42	76.02	0.45
AF20-46	33	Phenocryst	<500µ	Intermediate	48.38	0.05	32.39	0.76	0.14	16.15	2.16	0.07	0.05	0.05	100.21	19.42	80.09	0.40
AF20-46	33	Phenocryst	<500µ	Intermediate	48.10	0.08	32.10	0.75	0.16	16.21	2.04	0.05	0.07	0.06	99.62	18.50	81.11	0.27
AF20-46	33	Phenocryst	<500µ	Intermediate	48.23	0.07	32.43	0.70	0.15	16.34	2.11	0.07	0.11	0.06	100.28	18.81	80.65	0.42
AF20-46	33	Phenocryst	<500µ	Intermediate	48.27	0.07	32.19	0.76	0.17	15.94	2.34	0.07	0.07	0.05	99.92	20.91	78.62	0.39
AF20-46	33	Phenocryst	<500µ	Intermediate	48.44	0.05	32.08	0.73	0.17	15.67	2.31	0.06	0.04	0.03	99.59	21.00	78.59	0.36
AF20-46	33	Phenocryst	<500µ	Intermediate	48.61	0.09	31.93	0.77	0.17	16.06	2.31	0.07	0.05	0.06	100.12	20.55	78.90	0.43
AF20-46	33	Phenocryst	<500µ	Intermediate	49.62	0.09	31.08	0.77	0.16	14.93	2.98	0.10	0.10	0.05	99.86	26.37	72.98	0.57
AF20-46	33	Phenocryst	<500µ	rim	50.09	0.09	31.18	0.79	0.19	14.70	3.04	0.10	0.07	0.07	100.33	27.05	72.23	0.59
AF20-46	34	Phenocryst		Core	49.07	0.09	31.90	0.72	0.17	15.73	2.35	0.09	0.03	0.05	100.15	21.13	78.23	0.54
AF20-46	34	Phenocryst		Intermediate	49.18	0.08	31.98	0.69	0.17	15.65	2.58	0.07	0.03	0.06	100.44	22.88	76.60	0.40
AF20-46	34	Phenocryst		Intermediate	48.87	0.08	32.02	0.74	0.17	15.84	2.51	0.05	0.03	0.07	100.29	22.21	77.39	0.28
AF20-46	34	Phenocryst		Intermediate	48.93	0.07	32.26	0.73	0.17	15.68	2.51	0.06	0.06	0.06	100.48	22.36	77.16	0.37
AF20-46	34	Phenocryst		Intermediate	49.04	0.08	32.28	0.76	0.18	15.56	2.66	0.07	0.02	0.06	100.63	23.49	75.99	0.41
AF20-46	34	Phenocryst		Intermediate	48.83	0.08	32.51	0.67	0.17	15.91	2.34	0.06	0.12	0.07	100.71	20.94	78.56	0.37
AF20-46	34	Phenocryst		Intermediate	49.91	0.08	30.46	0.76	0.20	14.57	3.00	0.10	0.08	0.05	99.15	26.93	72.40	0.59
AF20-46	34	Phenocryst		Intermediate	51.23	0.09	30.50	0.72	0.22	14.21	3.40	0.09	0.08	0.07	100.53	30.02	69.31	0.54
AF20-46	34	Phenocryst		Intermediate	50.42	0.07	31.07	0.73	0.21	14.71	3.06	0.09	0.10	0.05	100.45	27.17	72.18	0.55
AF20-46	34	Phenocryst		Intermediate	50.31	0.09	31.22	0.74	0.21	14.82	3.12	0.09	0.06	0.05	100.64	27.43	71.94	0.54
AF20-46	34	Phenocryst		Intermediate	49.78	0.06	31.59	0.76	0.20	15.34	2.68	0.07	0.03	0.07	100.50	23.89	75.57	0.41
AF20-46	34	Phenocryst		Intermediate	49.93	0.06	31.53	0.73	0.20	15.25	2.78	0.07	0.07	0.06	100.61	24.70	74.76	0.43
AF20-46	34	Phenocryst		Intermediate	50.30	0.08	31.39	0.72	0.20	14.92	2.93	0.08	0.05	0.09	100.68	26.05	73.34	0.45
AF20-46	34	Phenocryst		Intermediate	48.91	0.07	32.36	0.73	0.18	15.79	2.49	0.06	0.06	0.05	100.64	22.07	77.47	0.37
AF20-46	34	Phenocryst		Intermediate	49.60	0.09	31.58	0.75	0.19	15.31	2.90	0.08	0.09	0.05	100.54	25.42	74.05	0.45
AF20-46	34	Phenocryst		Intermediate	49.15	0.07	32.34	0.72	0.17	15.55	2.51	0.06	0.05	0.05	100.62	22.49	77.06	0.36
AF20-46	34	Phenocryst		Rim	48.70	0.07	32.52	0.77	0.16	16.00	2.35	0.05	0.04	0.05	100.64	20.93	78.71	0.28
AF20-46		Phenocryst			54.95	0.12	28.31	0.87	0.17	11.31	4.85	0.26	0.07	0.09	100.93	42.97	55.35	1.53
AF20-46	35	Phenocryst		Core	48.66	0.31	31.45	1.81	0.17	15.20	2.52	0.14	0.10	0.08	100.24	22.87	76.17	0.82
AF20-46	35	Phenocryst		Intermediate	48.66	0.07	32.60	0.75	0.17	16.18	2.37	0.05	0.08	0.06	100.92	20.89	78.70	0.30
AF20-46	35	Phenocryst		Intermediate	48.43	0.06	32.48	0.82	0.16	16.05	2.29	0.05	0.07	0.05	100.40	20.44	79.17	0.30
AF20-46	35	Phenocryst		Intermediate	49.72	0.08	31.77	0.75	0.19	15.13	2.79	0.08	0.05	0.08	100.58	24.83	74.57	0.46
AF20-46	35	Phenocryst		Intermediate	49.52	0.06	31.99	0.70	0.19	15.44	2.61	0.08	0.06	0.07	100.65	23.31	76.12	0.45
AF20-46	35	Phenocryst		Intermediate	49.08	0.07	32.22	0.78	0.18	15.76	2.59	0.06	0.03	0.05	100.75	22.83	76.74	0.32
AF20-46	35	Phenocryst		Intermediate	49.01	0.06	32.19	0.69	0.18	15.69	2.45	0.07	0.04	0.05	100.36	21.90	77.61	0.41
AF20-46	35	Phenocryst		Intermediate	48.62	0.07	32.50	0.74	0.18	16.00	2.41	0.06	0.03	0.04	100.58	21.35	78.22	0.36
AF20-46	35	Phenocryst		Intermediate	48.54	0.06	32.54	0.70	0.17	16.14	2.23	0.06	0.06	0.05	100.48	19.88	79.66	0.37
AF20-46	35	Phenocryst		Intermediate	48.55	0.07	32.59	0.70	0.19	16.11	2.16	0.06	0.06	0.03	100.46	19.44	80.14	0.36
AF20-46	35	Phenocryst		Intermediate	49.26	0.06	32.30	0.71	0.19	15.67	2.44	0.07	0.09	0.04	100.76	21.88	77.65	0.39
AF20-46	35	Phenocryst		Intermediate	48.81	0.08	32.26	0.69	0.18	15.84	2.37	0.07	0.05	0.06	100.34	21.17	78.30	0.41

AF20-46	35	Phenocryst	Intermediate	48.94	0.08	32.06	0.72	0.21	15.71	2.52	0.07	0.04	0.04	100.33	22.39	77.11	0.42
AF20-46	35	Phenocryst	Intermediate	49.28	0.07	32.29	0.71	0.18	15.57	2.52	0.07	0.07	0.04	100.74	22.52	76.99	0.41
AF20-46	35	Phenocryst	Intermediate	49.39	0.08	31.91	0.70	0.20	15.49	2.57	0.07	0.06	0.05	100.46	22.95	76.54	0.42
AF20-46	35	Phenocryst	Intermediate	49.00	0.08	32.21	0.71	0.18	15.67	2.45	0.07	0.11	0.06	100.48	21.90	77.59	0.39
AF20-46	35	Phenocryst	Intermediate	49.58	0.09	31.80	0.69	0.19	15.27	2.70	0.07	0.07	0.07	100.44	24.08	75.39	0.40
AF20-46	35	Phenocryst	Intermediate	48.72	0.05	32.09	0.72	0.19	15.74	2.50	0.08	0.04	0.04	100.11	22.22	77.25	0.46
AF20-46	35	Phenocryst	Intermediate	49.08	0.08	31.95	0.72	0.18	15.63	2.51	0.07	0.10	0.06	100.31	22.42	77.07	0.41
AF20-46	35	Phenocryst	Intermediate	48.97	0.05	32.01	0.72	0.17	15.48	2.48	0.07	0.08	0.08	100.06	22.31	77.11	0.43
AF20-46	35	Phenocryst	Intermediate	49.12	0.08	32.14	0.74	0.18	15.70	2.55	0.06	0.07	0.05	100.62	22.60	76.95	0.36
AF20-46	35	Phenocryst	Intermediate	48.68	0.05	32.06	0.74	0.17	15.95	2.33	0.07	0.04	0.04	100.07	20.82	78.68	0.42
AF20-46	35	Phenocryst	Intermediate	48.40	0.05	32.71	0.73	0.16	16.11	2.20	0.07	0.05	0.09	100.49	19.73	79.69	0.42
AF20-46	35	Phenocryst	Intermediate	48.81	0.07	32.51	0.70	0.15	16.03	2.37	0.08	0.05	0.05	100.75	21.00	78.44	0.47
AF20-46	35	Phenocryst	Intermediate	48.97	0.07	32.46	0.79	0.16	15.98	2.30	0.06	0.08	0.07	100.86	20.54	78.97	0.36
AF20-46	35	Phenocryst	Intermediate	50.71	0.11	30.89	0.87	0.21	14.54	3.24	0.11	0.06	0.07	100.72	28.54	70.73	0.61
AF20-46	35	Phenocryst	Rim	54.76	0.17	27.85	0.96	0.16	11.15	4.95	0.28	0.10	0.07	100.41	43.78	54.47	1.63
AF20-46	36	Groundmass		58.53	0.34	25.04	1.23	0.12	8.86	5.33	0.91	0.07	0.10	100.41	49.15	45.12	5.54
AF20-46	36	Groundmass		56.42	0.22	26.50	1.22	0.15	9.77	5.04	0.57	0.10	0.04	99.90	46.56	49.89	3.47
AF20-46	37	Phenocryst	Core	50.29	0.29	29.47	1.98	0.68	14.33	3.05	0.16	0.06	0.07	100.18	27.49	71.43	0.94
AF20-46	37	Phenocryst	Intermediate	48.66	0.08	32.32	0.72	0.15	15.81	2.38	0.06	0.04	0.07	100.21	21.29	78.26	0.32
AF20-46	37	Phenocryst	Intermediate	48.93	0.07	32.34	0.74	0.17	15.71	2.50	0.05	0.10	0.07	100.60	22.25	77.32	0.31
AF20-46	37	Phenocryst	Intermediate	50.15	0.07	31.23	0.71	0.20	14.75	3.00	0.08	0.03	0.03	100.19	26.78	72.67	0.49
AF20-46	37	Phenocryst	Intermediate	48.60	0.06	32.27	0.72	0.18	16.18	2.34	0.06	0.05	0.06	100.44	20.63	78.93	0.35
AF20-46	37	Phenocryst	Intermediate	49.12	0.07	31.92	0.74	0.17	15.49	2.52	0.08	0.13	0.04	100.19	22.63	76.85	0.44
AF20-46	37	Phenocryst	Intermediate	48.32	0.09	32.29	0.77	0.16	15.80	2.29	0.05	0.08	0.03	99.80	20.69	78.97	0.29
AF20-46	37	Phenocryst	Intermediate	48.81	0.07	32.36	0.72	0.16	16.01	2.38	0.06	0.08	0.06	100.65	21.11	78.40	0.37
AF20-46	37	Phenocryst	Intermediate	48.54	0.08	31.97	0.75	0.16	15.61	2.48	0.07	0.04	0.06	99.71	22.22	77.26	0.42
AF20-46	37	Phenocryst	Rim	48.49	0.09	31.89	0.79	0.12	15.63	2.63	0.08	0.08	0.06	99.78	23.19	76.23	0.49
AF20-46	38	Phenocryst	Core	48.38	0.05	32.71	0.78	0.16	16.19	2.21	0.07	0.09	0.06	100.61	19.69	79.81	0.39
AF20-46	38	Phenocryst	Intermediate	48.62	0.07	32.06	0.77	0.18	15.78	2.47	0.07	0.10	0.06	100.11	21.98	77.52	0.39
AF20-46	38	Phenocryst	Intermediate	50.26	0.09	31.01	0.75	0.19	14.58	3.07	0.08	0.09	0.06	100.10	27.45	71.97	0.48
AF20-46	38	Phenocryst	Intermediate	49.30	0.07	31.89	0.73	0.18	15.49	2.63	0.07	0.09	0.08	100.48	23.38	76.08	0.41
AF20-46	38	Phenocryst	Intermediate	49.06	0.06	31.98	0.77	0.17	15.59	2.51	0.08	0.07	0.08	100.31	22.45	76.97	0.44
AF20-46	38	Phenocryst	Intermediate	48.64	0.06	32.04	0.72	0.16	15.90	2.42	0.07	0.08	0.06	100.08	21.45	78.05	0.39
AF20-46	38	Phenocryst	Intermediate	48.36	0.08	31.98	0.75	0.16	15.86	2.32	0.06	0.09	0.07	99.65	20.83	78.67	0.38
AF20-46	38	Phenocryst	Intermediate	49.25	0.06	31.83	0.74	0.17	15.46	2.59	0.08	0.10	0.05	100.25	23.11	76.35	0.44
AF20-46	38	Phenocryst	Intermediate	50.71	0.10	30.94	0.74	0.19	14.46	3.19	0.11	0.09	0.05	100.48	28.30	70.99	0.62
AF20-46	38	Phenocryst	Intermediate	51.28	0.12	30.36	0.82	0.19	13.86	3.43	0.13	0.12	0.06	100.30	30.63	68.47	0.78
AF20-46	38	Phenocryst	Rim	53.23	0.14	29.06	0.85	0.16	12.44	4.33	0.20	0.05	0.06	100.48	38.15	60.60	1.14
AF20-46	39	Phenocryst	Core	48.92	0.07	31.83	0.75	0.18	15.51	2.50	0.07	0.08	0.06	99.92	22.47	76.99	0.44
AF20-46	40	Phenocryst	Intermediate	48.91	0.09	32.27	0.74	0.16	15.79	2.38	0.06	0.03	0.05	100.40	21.36	78.19	0.36
AF20-46	40	Phenocryst	Intermediate	48.48	0.06	32.33	0.78	0.16	15.87	2.23	0.07	0.07	0.08	100.04	20.18	79.27	0.41
AF20-46	40	Phenocryst	Intermediate	48.96	0.07	32.52	0.72	0.16	15.98	2.14	0.07	0.05	0.05	100.66	19.42	80.05	0.43
AF20-46	40	Phenocryst	Intermediate	48.78	0.10	32.17	0.76	0.17	15.84	2.32	0.07	0.09	0.05	100.29	20.83	78.65	0.42
AF20-46	40	Phenocryst	Intermediate	48.97	0.08	31.87	0.75	0.17	15.61	2.43	0.09	0.05	0.04	99.99	21.85	77.54	0.54
AF20-46	40	Phenocryst	Intermediate	49.14	0.06	31.81	0.76	0.15	15.67	2.46	0.08	0.05	0.05	100.17	21.99	77.47	0.45
AF20-46	40	Phenocryst	Intermediate	48.06	0.05	32.66	0.72	0.15	16.39	2.18	0.06	0.06	0.06	100.31	19.28	80.24	0.36
AF20-46	40	Phenocryst	Intermediate	48.74	0.09	31.61	0.77	0.17	15.40	2.43	0.09	0.05	0.07	99.35	22.07	77.27	0.54
AF20-46	40	Phenocryst	Intermediate	50.21	0.09	30.49	0.80	0.20	14.18	3.11	0.12	0.04	0.06	99.22	28.20	70.97	0.71
AF20-46	40	Phenocryst	Intermediate	49.90	0.07	31.17	0.74	0.18	14.81	3.02	0.08	0.08	0.06	100.05	26.78	72.63	0.48
AF20-46	40	Phenocryst	Intermediate	49.30	0.08	31.93	0.75	0.17	15.36	2.56	0.06	0.08	0.07	100.29	23.05	76.48	0.34
AF20-46	40	Phenocryst	Intermediate	48.92	0.08	31.90	0.76	0.16	15.53	2.49	0.06	0.08	0.07	99.97	22.40	77.13	0.35
AF20-46	40	Phenocryst	Intermediate	50.20	0.07	31.04	0.78	0.18	14.61	3.11	0.09	0.08	0.05	100.13	27.67	71.72	0.53
AF20-46	40	Phenocryst	Intermediate	50.60	0.07	30.55	0.81	0.19	14.02	3.17	0.11	0.06	0.06	99.55	28.80	70.44	0.65
AF20-46	40	Phenocryst	Intermediate	50.23	0.06	30.98	0.75	0.19	14.61	3.18	0.09	0.07	0.05	100.13	28.08	71.32	0.52
AF20-46	40	Phenocryst	Intermediate	51.28	0.11	30.18	0.82	0.17	13.73	3.57	0.12	0.09	0.07	100.05	31.70	67.45	0.73
AF20-46	40	Phenocryst	Intermediate	52.62	0.10	29.49	0.84	0.19	13.07	4.04	0.15	0.04	0.06	100.51	35.51	63.52	0.86
AF20-46	40	Phenocryst	Rim	54.65	0.12	27.80	0.89	0.14	11.28	4.61	0.27	0.08	0.06	99.82	41.77	56.52	1.60

AF20-46	41	Micro-Phenocryst	Core	50.17	0.08	31.04	0.73	0.17	14.65	3.03	0.10	0.04	0.04	99.97	27.04	72.32	0.56
AF20-46	41	Micro-Phenocryst	Intermediate	49.95	0.07	31.77	0.73	0.17	15.12	2.85	0.08	0.10	0.04	100.82	25.31	74.16	0.46
AF20-46	41	Micro-Phenocryst	Intermediate	50.19	0.08	31.30	0.75	0.17	14.98	2.89	0.10	0.08	0.05	100.51	25.69	73.66	0.56
AF20-46	41	Micro-Phenocryst	Intermediate	51.71	0.12	30.16	0.80	0.20	13.66	3.73	0.12	0.08	0.06	100.55	32.78	66.41	0.71
AF20-46	41	Micro-Phenocryst	Intermediate	51.00	0.09	30.53	0.86	0.18	14.04	3.31	0.10	0.07	0.04	100.14	29.72	69.60	0.61
AF20-46	41	Micro-Phenocryst	Rim	52.82	0.12	29.43	0.88	0.18	12.64	4.01	0.18	0.07	0.06	100.29	36.03	62.83	1.04
AF-20-66		Phenocryst	Core	52.72	0.13	29.10	0.70	0.12	12.00	4.45	0.20	0.11	0.09	99.61	39.63	59.07	1.14
AF-20-66		Phenocryst	Rim	52.32	0.13	29.21	0.70	0.11	12.28	4.38	0.17	0.13	0.07	99.49	38.79	60.10	0.98
AF-20-66		Micro-Phenocryst	Core	51.65	0.12	29.82	0.80	0.15	12.91	3.91	0.16	0.10	0.07	99.67	35.01	63.94	0.93
AF-20-66		Groundmass	Core	53.92	0.17	28.15	0.86	0.11	11.09	4.96	0.29	0.09	0.07	99.69	43.91	54.28	1.69
AF-20-66		Phenocryst	Core	51.16	0.11	30.55	0.84	0.11	13.52	3.71	0.13	0.09	0.07	100.28	32.89	66.24	0.74
AF-20-66		Phenocryst	Rim	53.24	0.17	28.69	0.85	0.12	11.74	4.71	0.22	0.13	0.07	99.96	41.49	57.10	1.29
AF-20-66		Micro-Phenocryst	Core	52.32	0.11	29.37	0.86	0.17	12.54	4.30	0.20	0.10	0.09	100.06	37.80	60.92	1.13
AF-20-66		Micro-Phenocryst	Rim	54.61	0.20	27.30	0.97	0.12	10.24	5.37	0.33	0.11	0.10	99.33	47.67	50.26	1.90
AF-20-66		Phenocryst	Core	49.20	0.11	31.65	0.90	0.09	14.85	2.82	0.11	0.11	0.06	99.89	25.36	73.90	0.63
AF-20-66		Phenocryst	Core	49.54	0.11	30.96	0.89	0.14	14.46	3.10	0.09	0.08	0.06	99.45	27.77	71.57	0.55
AF-20-66		Phenocryst	Intermediate	53.53	0.15	28.42	0.81	0.13	11.38	4.84	0.26	0.08	0.08	99.66	42.79	55.58	1.50
AF-20-66		Phenocryst	Rim	53.50	0.17	28.53	0.80	0.12	11.37	4.85	0.24	0.08	0.07	99.74	42.89	55.59	1.40
AF-20-66		Groundmass		51.26	0.17	29.75	1.07	0.12	13.12	3.87	0.19	0.09	0.07	99.70	34.40	64.37	1.11
AF-20-66		Phenocryst	Core	47.06	0.06	33.10	0.66	0.14	16.74	1.81	0.04	0.12	0.07	99.80	16.28	83.34	0.26
AF-20-66		Phenocryst	Core	55.23	0.15	27.49	0.70	0.11	10.08	5.68	0.34	0.12	0.08	99.98	49.46	48.47	1.92
AF-20-66		Phenocryst	Core	53.59	0.16	28.55	0.83	0.12	11.55	4.81	0.26	0.11	0.06	100.02	42.29	56.11	1.50
AF-20-66		Phenocryst	Rim	60.16	0.15	24.48	0.66	0.06	6.24	7.52	0.90	0.11	0.13	100.41	64.90	29.77	5.10
AF-20-66		Micro-Phenocryst	Intermediate	47.15	0.09	32.83	0.88	0.09	16.41	1.91	0.06	0.09	0.05	99.56	17.28	82.24	0.38
AF-20-66		Micro-Phenocryst	Intermediate	47.73	0.06	32.46	0.84	0.10	15.78	2.25	0.06	0.12	0.06	99.46	20.38	79.18	0.34
AF-20-66		Micro-Phenocryst	Intermediate	48.63	0.10	31.80	0.81	0.12	15.23	2.62	0.07	0.10	0.07	99.53	23.62	75.84	0.42
AF-20-66		Micro-Phenocryst	Intermediate	47.10	0.09	32.75	0.80	0.10	16.52	2.00	0.06	0.07	0.04	99.52	17.88	81.72	0.32
AF-20-66		Micro-Phenocryst	Intermediate	48.14	0.08	32.08	0.77	0.11	15.64	2.40	0.07	0.12	0.03	99.44	21.61	77.92	0.42
AF-20-66		Micro-Phenocryst	Intermediate	48.04	0.08	32.75	0.82	0.10	16.06	2.17	0.05	0.07	0.06	100.20	19.59	80.03	0.27
AF-20-66		Micro-Phenocryst	Intermediate	53.03	0.12	28.45	0.82	0.14	11.80	4.68	0.17	0.11	0.06	99.37	41.32	57.57	1.00
AF-20-66		Micro-Phenocryst	Intermediate	53.43	0.14	28.52	0.81	0.13	11.66	4.78	0.19	0.12	0.07	99.83	42.05	56.71	1.12
AF-20-66		Micro-Phenocryst	Intermediate	53.20	0.13	28.64	0.82	0.13	11.50	4.66	0.22	0.10	0.07	99.48	41.70	56.87	1.32
AF-20-66		Micro-Phenocryst	Intermediate	54.42	0.15	27.51	0.79	0.11	9.90	5.80	0.34	0.09	0.07	99.16	50.42	47.52	1.94
AF-20-66		Phenocryst	Core	47.04	0.08	33.06	0.66	0.15	16.49	1.95	0.05	0.07	0.06	99.58	17.53	82.10	0.27
AF-20-66		Phenocryst	Intermediate	47.27	0.09	32.98	0.69	0.14	16.32	1.96	0.05	0.07	0.07	99.62	17.78	81.82	0.29
AF-20-66		Phenocryst	Rim	52.16	0.12	29.35	0.81	0.13	12.67	4.15	0.17	0.14	0.07	99.75	36.80	62.10	0.97
AF-20-66		Groundmass		51.80	0.15	29.59	0.88	0.14	12.69	4.14	0.20	0.09	0.06	99.73	36.65	62.09	1.15
AF-20-66		Groundmass		55.00	0.14	27.62	0.72	0.10	10.54	5.29	0.31	0.12	0.06	99.90	46.67	51.40	1.82
AF-20-66		Groundmass		52.30	0.15	29.24	0.80	0.16	12.41	4.27	0.17	0.10	0.07	99.66	37.95	60.97	0.97
AF-20-66		Groundmass		52.87	0.13	28.89	0.91	0.15	12.19	4.50	0.20	0.11	0.08	100.03	39.53	59.15	1.18
AF-20-66		Phenocryst	Core	47.35	0.05	32.73	0.70	0.15	16.47	1.98	0.05	0.05	0.06	99.58	17.78	81.85	0.27
AF-20-66		Phenocryst	Rim	52.15	0.14	29.52	0.82	0.15	12.68	4.10	0.15	0.12	0.07	99.90	36.56	62.43	0.89
AF-20-66		Micro-Phenocryst	Core	48.38	0.12	31.98	0.87	0.10	15.38	2.60	0.08	0.11	0.04	99.66	23.31	76.13	0.48
AF-20-66		Micro-Phenocryst	Intermediate	49.86	0.11	31.03	0.87	0.13	14.25	3.13	0.11	0.12	0.08	99.69	28.20	71.01	0.64
AF-20-66		Micro-Phenocryst	Rim	52.72	0.14	28.73	0.86	0.14	12.00	4.59	0.21	0.11	0.09	99.59	40.31	58.30	1.24
AF-20-25		Micro-Phenocryst	Core	53.17	0.12	28.79	0.67	0.14	11.76	4.46	0.18	0.11	0.07	99.47	40.19	58.63	1.04
AF-20-25		Micro-Phenocryst	Rim	50.38	0.11	30.63	0.78	0.16	14.15	3.30	0.12	0.05	0.06	99.74	29.46	69.75	0.68
AF-20-25		Groundmass		53.24	0.17	28.68	1.06	0.20	11.91	4.44	0.22	0.04	0.06	100.01	39.75	58.85	1.30
AF-20-25		Groundmass		52.95	0.17	28.61	1.06	0.19	11.86	4.40	0.24	0.09	0.07	99.64	39.55	58.90	1.43
AF-20-25		Phenocryst	Core	54.50	0.10	27.92	0.62	0.10	10.70	5.21	0.21	0.10	0.07	99.52	46.17	52.46	1.25
AF-20-25		Phenocryst	Rim	52.14	0.14	29.23	0.73	0.17	12.55	4.15	0.16	0.05	0.07	99.39	37.05	61.90	0.93
AF-20-25		Micro-Phenocryst	Core	46.71	0.08	33.09	0.60	0.11	16.59	1.87	0.05	0.07	0.06	99.20	16.85	82.76	0.29
AF-20-25		Micro-Phenocryst	Rim	49.32	0.09	30.81	0.83	0.17	14.53	3.10	0.12	0.06	0.06	99.07	27.63	71.59	0.67
AF-20-25		Phenocryst	Core	49.00	0.05	31.59	0.71	0.13	15.10	2.63	0.08	0.05	0.06	99.41	23.82	75.57	0.50
AF-20-25		Phenocryst	Intermediate	51.08	0.11	30.06	0.72	0.17	13.37	3.71	0.14	0.08	0.04	99.47	33.13	66.00	0.79
AF-20-25		Phenocryst	Rim	49.35	0.09	31.27	0.76	0.15	14.58	3.00	0.11	0.07	0.06	99.42	26.91	72.33	0.65
AF-20-25		Micro-Phenocryst	Core	50.62	0.10	30.41	0.70	0.13	13.77	3.40	0.12	0.11	0.06	99.42	30.60	68.59	0.69

AF-20-25	Micro-Phenocryst	Rim	51.13	0.14	30.12	0.90	0.16	13.56	3.51	0.16	0.08	0.07	99.82	31.58	67.35	0.95
AF-20-25	Micro-Phenocryst	Core	48.55	0.11	31.87	0.68	0.16	15.25	2.62	0.07	0.04	0.07	99.41	23.55	75.91	0.42
AF-20-25	Micro-Phenocryst	Rim	53.92	0.19	27.91	1.21	0.18	11.18	4.71	0.26	0.07	0.07	99.69	42.54	55.80	1.54
AF-20-25	Micro-Phenocryst	Core	48.03	0.08	32.35	0.72	0.15	15.73	2.37	0.05	0.08	0.06	99.61	21.33	78.26	0.31
AF-20-25	Micro-Phenocryst	Rim	50.63	0.14	30.07	1.00	0.21	13.69	3.47	0.15	0.06	0.07	99.50	31.15	67.82	0.90
AF-20-25	Groundmass		52.99	0.16	28.62	1.06	0.16	11.73	4.67	0.25	0.06	0.05	99.75	41.21	57.25	1.45
AF-20-25	Groundmass		52.83	0.16	28.62	0.96	0.18	11.84	4.58	0.23	0.09	0.08	99.57	40.57	57.96	1.33
AF-20-25	Groundmass		53.13	0.19	28.62	1.05	0.18	11.71	4.54	0.24	0.04	0.07	99.77	40.59	57.88	1.41
AF-20-25	Groundmass		53.10	0.19	28.59	1.23	0.19	11.68	4.43	0.25	0.06	0.07	99.78	40.07	58.34	1.47
AF-20-25	Groundmass		53.23	0.18	28.42	1.20	0.18	11.78	4.49	0.25	0.10	0.07	99.89	40.17	58.25	1.45
AF-20-25	Groundmass		53.24	0.20	28.50	1.08	0.17	11.72	4.44	0.24	0.07	0.07	99.73	40.06	58.41	1.41

Sample	Crystal	Type	Size	Zone	SiO_2 (wt%)	TiO_2	Al_2O_3	Cr_2O_3	FeO	MnO	NiO	MgO	CaO	Total	Fo	Fa	Tp
Lower Stratoids																	
H436		Phenocryst		Core	38.15	0.05	0.03	0.00	22.25	0.35	0.14	38.89	0.30	100.16	75.10	24.11	0.39
H436		Phenocryst		Rim	35.90	0.08	0.01	0.02	33.55	0.52	0.07	28.76	0.32	99.23	59.78	39.13	0.62
H436		Groundmass			33.62	0.11	0.01	0.08	44.66	0.75	0.04	19.06	0.38	98.71	42.53	55.91	0.94
H436		Micro-Phenocryst		Core	35.28	0.07	0.03	0.00	37.05	0.57	0.05	26.27	0.34	99.65	55.17	43.64	0.68
H436		Micro-Phenocryst		Rim	32.95	0.07	0.02	0.00	48.56	0.86	0.01	16.59	0.38	99.45	37.20	61.09	1.10
H436		Micro-Phenocryst		Rim	36.95	0.06	0.02	0.04	29.10	0.42	0.08	32.64	0.29	99.60	66.06	33.04	0.48
H436		Micro-Phenocryst		Rim	34.13	0.12	0.01	0.00	42.54	0.70	0.02	20.54	0.34	98.39	45.59	52.98	0.88
H436		Groundmass			34.62	0.08	0.02	0.01	42.74	0.71	0.02	21.61	0.36	100.17	46.73	51.84	0.87
H436		Groundmass			33.67	0.08	0.01	0.05	46.61	0.81	0.03	17.16	0.35	98.77	38.98	59.40	1.04
H436		Groundmass			35.81	0.04	0.02	0.00	34.43	0.52	0.05	28.14	0.31	99.34	58.66	40.25	0.62
H436		Groundmass			32.28	0.14	0.04	0.04	51.73	0.98	0.02	13.29	0.32	98.83	30.83	67.34	1.29
H436		Micro-Phenocryst		Rim	38.11	0.06	0.03	0.01	22.13	0.33	0.11	38.82	0.30	99.89	75.18	24.04	0.36
H436		Micro-Phenocryst		Rim	36.28	0.02	0.02	0.01	33.27	0.48	0.05	29.19	0.32	99.62	60.37	38.60	0.56
H436		Groundmass			34.14	0.07	0.01	0.00	43.79	0.69	0.04	20.69	0.35	99.79	45.07	53.53	0.86
H436		Groundmass			32.00	0.10	0.02	0.00	53.71	1.06	0.02	11.86	0.39	99.17	27.67	70.27	1.41
H436		Micro-Phenocryst		Rim	38.53	0.04	0.03	0.05	21.58	0.32	0.12	38.92	0.30	99.87	75.69	23.54	0.36
H436		Micro-Phenocryst		Rim	37.04	0.07	0.02	0.00	28.98	0.40	0.08	32.65	0.31	99.54	66.15	32.94	0.46
H436		Groundmass			34.96	0.07	0.03	0.00	40.23	0.63	0.04	23.33	0.35	99.64	50.16	48.53	0.77
H436		Groundmass		Rim	35.60	0.07	0.02	0.00	36.16	0.58	0.07	26.57	0.33	99.39	56.03	42.77	0.69
H436		Groundmass		Rim	33.44	0.11	0.02	0.02	46.31	0.83	0.00	17.63	0.36	98.71	39.76	58.59	1.07
Upper Stratoids																	
AF-20-04	1	Groundmass	<100µ		34.91	0.04	0.01	0.06	43.44	0.67	0.03	20.60	0.35	100.11	45.17	53.44	0.84
AF-20-04	2	Groundmass	<250µ	Core	35.46	0.05	0.01	0.00	41.21	0.62	0.03	22.74	0.32	100.44	48.97	49.78	0.76
AF-20-04	2	Groundmass	<250µ	Rim	35.43	0.07	0.04	0.06	41.47	0.55	0.04	22.72	0.31	100.68	48.84	50.01	0.67
AF-20-04	3	Groundmass	<500µ		34.47	0.05	0.01	0.00	44.73	0.65	0.05	20.09	0.33	100.38	43.88	54.80	0.81
AF-20-04	4	Groundmass	<250µ	Core	32.12	0.23	0.00	0.01	55.95	0.92	0.03	11.27	0.38	100.91	25.94	72.24	1.20
AF-20-04	5	Micro-Phenocryst	<500µ	Core	36.79	0.06	0.00	0.00	33.05	0.46	0.06	29.97	0.29	100.67	61.18	37.85	0.54
AF-20-04	6	Groundmass	<250µ	Rim	33.43	0.09	0.00	0.00	50.25	0.87	0.00	14.93	0.38	99.94	34.02	64.23	1.13
AF-20-04	7	Groundmass	<250µ	Core	34.35	0.07	0.01	0.04	42.96	0.64	0.00	20.64	0.36	99.08	45.51	53.12	0.80
AF-20-04	8	Groundmass	<250µ	Core	34.27	0.09	0.01	0.05	44.56	0.61	0.00	20.36	0.36	100.30	44.30	54.39	0.75
AF-20-04	8	Groundmass	<250µ	Core	32.49	0.09	0.03	0.07	54.99	0.87	0.02	11.77	0.41	100.75	27.12	71.06	1.14
AF-20-04	9	Micro-Phenocryst	<500µ	Rim	32.95	0.06	0.00	0.00	53.49	0.86	0.01	13.20	0.37	100.94	30.03	68.25	1.11
AF-20-04	10	Micro-Phenocryst	<500µ	Core	36.56	0.08	0.14	0.00	34.54	0.46	0.02	27.93	0.34	100.08	58.41	40.52	0.55
AF-20-04	11	Micro-Phenocryst	<500µ	Core	35.65	0.05	0.00	0.00	37.58	0.51	0.06	25.76	0.31	99.93	54.40	44.52	0.62
AF-20-04	11	Micro-Phenocryst	<500µ	Rim	33.77	0.06	0.00	0.00	48.19	0.74	0.01	17.19	0.33	100.29	38.30	60.23	0.93
AF-20-04	12	Micro-Phenocryst	<500µ	Core	35.45	0.06	0.03	0.00	36.89	0.56	0.04	26.53	0.30	99.86	55.55	43.34	0.67
AF-20-04	12	Micro-Phenocryst	<500µ	Rim	33.90	0.08	0.02	0.00	46.65	0.74	0.03	18.66	0.34	100.42	41.02	57.51	0.92
AF-20-04	12	Micro-Phenocryst	<500µ	Core	36.67	0.05	0.03	0.06	31.82	0.45	0.03	30.85	0.28	100.23	62.76	36.31	0.52
AF-20-04	12	Micro-Phenocryst	<500µ	Rim	33.20	0.08	0.02	0.02	48.58	0.74	0.00	16.53	0.36	99.52	37.17	61.30	0.94
AF-20-04	13	Micro-Phenocryst	<500µ	Core	36.35	0.06	0.02	0.00	33.82	0.47	0.03	29.59	0.27	100.60	60.36	38.70	0.54
AF-20-04	13	Micro-Phenocryst	<500µ	Rim	34.35	0.15	0.01	0.00	44.55	0.69	0.03	20.19	0.31	100.27	44.10	54.57	0.85
AF-20-04	14	Groundmass	<250µ	Core	34.05	0.08	0.02	0.04	45.58	0.67	0.03	19.43	0.34	100.23	42.59	56.04	0.84
AF-20-04	15	Groundmass	<250µ	Rim	32.79	0.12	0.02	0.00	51.68	0.87	0.01	14.05	0.38	99.91	32.08	66.17	1.12
AF-20-04	16	Groundmass	<250µ	Core	35.38	0.06	0.02	0.00	38.25	0.53	0.02	26.23	0.31	100.79	54.41	44.51	0.62
AF-20-04	16	Groundmass	<250µ	Rim	31.74	0.11	0.02	0.00	57.00	1.00	0.02	9.44	0.43	99.76	22.32	75.60	1.34
AF-20-04	17	Groundmass	<250µ	Core	32.97	0.06	0.02	0.00	49.70	0.78	0.01	16.48	0.35	100.37	36.57	61.89	0.98
AF-20-04	18	Groundmass	<250µ	Core	32.94	0.11	0.04	0.02	50.30	0.75	0.02	15.56	0.37	100.10	34.99	63.46	0.96
AF-20-04	19	Groundmass	<250µ	Core	35.13	0.04	0.02	0.00	39.27	0.52	0.02	25.18	0.33	100.51	52.74	46.14	0.62
AF-20-04	19	Groundmass	<250µ	Core	34.74	0.08	0.01	0.00	40.79	0.54	0.03	24.33	0.34	100.85	50.94	47.91	0.64
AF-20-04	19	Groundmass	<250µ	Rim	32.14	0.14	0.01	0.00	53.65	0.84	0.01	13.24	0.40	100.43	30.03	68.24	1.08
AF-20-04	20	Groundmass	<100µ	Core	34.00	0.10	0.02	0.06	44.74	0.63	0.03	20.84	0.36	100.78	44.78	53.91	0.77

AF-20-04	21	Groundmass	<250µ	Core	35.48	0.07	0.03	0.00	37.42	0.54	0.04	26.77	0.30	100.65	55.44	43.48	0.63
AF-20-04	22	Groundmass	<100µ	Core	33.43	0.09	0.02	0.01	48.15	0.75	0.01	17.57	0.39	100.43	38.79	59.64	0.95
AF-20-04	23	Groundmass	<250µ	Core	34.94	0.08	0.02	0.00	40.40	0.57	0.03	24.01	0.29	100.34	50.86	48.01	0.68
AF-20-04	23	Groundmass	<250µ	Rim	33.27	0.07	0.01	0.02	49.19	0.78	0.00	16.46	0.34	100.14	36.79	61.68	0.98
AF-20-04	24	Groundmass	<250µ	Core	34.91	0.08	0.02	0.02	41.27	0.60	0.00	23.10	0.34	100.33	49.33	49.43	0.72
AF-20-04	26	Groundmass	<100µ	Core	34.18	0.07	0.02	0.02	44.57	0.62	0.00	20.78	0.35	100.62	44.79	53.90	0.76
AF-20-04	29	Groundmass	<100µ	Core	35.85	0.06	0.01	0.01	37.77	0.53	0.03	25.94	0.33	100.53	54.42	44.45	0.63
AF-20-04					33.37	0.11	0.02	0.04	48.88	0.74	0.01	16.30	0.35	99.81	36.71	61.77	0.94
AF-20-04	32	Groundmass	<200µ	Core	33.96	0.05	0.01	0.00	46.01	0.71	0.03	19.07	0.37	100.21	41.87	56.66	0.88
AF-20-04	33	Groundmass	<50µ		30.52	0.17	0.01	0.04	61.16	1.29	0.00	5.76	0.36	99.49	14.03	83.55	1.78
AF-20-04	34	Groundmass	<50µ		31.01	0.17	0.02	0.03	59.79	1.12	0.00	7.21	0.33	99.89	17.32	80.59	1.52
AF-20-19	1	Groundmass			33.14	0.10	0.02	0.00	51.24	0.82	0.00	15.16	0.24	100.73	34.04	64.52	1.05
AF-20-19	2	Groundmass			33.26	0.13	0.01	0.01	49.99	0.77	0.04	15.62	0.26	100.09	35.26	63.33	0.99
AF-20-19	3	Groundmass			33.17	0.09	0.01	0.00	49.60	0.80	0.03	16.13	0.23	100.04	36.19	62.43	1.01
AF-20-19	4	Groundmass			33.29	0.13	0.01	0.00	51.10	0.80	0.03	15.16	0.23	100.74	34.11	64.50	1.02
AF-20-19	5	Groundmass			33.04	0.09	0.01	0.02	50.49	0.75	0.03	15.52	0.25	100.20	34.92	63.72	0.96
AF-20-19	6	Groundmass			32.60	0.15	0.02	0.00	51.13	0.82	0.03	14.57	0.26	99.58	33.19	65.33	1.06
Central Afar Gulf																	
AF-20-46	3	Groundmass			34.54	0.14	0.03	0.00	42.45	0.73	0.00	22.46	0.30	100.65	47.89	50.77	0.88
AF-20-46	6	Groundmass			34.92	0.12	0.04	0.02	39.94	0.66	0.03	23.78	0.34	99.83	50.80	47.87	0.80
AF-20-46	1	Micro-Phenocryst	<1500µ	Rim	36.85	0.04	0.07	0.03	30.59	0.46	0.03	31.06	0.39	99.52	63.70	35.19	0.54
AF-20-46	8	Groundmass	<150µ		33.47	0.16	0.02	0.01	48.29	0.83	0.02	17.46	0.38	100.64	38.55	59.81	1.04
AF-20-46	9	Groundmass	<150µ		34.57	0.08	0.02	0.00	43.60	0.74	0.01	21.44	0.36	100.81	46.03	52.51	0.90
AF-20-46	10			Rim	35.56	0.06	0.04	0.00	37.65	0.60	0.04	25.77	0.31	100.03	54.30	44.51	0.72
AF-20-46	11	Groundmass	<150µ		35.09	0.09	0.04	0.00	41.43	0.72	0.00	22.54	0.32	100.21	48.56	50.08	0.88
AF-20-46	12	Groundmass	<150µ		35.05	0.09	0.02	0.00	41.32	0.72	0.02	23.23	0.38	100.83	49.33	49.22	0.87
AF-20-46	13	Groundmass	<150µ		33.81	0.16	0.11	0.01	45.95	0.85	0.02	18.15	0.39	99.44	40.61	57.68	1.09
AF-20-46	14	Groundmass	<150µ		35.14	0.12	0.04	0.00	39.86	0.69	0.03	23.70	0.32	99.90	50.76	47.90	0.84
AF-20-46	15	Groundmass	<150µ	Core	37.08	0.06	0.04	0.00	29.39	0.41	0.05	33.03	0.30	100.36	66.11	33.00	0.47
AF-20-46	16	Groundmass	<150µ	Rim	36.14	0.09	0.04	0.00	33.76	0.56	0.05	28.94	0.34	99.91	59.74	39.09	0.66
AF-20-46	17	Groundmass	<150µ		34.71	0.09	0.02	0.02	40.12	0.67	0.01	23.11	0.37	99.11	49.96	48.65	0.82
AF-20-46	18	Micro-Phenocryst	<1000µ	Core	39.09	0.04	0.03	0.03	19.96	0.32	0.07	40.87	0.30	100.70	77.90	21.34	0.34
AF-20-46	18	Micro-Phenocryst	<1000µ	Rim	36.90	0.06	0.09	0.04	31.40	0.47	0.04	31.61	0.31	100.92	63.58	35.43	0.54
AF-20-46	19	Groundmass			36.02	0.08	0.03	0.02	35.28	0.55	0.03	27.88	0.28	100.17	57.86	41.07	0.65
AF-20-46	20	Micro-Phenocryst	<500µ	Core	39.12	0.04	0.03	0.01	20.75	0.30	0.05	40.07	0.30	100.68	76.91	22.35	0.32
AF-20-46	20	Micro-Phenocryst	<500µ	Intermediate	37.26	0.04	0.02	0.00	30.28	0.49	0.04	32.39	0.30	100.82	64.95	34.06	0.56
AF-20-46	20	Micro-Phenocryst	<500µ	Rim	36.46	0.08	0.02	0.00	33.55	0.56	0.02	29.49	0.30	100.48	60.38	38.53	0.65
AF-20-46	21	Micro-Phenocryst	<1000µ	Core	39.38	0.04	0.12	0.06	20.24	0.34	0.05	40.36	0.36	100.94	77.38	21.76	0.37
AF-20-46	21	Micro-Phenocryst	<1000µ	Intermediate	38.94	0.06	0.04	0.00	20.73	0.33	0.07	40.34	0.31	100.81	77.02	22.20	0.35
AF-20-46	21	Micro-Phenocryst	<1000µ	Intermediate	38.98	0.04	0.03	0.03	20.91	0.31	0.07	40.16	0.32	100.84	76.80	22.43	0.33
AF-20-46	21	Micro-Phenocryst	<1000µ	Intermediate	39.03	0.03	0.03	0.01	20.58	0.30	0.08	40.46	0.31	100.84	77.21	22.03	0.33
AF-20-46	21	Micro-Phenocryst	<1000µ	Intermediate	38.97	0.04	0.03	0.00	20.81	0.30	0.09	40.23	0.30	100.74	76.94	22.32	0.32
AF-20-46	21	Micro-Phenocryst	<1000µ	Intermediate	36.88	0.06	0.01	0.01	32.08	0.51	0.03	30.80	0.30	100.68	62.47	36.50	0.59
AF-20-46	21	Micro-Phenocryst	<1000µ	Intermediate	36.39	0.07	0.03	0.00	34.92	0.58	0.02	28.45	0.33	100.79	58.54	40.30	0.68
AF-20-46	21	Micro-Phenocryst	<1000µ	Rim	36.07	0.05	0.02	0.01	36.08	0.56	0.03	27.24	0.32	100.37	56.72	42.14	0.66
AF-20-46	22	Phenocryst	<1500µ	Core	39.24	0.05	0.03	0.00	20.20	0.29	0.08	40.14	0.30	100.34	77.41	21.85	0.32
AF-20-46	22	Phenocryst	<1500µ	Intermediate	39.08	0.04	0.04	0.08	20.31	0.30	0.06	40.52	0.30	100.73	77.47	21.79	0.33
AF-20-46	22	Phenocryst	<1500µ	Intermediate	39.20	0.02	0.03	0.02	20.59	0.31	0.08	40.39	0.32	100.96	77.16	22.07	0.33
AF-20-46	22	Phenocryst	<1500µ	Intermediate	39.18	0.03	0.03	0.03	20.47	0.33	0.08	40.42	0.30	100.86	77.28	21.95	0.36
AF-20-46	22	Phenocryst	<1500µ	Intermediate	39.26	0.05	0.03	0.03	20.75	0.31	0.10	40.11	0.31	100.94	76.92	22.32	0.34
AF-20-46	22	Phenocryst	<1500µ	Intermediate	39.71	0.04	0.13	0.01	20.55	0.31	0.07	39.11	0.35	100.27	76.59	22.57	0.35
AF-20-46	22	Phenocryst	<1500µ	Intermediate	39.80	0.04	0.11	0.01	20.35	0.28	0.05	38.73	0.37	99.74	76.59	22.57	0.31
AF-20-46	22	Phenocryst	<1500µ	Intermediate	39.47	0.05	0.08	0.00	21.06	0.34	0.03	39.29	0.33	100.64	76.24	22.93	0.37
AF-20-46	22	Phenocryst	<1500µ	Intermediate	37.24	0.03	0.02	0.00	30.82	0.47	0.04	31.64	0.34	100.58	64.00	34.97	0.53

AF-20-46	22	Phenocryst	<1500µ	Rim	36.67	0.07	0.02	0.00	33.83	0.56	0.02	28.77	0.34	100.29	59.55	39.28	0.66
AF20-66		Groundmass		Core	37.26	0.05	0.03	0.00	27.92	0.50	0.05	34.22	0.35	100.36	67.88	31.07	0.56
AF20-66		Groundmass		Rim	33.60	0.11	0.02	0.07	43.38	0.97	0.03	20.23	0.33	98.73	44.61	53.65	1.21
AF20-66		Groundmass			33.22	0.11	0.04	0.00	44.29	1.05	0.03	19.40	0.44	98.58	42.96	55.02	1.32
AF20-66		Groundmass		Core	36.16	0.05	0.02	0.00	32.05	0.57	0.02	30.00	0.35	99.22	61.79	37.02	0.67
AF20-66		Groundmass		Rim	32.94	0.44	0.02	0.01	48.36	1.01	0.00	16.36	0.28	99.41	36.96	61.30	1.29
AF20-66		Groundmass			33.98	0.14	0.02	0.01	43.50	1.00	0.01	20.19	0.40	99.25	44.42	53.69	1.25
AF20-66	1	Micro-Phenocryst		Core	37.89	0.03	0.02	0.04	23.99	0.36	0.08	37.89	0.29	100.60	73.19	26.00	0.40
AF20-66	1	Micro-Phenocryst		Rim	36.20	0.03	0.02	0.01	31.40	0.57	0.06	30.41	0.33	99.02	62.60	36.25	0.67
AF20-66	1	Micro-Phenocryst		Rim	36.66	0.07	0.03	0.01	30.15	0.54	0.04	31.80	0.32	99.62	64.57	34.34	0.63
AF20-66	2	Micro-Phenocryst		Core	38.04	0.05	0.03	0.00	22.79	0.39	0.09	38.02	0.29	99.69	74.21	24.95	0.44
AF20-66	2	Micro-Phenocryst		Rim	34.64	0.06	0.01	0.03	40.10	0.85	0.03	22.88	0.34	98.95	49.63	48.79	1.05
AF20-66	3	Micro-Phenocryst		Core	36.66	0.03	0.02	0.01	30.43	0.57	0.00	31.68	0.29	99.69	64.28	34.64	0.65
AF20-66	3	Micro-Phenocryst		Rim	35.52	0.06	0.02	0.03	36.25	0.68	0.02	27.32	0.36	100.27	56.56	42.11	0.80
AF20-66		Groundmass			35.71	0.07	0.02	0.02	33.79	0.62	0.02	29.04	0.33	99.61	59.77	39.01	0.73
AF20-66		Micro-Phenocryst		Core	36.55	0.07	0.03	0.00	30.71	0.58	0.03	30.98	0.33	99.27	63.52	35.32	0.67
AF20-66		Micro-Phenocryst		Rim	35.72	0.06	0.02	0.00	33.85	0.65	0.01	28.58	0.35	99.22	59.31	39.41	0.76
AF20-66		Groundmass			33.65	0.15	0.04	0.01	44.93	1.02	0.00	18.96	0.41	99.16	42.09	55.97	1.29
AF20-66		Groundmass		Core	36.59	0.04	0.02	0.00	29.98	0.52	0.05	32.68	0.29	100.17	65.35	33.64	0.59
AF20-66		Groundmass		Rim	34.77	0.08	0.01	0.00	39.90	0.87	0.01	24.18	0.34	100.14	51.11	47.32	1.05
AF20-66		Groundmass		Core	36.27	0.05	0.03	0.02	30.68	0.54	0.03	31.42	0.30	99.34	63.92	35.02	0.63
AF20-66		Groundmass			33.27	0.10	0.02	0.00	44.99	1.12	0.00	18.64	0.40	98.54	41.61	56.34	1.42
AF20-66		Micro-Phenocryst		Core	38.01	0.04	0.05	0.00	21.39	0.36	0.09	39.44	0.32	99.69	76.04	23.13	0.40
AF20-66		Micro-Phenocryst		Rim	35.71	0.08	0.02	0.00	33.55	0.68	0.04	28.29	0.32	98.67	59.28	39.43	0.81
AF20-66		Groundmass			33.95	0.12	0.01	0.00	43.20	1.02	0.00	20.57	0.39	99.25	45.06	53.07	1.27
AF-20-25		Micro-Phenocryst		Core	38.68	0.03	0.03	0.00	19.78	0.32	0.10	40.55	0.25	99.75	77.97	21.34	0.35
AF-20-25		Groundmass			35.59	0.11	0.04	0.00	33.58	0.61	0.03	28.42	0.29	98.66	59.44	39.40	0.72
AF-20-25		Groundmass			35.06	0.16	0.03	0.00	35.82	0.67	0.03	26.72	0.30	98.79	56.36	42.38	0.80
AF-20-25		Micro-Phenocryst		Core	38.64	0.03	0.04	0.03	18.62	0.29	0.13	41.73	0.27	99.76	79.45	19.88	0.31
AF-20-25		Micro-Phenocryst		Core	38.39	0.06	0.03	0.00	20.54	0.33	0.08	39.81	0.26	99.50	76.99	22.28	0.37
AF-20-25		Micro-Phenocryst		Rim	36.53	0.07	0.04	0.02	30.29	0.48	0.05	31.81	0.28	99.57	64.56	34.48	0.55
AF-20-25		Micro-Phenocryst		Core	38.20	0.03	0.03	0.02	21.12	0.35	0.08	39.40	0.24	99.48	76.33	22.95	0.38
AF-20-25		Micro-Phenocryst		Core	37.96	0.03	0.03	0.01	23.57	0.38	0.06	37.46	0.24	99.74	73.36	25.89	0.42
AF-20-25		Micro-Phenocryst		Core	37.96	0.05	0.03	0.00	21.33	0.38	0.10	39.21	0.25	99.31	76.03	23.20	0.42
AF-20-25		Phenocryst		Core	38.64	0.05	0.04	0.05	20.19	0.30	0.12	40.83	0.26	100.46	77.76	21.57	0.32
AF-20-25		Phenocryst		Rim	37.16	0.07	0.03	0.02	28.13	0.47	0.06	33.17	0.30	99.41	67.10	31.93	0.54
AF-20-25		Groundmass			35.74	0.10	0.05	0.00	30.34	0.50	0.06	31.02	0.33	98.13	63.88	35.05	0.59
AF-20-25		Phenocryst		Core	38.56	0.02	0.03	0.00	19.99	0.31	0.12	40.27	0.26	99.56	77.67	21.63	0.34
AF-20-25		Phenocryst		Rim	36.53	0.10	0.03	0.00	29.62	0.47	0.06	32.25	0.27	99.33	65.38	33.69	0.54
AF-20-25		Groundmass			35.67	0.15	0.04	0.02	33.77	0.61	0.03	28.23	0.36	98.86	59.09	39.66	0.72
AF-20-25		Groundmass			36.69	0.10	0.04	0.02	27.55	0.44	0.04	33.64	0.35	98.87	67.82	31.17	0.51
AF-20-25		Groundmass			34.82	0.14	0.04	0.06	35.86	0.69	0.04	26.31	0.32	98.28	55.92	42.76	0.83
AF-20-25		Groundmass			34.24	0.15	0.05	0.00	39.46	0.76	0.02	23.12	0.33	98.12	50.34	48.21	0.94
AF-20-25		Groundmass			35.54	0.13	0.04	0.00	33.39	0.61	0.01	28.46	0.32	98.51	59.58	39.21	0.73
AF-20-25		Groundmass			35.66	0.14	0.13	0.01	35.44	0.66	0.04	26.55	0.30	98.93	56.46	42.28	0.80
AF-20-25		Groundmass			35.54	0.14	0.17	0.00	32.38	0.64	0.04	30.32	0.25	99.49	61.84	37.05	0.74
AF-20-25		Groundmass			35.19	0.18	0.03	0.00	36.78	0.78	0.01	25.96	0.29	99.21	54.95	43.68	0.93
AF-20-25		Groundmass		Core	36.87	0.09	0.05	0.00	26.33	0.47	0.06	35.01	0.36	99.24	69.59	29.36	0.53
AF-20-25		Groundmass		Rim	36.10	0.14	0.21	0.03	33.60	0.67	0.04	28.22	0.39	99.39	59.13	39.49	0.80
AF-20-25		Groundmass			35.07	0.15	0.04	0.02	35.33	0.65	0.03	27.01	0.36	98.66	56.92	41.76	0.77
AF-20-25		Groundmass		Core	36.67	0.07	0.03	0.00	27.71	0.46	0.07	33.48	0.33	98.82	67.61	31.38	0.53
AF-20-25		Groundmass		Rim	34.51	0.14	0.03	0.00	38.84	0.72	0.01	24.12	0.26	98.63	51.87	46.86	0.88
AF-20-25		Groundmass			35.86	0.10	0.04	0.00	31.58	0.58	0.03	30.54	0.33	99.07	62.55	36.29	0.68
AF-20-25		Groundmass			36.31	0.12	0.04	0.02	30.51	0.52	0.04	31.83	0.37	99.75	64.29	34.58	0.60
AF-20-25		Groundmass			36.46	0.11	0.05	0.02	33.65	0.66	0.03	27.98	0.35	99.31	58.93	39.76	0.79

Sample	Crystal	Type	Size	Zone	SiO_2 (wt%)	TiO_2	Al_2O_3	Cr_2O_3	Fe_2O_3	FeO	MnO	NiO	MgO	CaO	Na_2O	K_2O	sum	En	Fe	Wo	Mg#
Lower Stratoids																					
H436	1	Micro-Phenocryst		Core	48.88	1.46	4.43	0.22	2.90	6.33	0.18	0.00	14.41	20.39	0.31	0.00	99.51	42.16	14.97	42.87	0.74
H436	1	Micro-Phenocryst		Rim	50.32	1.37	1.91	0.00	0.53	12.14	0.31	0.00	13.25	18.77	0.27	0.00	98.87	38.99	21.33	39.68	0.65
H436		Groundmass			50.87	1.12	2.59	0.15	1.37	8.25	0.19	0.00	15.16	19.49	0.30	0.01	99.49	43.81	15.70	40.49	0.74
H436		Groundmass			50.37	1.32	2.40	0.02	0.93	9.15	0.20	0.00	14.37	19.56	0.30	0.00	98.62	42.08	16.75	41.18	0.72
H436		Groundmass			50.67	1.01	1.22	0.01	0.52	13.43	0.35	0.00	13.18	17.91	0.27	0.00	98.57	38.72	23.47	37.81	0.62
H436		Groundmass			51.48	1.03	2.27	0.10	0.76	8.53	0.24	0.00	15.09	19.97	0.26	0.01	99.73	43.42	15.27	41.30	0.74
H436		Groundmass			51.36	1.15	1.80	0.01	0.47	10.64	0.27	0.00	14.20	19.26	0.33	0.00	99.48	41.28	18.49	40.24	0.69
H436		Groundmass			50.62	1.23	2.19	0.04	1.04	9.19	0.29	0.00	14.44	19.62	0.27	0.01	98.92	41.98	17.01	41.01	0.71
Upper Stratoids																					
AF20-04	1	Groundmass	<100µ		51.70	1.32	1.86	0.05	0.00	13.20	0.32	0.00	14.63	17.41	0.21	0.00	100.69	42.13	21.84	36.03	0.66
AF20-04	2	Groundmass	<250µ		52.93	0.91	1.54	0.07	0.00	9.99	0.24	0.00	15.62	18.97	0.25	0.01	100.52	44.63	16.41	38.96	0.73
AF20-04	3	Groundmass	<250µ	Core	51.51	1.31	1.96	0.00	0.00	11.96	0.34	0.02	14.42	17.81	0.22	0.02	99.55	42.26	20.23	37.51	0.68
AF20-04	3	Groundmass	<250µ	Rim	51.99	0.70	1.00	0.01	0.00	17.70	0.47	0.00	14.16	13.70	0.19	0.00	99.93	41.40	29.81	28.79	0.58
AF20-04	4	Groundmass	<250µ		52.07	1.13	2.00	0.06	0.00	10.96	0.26	0.00	15.45	18.02	0.27	0.00	100.23	44.52	18.15	37.33	0.71
AF20-04	5	Groundmass	<250µ	Core	51.78	1.19	1.93	0.03	0.74	11.63	0.29	0.01	14.99	18.07	0.26	0.00	100.92	42.78	20.15	37.06	0.68
AF20-04	5	Groundmass	<250µ	Rim	51.36	1.11	1.94	0.01	1.79	10.76	0.34	0.00	15.05	18.13	0.26	0.01	100.76	42.75	20.26	36.99	0.68
AF20-04	6	Groundmass	<250µ		52.83	0.93	1.61	0.06	0.00	10.61	0.27	0.03	15.46	18.58	0.21	0.00	100.58	44.27	17.49	38.24	0.72
AF20-04	8	Groundmass	<250µ		52.64	0.90	1.41	0.02	0.00	11.65	0.32	0.00	15.32	17.61	0.18	0.01	100.06	44.16	19.36	36.48	0.70
AF20-04	9	Micro-Phenocryst	<500µ	Core	51.90	1.03	2.06	0.23	0.12	9.63	0.27	0.02	15.76	18.68	0.23	0.00	99.92	45.29	16.13	38.58	0.74
AF20-04	9	Micro-Phenocryst	<500µ	Rim	51.33	1.02	1.68	0.00	0.00	15.94	0.42	0.00	12.97	16.85	0.19	0.01	100.41	37.85	26.80	35.35	0.59
AF20-04	10	Groundmass	<250µ		52.39	1.02	1.49	0.04	0.16	12.09	0.30	0.02	15.23	17.98	0.21	0.00	100.92	43.28	20.00	36.73	0.68
AF20-04	11	Groundmass	<250µ		52.48	0.94	1.58	0.02	0.00	10.72	0.27	0.02	15.68	18.21	0.20	0.00	100.12	44.88	17.65	37.47	0.72
AF20-04	12	Groundmass	<250µ		51.59	1.01	1.92	0.10	0.00	10.65	0.27	0.02	15.03	18.45	0.20	0.00	99.24	43.67	17.80	38.53	0.71
AF20-04	13	Groundmass	<250µ		51.97	1.10	1.96	0.07	0.00	10.81	0.28	0.00	15.51	18.18	0.19	0.00	100.07	44.58	17.88	37.54	0.71
AF20-04	13	Groundmass	<250µ		51.99	1.10	1.72	0.01	0.00	12.29	0.29	0.01	14.64	17.90	0.24	0.01	100.18	42.36	20.42	37.22	0.67
AF20-04	15	Groundmass	<250µ	Core	52.02	0.95	1.73	0.10	0.86	9.12	0.26	0.00	15.94	18.85	0.24	0.00	100.06	45.31	16.18	38.51	0.74
AF20-04	15	Groundmass	<250µ	Rim	47.87	0.85	1.33	0.01	4.77	15.12	0.49	0.00	10.77	17.02	0.27	0.05	98.55	31.51	32.70	35.79	0.49
AF20-04	15	Groundmass	<250µ	Core	50.77	1.02	1.57	0.02	1.40	14.59	0.38	0.00	13.43	16.79	0.25	0.02	100.22	38.82	26.31	34.87	0.60
AF20-04	16	Groundmass	<250µ		51.24	1.20	1.90	0.02	1.24	11.10	0.32	0.00	15.21	17.78	0.22	0.01	100.24	43.42	20.10	36.48	0.68
AF20-04	22	Groundmass	<100µ	Core	51.55	1.03	1.46	0.01	1.60	11.43	0.31	0.00	15.17	17.48	0.30	0.01	100.34	43.18	21.06	35.76	0.67
AF20-04	22	Groundmass	<100µ	Core	50.63	1.05	1.71	0.01	1.57	14.46	0.39	0.00	13.62	16.62	0.23	0.00	100.27	39.27	26.30	34.43	0.60
AF20-04	23	Groundmass	<100µ	Core	51.88	0.93	1.61	0.08	1.65	8.24	0.24	0.00	16.33	18.78	0.26	0.01	100.01	46.10	15.80	38.11	0.74
AF20-04	24	Groundmass	<100µ	Core	51.17	1.19	1.92	0.04	1.46	11.10	0.32	0.00	15.21	17.57	0.26	0.00	100.23	43.48	20.42	36.10	0.68
AF20-04	24	Groundmass	<100µ	Rim	49.34	0.54	0.58	0.00	1.34	30.74	0.73	0.00	11.31	5.76	0.09	0.01	100.43	33.48	54.27	12.25	0.38
AF20-04	25	Groundmass	<100µ	Core	51.16	1.16	1.84	0.03	1.59	10.24	0.30	0.00	15.01	18.45	0.27	0.01	100.05	42.91	19.20	37.89	0.69
AF20-04	26	Groundmass	<250µ	Core	50.36	1.26	2.03	0.02	1.55	12.59	0.35	0.00	14.14	17.12	0.27	0.01	99.69	41.00	23.32	35.68	0.64
AF20-04	26	Groundmass	<250µ	Core	50.54	1.00	1.62	0.01	2.14	14.56	0.40	0.00	13.37	16.55	0.28	0.00	100.48	38.49	27.28	34.23	0.59
AF20-04	27	Groundmass	<250µ	Core	50.65	0.98	1.58	0.00	2.03	15.12	0.43	0.00	14.42	14.85	0.25	0.00	100.31	41.39	27.97	30.63	0.60
AF20-04	17	Groundmass	<100µ	Core	52.56	0.91	1.59	0.07	0.89	9.39	0.27	0.00	16.06	18.95	0.24	0.01	100.91	45.18	16.50	38.32	0.73
AF20-04	18	Groundmass	<100µ	Core	51.76	1.00	1.54	0.03	1.48	10.06	0.26	0.00	15.50	18.58	0.23	0.00	100.43	43.79	18.48	37.73	0.70
AF20-04	19	Groundmass	<100µ	Core	51.30	1.12	2.00	0.05	1.28	9.57	0.29	0.00	15.67	18.14	0.27	0.01	99.70	44.92	17.72	37.37	0.72
AF20-04	20	Groundmass	<100µ	Core	51.03	1.28	1.95	0.00	1.21	13.00	0.32	0.00	13.97	17.67	0.28	0.00	100.71	40.20	23.26	36.54	0.63
AF20-04	29	Groundmass	<250µ		51.82	1.03	1.73	0.05	1.02	9.53	0.27	0.00	15.52	18.95	0.25	0.00	100.16	44.15	17.11	38.74	0.72
AF20-04	28	Groundmass	<250µ	Core	51.32	1.29	1.93	0.03	1.26	11.29	0.29	0.00	15.09	17.77	0.27	0.00	100.54	43.11	20.39	36.50	0.68
AF20-04	21	Groundmass	<250µ	Core	51.28	0.94	1.30	0.01	1.17	13.80	0.35	0.00	13.97	17.10	0.25	0.02	100.19	40.15	24.52	35.34	0.62
AF20-04	21	Groundmass	<250µ	Core	52.09	0.95	1.73	0.08	0.80	9.56	0.27	0.00	15.76	18.77	0.25	0.00	100.25	44.81	16.84	38.35	0.73
AF20-04	30	Groundmass	<100µ	Core	52.28	1.01	1.59	0.01	0.38	11.37	0.28	0.00	15.45	17.96	0.26	0.00	100.59	44.04	19.18	36.78	0.70
AF20-04	31	Groundmass	<100µ	Core	50.94	0.92	1.48	0.00	0.38	16.43	0.39	0.00	12.11	17.11	0.29	0.02	100.07	35.58	28.29	36.13	0.56
AF20-04	32	Groundmass	<250µ	Core	52.87	0.83	1.73	0.11	0.00	9.77	0.26	0.00	16.17	18.80	0.21	0.00	100.74	45.79	15.93	38.28	0.74
AF20-04	32	Groundmass	<250µ	Core	50.68	1.27	1.99	0.01	1.03	13.74	0.39	0.00	13.66	17.24	0.25	0.00	100.27	39.60	24.49	35.91	0.62
AF20-04	33	Groundmass	<250µ		51.97	1.04	1.97	0.09	0.17	9.94	0.26	0.00	15.44	18.94	0.23	0.01	100.06	44.30	16.66	39.05	0.73
AF20-04	34	Groundmass	<250µ		51.08	1.32	1.88	0.02	0.86	12.45	0.35	0.00	14.23	17.72	0.30	0.00	100.19	41.15	22.02	36.83	0.65
AF20-04	35	Groundmass	<100µ	Core	51.43	1.13	1.92	0.05	1.22	10.52	0.31	0.00	15.40	18.13	0.22	0.00	100.32	43.85	19.05	37.10	0.70
AF20-04	35	Groundmass	<100µ	Intermediate	50.78	0.88	1.43	0.00	1.00	17.36	0.45	0.00	13.32	14.81	0.21	0.01	100.24	38.65	30.47	30.88	0.56
AF20-04	36	Groundmass	<100µ	Core	52.35	0.98	1.52	0.05	0.36	10.63	0.26	0.00	16.04	17.95	0.21	0.01	100.36	45.52	17.87	36.61	0.72
AF20-04	37	Groundmass	<50µ	Core	51.22	1.23	1.78	0.01	0.17	14.18	0.39	0.00	13.80	17.26	0.22	0.01	100.28	40.04	23.98	35.98	0.63
AF20-04	38	Groundmass	<50µ	Core	51.40	1.10	2.43	0.17	0.89	10.18	0.30	0.00	15.61	17.88	0.27	0.00	100.22	44.86	18.19	36.95	0.71

AF20-04	39	Groundmass	<50µ	Core	52.01	1.01	1.89	0.11	0.00	10.22	0.25	0.00	15.45	18.56	0.25	0.00	99.75	44.56	16.95	38.48	0.72
AF20-04	40	Groundmass	<50µ	Core	51.72	1.06	2.20	0.15	0.32	10.39	0.28	0.00	16.13	17.49	0.21	0.00	99.94	46.29	17.64	36.07	0.72
AF20-04	41	Groundmass	<100µ	Core	52.03	1.18	1.94	0.06	0.52	10.94	0.31	0.00	15.37	18.34	0.24	0.00	100.92	43.76	18.72	37.52	0.70
AF20-04	42	Groundmass	<250µ	Core	52.31	0.87	1.61	0.06	0.48	9.76	0.27	0.00	15.82	18.73	0.24	0.01	100.15	45.00	16.71	38.29	0.73
AF20-04	42	Groundmass	<250µ	Core	51.94	0.95	1.40	0.02	0.29	13.10	0.36	0.00	15.21	16.69	0.22	0.00	100.17	43.58	22.06	34.36	0.66
AF20-04					52.61	0.87	1.57	0.08	0.33	9.38	0.28	0.00	15.84	19.33	0.22	0.00	100.51	44.85	15.81	39.34	0.74
AF20-04					51.00	1.28	1.90	0.00	0.54	13.73	0.34	0.00	13.63	17.57	0.26	0.01	100.26	39.60	23.72	36.68	0.63
AF20-19	1	Groundmass		Core	51.75	1.11	1.77	0.00	0.28	12.04	0.32	0.00	14.75	17.94	0.26	0.01	100.24	42.47	20.38	37.14	0.68
AF20-19	1	Groundmass		Rim	51.99	0.44	0.49	0.00	0.00	24.30	0.64	0.00	17.50	4.05	0.06	0.01	99.47	50.86	40.68	8.46	0.56
AF20-19	2	Micro-Phenocryst		Core	49.86	1.71	3.51	0.00	1.74	9.79	0.25	0.00	14.11	19.09	0.33	0.00	100.38	41.08	18.98	39.95	0.68
AF20-19	2	Micro-Phenocryst		Intermediate	48.62	2.09	4.62	0.02	1.23	11.89	0.30	0.00	13.25	17.99	0.25	0.00	100.27	39.39	22.18	38.43	0.64
AF20-19	2	Micro-Phenocryst		Rim	51.62	0.54	0.64	0.00	0.00	24.69	0.68	0.00	17.11	4.41	0.06	0.01	99.74	49.57	41.24	9.18	0.55
AF20-19	3	Micro-Phenocryst		Core	49.54	1.69	3.74	0.01	1.42	10.54	0.30	0.00	14.20	18.07	0.31	0.00	99.81	41.79	20.00	38.21	0.68
AF20-19	3	Micro-Phenocryst		Rim	50.33	1.09	2.07	0.01	1.06	14.76	0.37	0.00	12.93	16.83	0.30	0.01	99.76	37.97	26.51	35.52	0.59
AF20-19	4	Groundmass			52.23	0.43	0.55	0.00	0.00	23.36	0.57	0.00	18.47	4.19	0.07	0.01	99.87	52.91	38.46	8.62	0.58
AF20-19	5	Groundmass			50.12	1.38	2.43	0.01	1.03	14.26	0.37	0.00	12.84	17.55	0.25	0.00	100.24	37.56	25.55	36.90	0.60
AF20-19	6	Groundmass		Core	51.84	1.13	1.76	0.00	0.48	11.10	0.25	0.00	14.94	18.50	0.29	0.00	100.28	42.88	18.96	38.16	0.69
AF20-19	6	Groundmass		Rim	51.32	0.45	0.52	0.01	0.00	27.18	0.64	0.00	15.66	4.15	0.08	0.01	100.01	45.71	45.58	8.71	0.50
AF20-19	7	Groundmass			51.20	1.18	2.00	0.00	0.14	12.16	0.34	0.00	13.92	18.49	0.27	0.01	99.71	40.60	20.65	38.75	0.66
AF20-19	8	Groundmass			50.77	0.46	0.45	0.00	0.00	28.37	0.68	0.00	14.67	4.28	0.07	0.01	99.76	43.09	47.87	9.04	0.47
AF20-19	9	Groundmass			52.37	0.41	0.50	0.00	0.00	23.19	0.65	0.00	18.44	4.09	0.08	0.00	99.74	53.05	38.48	8.46	0.58
AF20-19	10	Groundmass			51.44	1.09	1.80	0.00	0.75	11.51	0.33	0.00	14.66	18.32	0.23	0.00	100.12	42.06	20.16	37.78	0.68
AF20-19	11	Groundmass			51.90	0.42	0.52	0.01	0.00	24.17	0.56	0.00	17.78	4.17	0.07	0.00	99.61	51.30	40.04	8.65	0.56
Central Afar Gulf																					
AF20-46	1	Micro-Phenocryst	<500µ	Core	51.20	0.97	3.22	0.33	1.65	5.39	0.16	0.00	15.99	20.77	0.31	0.01	99.98	45.86	11.33	42.81	0.80
AF20-46	1	Micro-Phenocryst	<500µ	Rim	50.43	1.32	2.69	0.04	1.66	10.90	0.28	0.00	15.27	17.04	0.27	0.01	99.90	44.10	20.54	35.36	0.68
AF20-46	2	Micro-Phenocryst	<500µ	Rim	51.65	0.97	3.23	0.37	1.00	6.05	0.15	0.00	16.05	20.74	0.27	0.01	100.48	45.92	11.41	42.66	0.80
AF20-46	2	Micro-Phenocryst	<500µ	Core	53.12	0.62	1.92	0.22	0.43	6.74	0.20	0.00	17.44	19.51	0.23	0.00	100.42	49.02	11.55	39.43	0.81
AF20-46	3	Micro-Phenocryst	<250µ	Core	53.43	0.69	1.48	0.10	0.43	10.27	0.30	0.00	19.18	14.83	0.16	0.01	100.87	53.30	17.09	29.61	0.76
AF20-46	3	Micro-Phenocryst	<250µ	Intermediate	50.23	1.30	3.84	0.13	2.14	7.39	0.25	0.00	15.22	19.53	0.31	0.01	100.34	43.95	15.51	40.53	0.74
AF20-46	3	Micro-Phenocryst	<250µ	Rim	49.88	1.91	3.58	0.03	0.43	11.68	0.32	0.00	14.24	17.56	0.32	0.01	99.93	42.11	20.55	37.34	0.67
AF20-46	3	Micro-Phenocryst	<250µ	Intermediate	51.18	1.25	2.81	0.06	0.97	9.47	0.25	0.00	15.12	19.02	0.27	0.01	100.40	43.53	17.11	39.36	0.72
AF20-46	4	Groundmass	<150µ		49.43	2.14	4.33	0.08	0.83	10.52	0.26	0.00	14.74	17.66	0.28	0.01	100.28	43.47	19.09	37.44	0.69
AF20-46	5	Groundmass	<150µ		51.68	1.12	1.90	0.03	0.27	11.89	0.33	0.00	15.51	17.19	0.18	0.03	100.13	44.49	20.07	35.45	0.69
AF20-46	6	Groundmass	<150µ		51.80	1.03	1.65	0.00	0.73	13.12	0.38	0.00	15.15	16.46	0.26	0.02	100.58	43.38	22.74	33.88	0.66
AF20-46	7	Groundmass	<50µ	Core	49.74	1.58	3.95	0.06	1.65	9.07	0.27	0.00	15.06	18.26	0.27	0.01	99.92	43.97	17.72	38.31	0.71
AF20-46	8	Groundmass		Rim	50.85	1.19	2.00	0.01	1.27	11.80	0.37	0.00	14.35	17.70	0.30	0.02	99.84	41.54	21.63	36.83	0.66
AF20-46	9	Groundmass			50.99	1.17	2.29	0.05	0.66	12.65	0.35	0.00	15.99	15.26	0.21	0.00	99.61	46.24	22.05	31.71	0.68
AF20-46	10	Groundmass			48.56	2.14	4.24	0.08	2.39	9.48	0.28	0.00	13.82	18.73	0.34	0.01	100.06	40.70	19.67	39.63	0.67
AF20-46	11	Groundmass			49.81	1.70	3.06	0.02	1.30	12.59	0.34	0.00	14.25	16.43	0.35	0.02	99.87	41.95	23.29	34.75	0.64
AF20-46	12	Groundmass			49.56	1.84	2.90	0.00	1.96	13.19	0.39	0.00	13.80	16.56	0.32	0.01	100.53	40.22	25.09	34.69	0.62
AF20-46	13	Groundmass		Core	51.32	1.20	2.53	0.05	0.07	11.62	0.33	0.00	15.76	16.59	0.24	0.00	99.71	45.77	19.58	34.65	0.70
AF20-46	14	Groundmass		Rim	49.64	1.88	3.72	0.06	0.90	11.55	0.29	0.00	14.46	17.09	0.31	0.03	99.91	42.73	20.98	36.29	0.67
AF20-46	15	Groundmass	<150µ		52.97	0.67	1.70	0.13	0.96	8.83	0.25	0.00	19.11	15.62	0.16	0.01	100.40	53.22	15.53	31.25	0.77
AF20-46	16	Groundmass	<150µ		51.11	1.44	3.34	0.12	0.71	10.10	0.25	0.00	15.88	17.57	0.26	0.00	100.77	45.81	17.77	36.42	0.72
AF20-46	17	Groundmass	<150µ		49.94	1.58	2.72	0.00	1.74	12.41	0.34	0.00	14.00	17.19	0.29	0.01	100.23	40.71	23.36	35.93	0.64
AF20-46	18	Groundmass	<150µ		50.34	1.51	3.23	0.10	1.68	9.81	0.27	0.00	15.22	17.85	0.30	0.02	100.33	44.05	18.82	37.13	0.70
AF20-46	19	Groundmass	<150µ		50.04	1.67	3.28	0.12	1.41	10.16	0.30	0.00	13.86	19.28	0.31	0.02	100.43	40.41	19.19	40.40	0.68
AF20-46	20	Groundmass	<50µ		50.80	1.34	2.68	0.07	0.08	13.22	0.32	0.00	14.75	16.32	0.25	0.01	99.85	43.23	22.40	34.38	0.66
AF20-46	21	Groundmass	<50µ		49.66	1.90	3.68	0.00	0.10	14.05	0.38	0.00	13.10	16.29	0.42	0.16	99.73	39.76	24.73	35.51	0.62
AF20-46	22	Groundmass	<50µ		51.33	0.97	2.04	0.00	1.27	11.74	0.38	0.00	16.00	15.88	0.26	0.02	99.91	45.90	21.36	32.73	0.68
AF20-46	23	Groundmass	<150µ	Core	50.72	1.20	3.94	0.29	1.56	6.66	0.14	0.00	15.52	20.16	0.30	0.02	100.50	44.84	13.31	41.85	0.77
AF20-46	24	Groundmass	<150µ	Rim	50.02	1.67	3.14	0.01	2.10	11.45	0.31	0.00	14.09	17.74	0.36	0.01	100.90	40.84	22.21	36.95	0.65
AF20-46	25	Groundmass	<150µ		51.13	1.13	2.14	0.01	0.62	13.00	0.35	0.00	15.48	15.59	0.27	0.00	99.71	44.88	22.63	32.49	0.66
AF20-46	26	Groundmass	<150µ		50.62	1.43	2.51	0.01	1.32	11.45	0.31	0.00	14.00	18.21	0.37	0.02	100.25	40.75	21.16	38.10	0.66
AF20-46	27	Micro-Phenocryst	<500µ	Core	51.12	1.01	3.31	0.35	1.95	5.28	0.14	0.00	16.06	20.84	0.28	0.00	100.33	45.80	11.48	42.72	0.80
AF20-46	28	Micro-Phenocryst	<1000µ	Core	52.20	0.85	2.90	0.39	0.65	6.25	0.16	0.00	16.23	20.76	0.27	0.00	100.64	46.28	11.18	42.54	0.81
AF20-46	28	Micro-Phenocryst	<1000µ	Rim	50.92	1.28	3.66	0.19	1.44	7.37	0.18	0.00	15.45	20.05	0.27	0.00	100.82	44.37	14.25	41.37	0.76
AF20-46	29			Core	49.59	1.57	3.84	0.07	1.71	9.74	0.25	0.00	14.26	18.55	0.33	0.01	99.91	41.86	19.00	39.15	0.69
AF20-46	29			Rim	49.83	1.73	3.81	0.16	1.41	9.70	0.26	0.00	15.35	17.61	0.27	0.00	100.12	44.75	18.36	36.89	0.71

AF20-46	30	Micro-Phenocryst	<1000µ	Core	51.60	0.98	3.34	0.28	1.23	6.60	0.16	0.00	16.21	19.90	0.31	0.00	100.60	46.42	12.63	40.96	0.79
AF20-46	30	Micro-Phenocryst	<1000µ	Intermediate	51.98	0.97	1.68	0.01	0.49	12.59	0.35	0.00	15.87	16.02	0.27	0.01	100.24	45.48	21.53	33.00	0.68
AF20-46	30	Micro-Phenocryst	<1000µ	Intermediate	51.75	1.06	1.78	0.00	0.05	12.58	0.33	0.00	14.94	17.23	0.26	0.01	99.98	43.19	21.02	35.79	0.67
AF-20-66		Groundmass			48.31	2.41	4.03	0.05	3.07	8.08	0.29	0.00	13.80	19.44	0.44	0.01	99.92	40.57	18.36	41.07	0.69
AF-20-66	1	Micro-Phenocryst		Core	51.18	1.12	2.38	0.08	1.37	7.25	0.24	0.00	16.06	19.16	0.33	0.00	99.18	46.26	14.10	39.64	0.77
AF-20-66		Groundmass			46.55	2.70	5.70	0.09	4.07	6.22	0.25	0.00	13.30	19.96	0.50	0.01	99.34	39.90	17.05	43.05	0.70
AF-20-66	1	Micro-Phenocryst		Rim	50.28	1.58	2.35	0.01	1.64	8.37	0.27	0.00	14.36	19.96	0.38	0.00	99.20	41.78	16.51	41.72	0.72
AF-20-66		Groundmass			50.94	1.06	1.09	0.00	0.93	12.56	0.44	0.00	14.15	17.45	0.27	0.01	98.90	41.05	22.55	36.40	0.65
AF-20-66		Groundmass			51.00	1.33	2.43	0.06	1.61	8.07	0.28	0.00	16.27	18.35	0.28	0.00	99.69	46.53	15.75	37.72	0.75
AF-20-66	2	Micro-Phenocryst		Core	50.71	1.29	2.49	0.11	2.15	6.28	0.21	0.00	15.53	20.44	0.30	0.01	99.53	44.44	13.54	42.02	0.77
AF-20-66	2	Micro-Phenocryst		Rim	50.22	1.56	2.67	0.03	2.07	7.72	0.27	0.00	14.35	20.30	0.41	0.00	99.59	41.63	16.04	42.33	0.72
AF-20-66	3	Micro-Phenocryst		Core	51.38	1.10	2.28	0.11	1.28	8.20	0.30	0.00	17.12	17.47	0.22	0.00	99.46	48.79	15.44	35.77	0.76
AF-20-66	3	Micro-Phenocryst		Intermediate	48.41	2.07	4.72	0.15	2.65	6.22	0.19	0.00	14.03	20.69	0.39	0.00	99.52	41.47	14.58	43.95	0.74
AF-20-66	3	Micro-Phenocryst		Rim	49.99	1.61	2.81	0.01	2.13	7.53	0.22	0.00	14.31	20.37	0.40	0.00	99.38	41.64	15.78	42.58	0.73
AF-20-66		Groundmass			51.20	1.05	1.13	0.01	0.14	12.21	0.45	0.00	13.41	18.89	0.29	0.02	98.78	39.25	21.00	39.76	0.65
AF-20-66		Groundmass			50.81	1.33	2.29	0.01	2.25	7.47	0.27	0.00	14.90	20.06	0.41	0.01	99.82	42.82	15.74	41.44	0.73
AF-20-66		Groundmass			51.02	1.34	2.08	0.01	1.05	8.38	0.25	0.00	14.73	20.10	0.34	0.00	99.30	42.63	15.55	41.81	0.73
AF-20-66		Groundmass			50.24	1.45	2.06	0.02	1.90	8.84	0.30	0.00	14.10	19.62	0.42	0.01	98.97	41.11	17.76	41.13	0.70
AF-20-66		Groundmass			50.30	1.38	2.63	0.15	1.53	9.15	0.28	0.00	15.91	17.41	0.27	0.02	99.04	46.13	17.60	36.27	0.72
AF-20-66		Groundmass			51.11	1.16	2.30	0.15	0.67	9.89	0.31	0.00	16.70	16.48	0.23	0.00	98.99	48.26	17.51	34.23	0.73
AF-20-66		Groundmass			49.25	1.73	3.42	0.13	1.24	9.12	0.28	0.00	14.63	18.40	0.30	0.00	98.50	43.34	17.48	39.18	0.71
AF-20-66		Groundmass			47.62	2.42	4.74	0.28	2.63	7.60	0.22	0.00	13.99	19.10	0.41	0.00	98.99	41.85	17.09	41.06	0.71
AF-20-66		Groundmass			50.08	1.44	2.94	0.15	1.86	9.67	0.31	0.00	16.44	16.06	0.28	0.01	99.23	47.62	18.94	33.44	0.72
AF-20-66		Groundmass			49.92	1.47	2.79	0.11	1.64	8.26	0.26	0.00	14.63	19.50	0.31	0.00	98.88	42.71	16.38	40.92	0.72
AF-20-66	1	Micro-Phenocryst		Core	50.05	1.17	4.31	0.53	0.00	7.15	0.17	0.00	15.27	20.25	0.00	0.00	98.90	44.99	12.11	42.90	0.79
AF-20-66	1	Micro-Phenocryst		Rim	50.73	0.96	3.53	0.46	0.14	6.75	0.15	0.00	16.00	20.38	0.00	0.00	99.08	46.26	11.38	42.36	0.80
AF-20-66	1	Micro-Phenocryst		Core	50.47	1.26	3.13	0.06	2.29	7.11	0.26	0.00	15.50	19.42	0.35	0.00	99.83	44.60	15.23	40.18	0.75
AF-20-66		Groundmass			49.12	1.74	3.41	0.17	2.97	7.90	0.25	0.00	14.70	19.00	0.33	0.02	99.61	42.69	17.64	39.66	0.71
AF-20-66		Groundmass			48.82	1.88	3.79	0.24	2.40	8.11	0.28	0.00	14.77	18.46	0.35	0.02	99.13	43.48	17.45	39.07	0.71
AF20-25		Groundmass			49.75	1.60	3.37	0.16	2.13	8.33	0.32	0.00	14.72	19.04	0.34	0.02	99.78	42.88	17.26	39.86	0.71
AF20-25		Groundmass			49.28	1.88	3.91	0.19	2.19	8.13	0.22	0.00	14.88	18.89	0.33	0.01	99.91	43.45	16.91	39.64	0.72
AF20-25		Groundmass			47.83	2.24	4.51	0.17	3.00	8.04	0.26	0.00	14.00	18.84	0.39	0.00	99.28	41.54	18.30	40.16	0.69
AF20-25		Groundmass			49.54	1.58	3.33	0.13	1.99	7.78	0.25	0.00	14.75	19.40	0.31	0.02	99.07	43.13	16.10	40.77	0.73
AF20-25		Groundmass			49.64	1.70	3.52	0.13	1.78	8.58	0.27	0.00	15.29	18.22	0.31	0.00	99.45	44.64	17.12	38.24	0.72
AF20-25		Groundmass			51.35	1.09	2.28	0.04	0.44	12.09	0.35	0.00	16.68	14.88	0.22	0.04	99.46	48.23	20.84	30.93	0.70
AF20-25		Groundmass			49.57	1.76	3.57	0.26	1.62	7.87	0.20	0.00	14.79	19.46	0.31	0.02	99.43	43.34	15.67	41.00	0.73
AF20-25		Groundmass			49.52	1.75	3.79	0.14	2.11	9.35	0.30	0.00	15.51	17.17	0.32	0.00	99.96	45.19	18.88	35.94	0.71
AF20-25		Groundmass			50.15	1.49	2.29	0.00	2.05	12.40	0.50	0.00	15.35	15.13	0.32	0.06	99.75	44.49	24.00	31.51	0.65
AF20-25		Groundmass			50.02	1.61	3.74	0.22	1.46	8.78	0.27	0.00	15.31	18.17	0.33	0.04	99.94	44.79	17.01	38.20	0.72

Sample	Crystal	Type	Size	Zone	SiO_2 (wt%)	TiO_2	Al_2O_3	V_2O_3	Cr_2O_3	Fe_2O_3	FeO	MnO	NiO	MgO	CaO	ZnO	sum	ILM'	HEM'	USP'	MT'
Lower Stratoids																					
H436		Groundmass			0.03	50.84	0.07	0.35	0.00	2.88	42.54	0.53	0.01	1.41	0.09	0.05	98.76	97.06	2.94	-	-
H436		Groundmass			0.08	25.02	1.55	0.85	0.03	18.02	51.55	0.49	0.02	1.46	0.04	0.11	99.10	-	-	73.29	26.71
H436		Groundmass			0.11	25.12	1.21	0.63	0.08	18.54	52.21	0.54	0.03	1.16	0.04	0.09	99.65	-	-	72.79	27.21
H436		Groundmass			0.09	25.02	1.29	0.71	0.04	18.74	52.05	0.50	0.00	1.25	0.04	0.11	99.72	-	-	72.52	27.48
H436		Groundmass			0.09	25.27	1.47	0.73	0.01	18.12	52.39	0.52	0.00	1.21	0.04	0.11	99.84	-	-	73.38	26.62
H436		Groundmass			0.04	50.54	0.08	0.32	0.00	4.45	42.76	0.51	0.02	1.15	0.11	0.03	99.96	95.55	4.45	-	-
H436		Groundmass			0.06	23.67	2.17	0.83	0.00	19.67	49.64	0.50	0.01	1.72	0.13	0.11	98.39	-	-	70.38	29.62
Upper Stratoids																					
AF20-04	1	Micro-Phenocryst	<500µ		0.15	47.56	0.14	-	0.02	9.39	40.36	0.45	0.00	1.12	0.11	-	99.30	90.53	9.47	-	-
AF20-04	1	Micro-Phenocryst	<500µ		0.02	48.14	0.14	-	0.00	8.63	40.74	0.46	0.00	1.13	0.06	-	99.33	91.33	8.67	-	-
AF20-04	1	Micro-Phenocryst	<500µ		0.01	48.61	0.15	-	0.00	7.36	40.80	0.55	0.00	1.27	0.08	-	98.83	92.53	7.47	-	-
AF20-04	2	Groundmass	<250µ	Core	0.05	47.72	0.16	-	0.00	9.43	40.75	0.47	0.00	0.94	0.05	-	99.57	90.59	9.41	-	-
AF20-04	3	Groundmass	<250µ	Rim	0.02	47.06	0.09	-	0.00	11.36	40.14	0.48	0.02	0.89	0.08	-	100.16	88.74	11.26	-	-
AF20-04	3	Groundmass	<250µ		0.02	47.06	0.18	-	0.00	10.81	40.02	0.52	0.01	0.91	0.14	-	99.65	89.23	10.77	-	-
AF20-04	4	Groundmass	<250µ		0.03	47.83	0.13	-	0.01	10.27	40.99	0.52	0.00	0.82	0.06	-	100.66	89.90	10.10	-	-
AF20-04	5	Groundmass	<250µ	Core	0.03	49.11	0.08	-	0.04	8.37	41.67	0.57	0.04	1.04	0.05	-	100.99	91.73	8.27	-	-
AF20-04	6	Groundmass	<250µ		0.03	48.70	0.08	-	0.00	9.07	41.44	0.53	0.01	1.00	0.04	-	100.89	91.05	8.95	-	-
AF20-04	7	Groundmass	<250µ		0.52	20.92	1.65	0.00	0.06	24.87	49.97	0.46	0.01	0.39	0.09	0.00	98.94	-	-	62.41	37.59
AF20-04	8	Groundmass	<100µ		0.02	47.73	0.11	-	0.03	10.13	41.01	0.50	0.00	0.74	0.08	-	100.34	90.03	9.97	-	-
AF20-04	9	Micro-Phenocryst	<500µ	Core	0.09	49.38	0.12	-	0.00	6.09	41.67	0.57	0.01	1.24	0.03	-	99.20	93.84	6.16	-	-
AF20-04	9	Micro-Phenocryst	<500µ	Rim	0.19	22.69	1.68	0.00	0.05	22.07	51.29	0.50	0.02	0.27	0.07	0.00	98.83	-	-	66.99	33.01
AF20-04	10	Groundmass	<250µ	Core	0.01	49.68	0.06	0.27	0.03	6.10	41.62	0.56	0.00	1.33	0.10	0.00	99.76	93.83	6.17	-	-
AF20-04	10	Groundmass	<250µ	Rim	0.09	22.10	1.63	0.65	0.02	23.82	49.91	0.51	0.00	0.80	0.07	0.21	99.58	-	-	64.67	35.33
AF20-04	12	Groundmass	<250µ	Core	0.06	47.23	0.12	0.71	0.04	10.72	40.38	0.45	0.01	0.90	0.07	0.00	100.68	89.36	10.64	-	-
AF20-04	14	Groundmass	<100µ		0.14	21.64	1.45	0.64	0.03	24.08	49.75	0.46	0.00	0.49	0.09	0.23	98.74	-	-	63.96	36.04
AF20-04	15	Groundmass	<100µ	Core	0.03	47.94	0.13	0.71	0.00	8.69	40.69	0.48	0.00	1.02	0.11	0.00	99.80	91.28	8.72	-	-
AF20-04	16	Groundmass	<100µ	Core	0.16	17.34	1.62	0.43	0.00	33.39	46.60	0.44	0.03	0.38	0.03	0.15	100.41	-	-	50.58	49.42
AF20-04					0.02	49.44	0.11	0.43	0.00	7.10	41.55	0.53	0.00	1.23	0.07	0.12	100.47	92.90	7.10	-	-
AF20-04					0.08	20.40	2.14	1.21	0.02	24.81	48.36	0.48	0.00	0.67	0.05	0.07	98.22	-	-	61.87	38.13
AF20-04					0.11	21.59	1.63	1.17	0.00	24.94	50.17	0.46	0.00	0.62	0.05	0.25	100.75	-	-	63.09	36.91
AF20-04	17	Groundmass	<100µ	Core	0.01	49.98	0.08	0.29	0.00	6.18	41.90	0.51	0.02	1.36	0.04	0.05	100.38	93.80	6.20	-	-
AF20-04	17	Groundmass	<100µ	Rim	0.12	22.15	1.77	0.72	0.00	23.14	49.88	0.48	0.01	0.81	0.09	0.22	99.16	-	-	65.40	34.60
AF20-04					0.02	48.68	0.13	0.60	0.01	7.36	41.43	0.61	0.00	0.93	0.07	0.00	99.82	92.63	7.37	-	-
AF20-04	13	Groundmass	<250µ		0.20	18.97	1.81	0.51	0.01	28.62	47.44	0.52	0.03	0.45	0.07	0.14	98.62	-	-	56.60	43.40
AF20-04	19	Groundmass	<250µ	Rim	0.12	23.19	1.23	1.07	0.03	20.98	51.17	0.59	0.03	0.45	0.08	0.16	98.93	-	-	68.53	31.47
AF20-04	20	Groundmass	<250µ	Core	0.04	48.61	0.19	0.79	0.04	8.06	40.94	0.48	0.02	1.26	0.04	0.02	100.45	91.90	8.10	-	-
AF20-04	20	Groundmass	<250µ	Rim	0.03	48.49	0.14	0.78	0.03	8.37	40.69	0.50	0.01	1.26	0.10	0.07	100.39	91.57	8.43	-	-
AF20-04	21	Groundmass	<250µ	Core	0.04	49.04	0.16	0.73	0.00	7.32	41.50	0.48	0.03	1.10	0.10	0.05	100.50	92.69	7.31	-	-
AF20-04	21	Groundmass	<250µ	Rim	0.12	20.83	2.46	1.76	0.08	57.39	17.76	0.23	0.00	0.31	0.05	0.31	100.99	-	-	43.25	56.75
AF20-04	22	Groundmass	<250µ	Core	0.00	47.75	0.14	0.69	0.00	10.02	40.93	0.45	0.00	0.82	0.05	0.02	100.85	90.12	9.88	-	-
AF20-04		Groundmass			0.53	20.54	1.81	0.41	0.00	25.49	49.25	0.54	0.01	0.43	0.34	0.16	99.33	-	-	61.34	38.66
AF20-04		Groundmass			0.18	20.74	1.65	0.48	0.01	25.72	49.28	0.53	0.03	0.40	0.06	0.09	99.08	-	-	61.37	38.63
AF20-19	1	Groundmass			0.12	19.74	1.24	0.54	0.03	29.17	47.58	0.40	0.01	1.02	0.18	0.03	100.03	-	-	57.20	42.80
AF20-19	2	Groundmass			0.00	49.64	0.08	0.29	0.00	6.46	40.61	0.55	0.00	1.88	0.08	0.02	99.58	93.35	6.65	-	-
AF20-19	3	Groundmass		Core	0.10	20.65	1.26	0.58	0.00	26.82	48.91	0.36	0.03	0.60	0.10	0.13	99.42	-	-	60.37	39.63
AF20-19	3	Groundmass		Rim	0.01	49.38	0.04	0.27	0.00	5.83	41.77	0.47	0.05	1.11	0.09	0.05	99.02	94.12	5.88	-	-
AF20-19	4	Groundmass			0.06	24.92	0.91	0.62	0.04	20.00	52.17	0.47	0.05	1.13	0.08	0.08	100.43	-	-	71.13	28.87
AF20-19	6	Groundmass		Rim	0.06	20.19	1.12	0.65	0.02	28.51	48.62	0.42	0.06	0.57	0.12	0.13	100.35	-	-	58.31	41.69
AF20-19	6	Groundmass		Core	0.04	48.58	0.05	0.28	0.01	7.60	41.26	0.58	0.00	0.92	0.19	0.00	99.50	92.38	7.62	-	-
AF20-19	7	Groundmass			0.04	49.77	0.07	0.33	0.02	6.27	40.87	0.52	0.03	1.82	0.05	0.06	99.78	93.57	6.43	-	-
Central Afar Gulf																					
AF20-46	1	Groundmass	<150µ		0.22	22.99	1.51	0.61	0.00	22.64	50.26	0.52	0.02	1.30	0.17	0.09	100.25	-	-	66.71	33.29
AF20-46	2	Groundmass	<150µ		0.09	22.83	1.54	0.54	0.04	23.38	50.04	0.55	0.00	1.30	0.16	0.04	100.47	-	-	65.81	34.19
AF20-46	3	Groundmass	<50µ		0.14	22.03	1.20	0.50	0.00	25.27	49.23	0.55	0.03	1.16	0.32	0.15	100.43	-	-	63.22	36.78
AF20-46	4	Groundmass	<50µ		0.10	20.74	1.32	0.51	0.03	27.03	47.92	0.49	0.02	1.09	0.27	0.17	99.51	-	-	60.21	39.79
AF20-46	6	Groundmass	<150µ		0.13	21.44	1.51	0.47	0.05	24.71	48.55	0.57	0.00	1.07	0.14	0.09	98.63	-	-	63.08	36.92
AF20-46	7	Groundmass	<150µ		0.12	22.12	1.53	0.57	0.05	23.71	49.14	0.56	0.02	1.13	0.23	0.07	99.17	-	-	64.76	35.24

AF20-46	8	Groundmass	<150µ		0.11	24.41	1.38	0.51	0.00	19.29	51.20	0.52	0.00	1.14	0.21	0.05	98.77	-	-	71.43	28.57
AF20-66		Groundmass			0.07	24.78	1.05	0.48	0.07	19.73	51.64	0.65	0.00	1.15	0.12	0.13	99.75	-	-	71.20	28.80
AF20-66		Groundmass			0.04	51.34	0.08	0.36	0.04	4.43	41.26	0.76	0.03	2.24	0.12	0.03	100.69	95.41	4.59	-	-
AF20-66		Groundmass			0.03	50.66	0.06	0.34	0.00	5.60	41.11	0.75	0.02	1.91	0.20	0.04	100.68	94.26	5.74	-	-
AF20-66		Groundmass			0.08	25.90	0.89	0.49	0.01	18.38	51.78	0.69	0.00	1.82	0.09	0.08	100.12	-	-	73.49	26.51
AF20-66		Groundmass			0.04	51.06	0.08	0.38	0.01	3.98	41.08	0.66	0.01	2.24	0.14	0.05	99.65	95.85	4.15	-	-
AF20-66		Groundmass			0.09	24.48	0.29	0.32	0.03	21.10	51.61	0.72	0.02	0.75	0.24	0.12	99.65	-	-	69.52	30.48
AF20-66		Groundmass			0.09	23.48	1.30	0.61	0.04	22.27	50.31	0.68	0.05	1.30	0.16	0.12	100.29	-	-	67.45	32.55
AF20-66		Groundmass			0.02	51.23	0.13	0.33	0.05	4.05	41.77	0.73	0.00	1.89	0.17	0.00	100.37	95.85	4.15	-	-
AF20-66		Groundmass			0.10	24.68	1.00	0.50	0.00	20.45	50.83	0.73	0.02	1.69	0.07	0.10	100.07	-	-	70.34	29.66
AF20-66		Groundmass			0.10	25.87	0.81	0.47	0.01	18.35	51.92	0.72	0.00	1.69	0.04	0.12	99.97	-	-	73.50	26.50
AF20-66		Groundmass			0.03	50.97	0.08	0.30	0.00	4.73	40.83	0.78	0.00	2.26	0.15	0.02	100.15	95.07	4.93	-	-
AF20-66		Groundmass			0.12	21.56	1.18	0.60	0.05	26.05	48.52	0.67	0.03	1.32	0.18	0.10	100.28	-	-	61.90	38.10
AF20-66		Groundmass			0.10	25.84	0.70	0.44	0.03	17.73	52.98	0.68	0.03	0.85	0.08	0.11	99.44	-	-	74.17	25.83
AF20-66		Groundmass			0.14	20.32	1.55	0.68	0.04	27.16	47.35	0.64	0.01	1.16	0.25	0.16	99.28	-	-	59.50	40.50
AF20-66		Groundmass			0.04	50.68	0.09	0.29	0.02	5.22	40.80	0.79	0.02	1.99	0.35	0.02	100.28	94.62	5.38	-	-
AF20-66		Groundmass			0.06	50.44	0.06	0.27	0.00	4.42	40.77	0.72	0.00	1.92	0.37	0.04	99.03	95.40	4.60	-	-
AF20-66		Groundmass			0.15	20.14	1.52	0.69	0.11	26.85	46.98	0.61	0.05	1.15	0.25	0.13	98.51	-	-	59.57	40.43
AF20-66		Groundmass			0.14	19.62	1.95	0.54	0.07	27.58	46.75	0.48	0.02	1.19	0.17	0.09	98.49	-	-	58.37	41.63
AF20-66		Groundmass			0.08	22.04	1.74	0.52	0.00	24.24	48.57	0.56	0.01	1.57	0.14	0.11	99.46	-	-	64.18	35.82
AF20-66		Groundmass		Core	0.86	47.28	0.19	0.26	0.02	9.15	39.02	0.79	0.01	1.92	0.22	0.01	99.71	90.33	9.67	-	-
AF20-66		Groundmass			0.10	21.54	2.05	0.43	0.02	24.23	47.56	0.59	0.06	1.62	0.30	0.07	98.48	-	-	63.63	36.37
AF20-66		Groundmass			0.10	16.90	2.53	0.50	0.04	32.40	43.90	0.52	0.06	1.30	0.26	0.11	98.51	-	-	50.60	49.40
AF20-66		Groundmass			0.18	49.03	0.12	0.24	0.00	8.10	39.28	0.63	0.02	2.22	0.32	0.02	100.14	91.57	8.43	-	-
AF20-25		Groundmass			0.12	12.68	2.81	0.46	0.00	39.77	40.87	0.37	0.02	0.84	0.28	0.08	98.22	-	-	38.53	61.47
AF20-25		Groundmass			0.17	47.68	0.19	0.28	0.03	10.04	38.08	0.77	0.02	2.13	0.31	0.00	99.70	89.48	10.52	-	-
AF20-25		Groundmass			0.11	16.82	1.90	0.43	0.04	33.54	44.13	0.49	0.03	1.18	0.23	0.11	98.89	-	-	49.64	50.36
AF20-25		Groundmass			0.13	12.66	2.39	0.41	0.04	41.08	40.45	0.47	0.03	1.17	0.25	0.12	99.09	-	-	37.63	62.37
AF20-25		Groundmass			0.08	21.78	1.82	0.47	0.01	24.69	48.04	0.61	0.03	1.70	0.17	0.04	99.41	-	-	63.44	36.56
AF20-25		Groundmass			0.10	13.51	2.26	0.62	0.03	39.01	41.40	0.45	0.01	1.00	0.19	0.10	98.59	-	-	40.44	59.56
AF20-25		Groundmass			0.05	48.16	0.11	0.30	0.00	9.69	38.70	0.64	0.00	2.08	0.24	0.01	99.98	89.95	10.05	-	-
AF20-25		Groundmass			0.16	46.96	0.10	0.33	0.00	11.47	38.38	0.65	0.00	1.72	0.22	0.02	99.97	88.20	11.80	-	-
AF20-25		Groundmass			0.08	20.54	1.72	0.48	0.00	26.51	46.82	0.59	0.01	1.50	0.27	0.06	98.51	-	-	60.38	39.62

Table S3. CIPW norm and major and trace elements analysis of the Lower Stratoids, Upper Stratoids, CAG and Axial Series samples. Data of silicic central volcanoes whose products are interlayered in the upper part of the Upper Stratoids Series are from Santarnecchi (1978).
Note. * Second batch of analysis and relative reference material. For the second batch Sc has been analysed by means of ICP-OES. The analyses of Santarnecchi (1978) have been made by means of X-Ray Fluorescence.

Sample	Lat	Long	Region	Major elements wt.%												CIPW Norm wt.%											
				SiO_2	TiO_2	Al_2O_3	FeO_{tot}	MnO	MgO	CaO	Na_2O	K_2O	P_2O_5	LOI	Tot.	Qz	Pl	Or	Nph	Di	Hyp	Ol	Acm	Na_2SiO_3	Ilm	Mag	Ap
Lower Stratoids Series																											
AF20-03	*10.44*	*40.72*	*Gewane city*	50.20	3.24	12.47	13.87	0.23	4.63	9.12	2.63	0.56	0.45	1.24	98.64	4.78	43.88	3.39	-	18.67	19.58	-	-	-	6.31	2.29	1.09
AF20-80*	*11.13*	*40.76*	*Awash valley*	51.90	3.04	13.19	12.67	0.25	3.84	7.63	3.30	0.82	0.74	1.91	99.29	5.87	47.85	4.97	-	12.29	19.22	-	-	-	5.92	2.09	1.80
AF20-60b	*11.44*	*40.77*	*Awash valley*	48.78	2.37	13.36	12.07	0.20	6.47	11.30	2.42	0.26	0.28	0.29	97.80	0.03	46.39	1.57	-	24.87	19.86	-	-	-	4.61	1.99	0.68
AF20-61*	*11.43*	*40.76*	*Awash valley*	56.80	1.42	16.43	7.02	0.12	3.75	7.74	3.03	1.52	0.14	1.78	99.75	10.52	53.40	9.16	-	9.01	13.10	-	-	-	2.75	1.73	0.34
AF20-62a*	*11.43*	*40.76*	*Awash valley*	55.68	1.47	16.13	7.60	0.13	4.08	7.77	3.23	1.43	0.13	1.32	98.97	7.98	53.81	8.64	-	10.44	14.08	-	-	-	2.85	1.88	0.31
H323*	*10.86*	*41.30*	*Manda Eli Tadda Do graben*	47.57	3.25	12.62	14.95	0.23	4.85	9.89	2.70	0.59	0.38	1.15	98.18	-	44.66	3.59	-	22.45	18.03	1.52	-	-	6.35	2.48	0.93
H332*	*10.86*	*41.30*	*Manda Eli Tadda Do graben*	49.15	3.41	12.40	15.18	0.23	4.51	8.96	2.87	0.86	0.52	-0.20	97.89	1.20	43.44	5.17	-	19.38	20.48	-	-	-	6.59	2.49	1.25
H436*	*10.89*	*41.69*	*Dulul Graben*	49.24	2.62	13.92	13.11	0.21	5.44	10.62	2.86	0.72	0.38	-0.04	99.08	-	47.56	4.29	-	22.81	12.72	4.59	-	-	5.01	2.13	0.91
H449*	*10.84*	*41.87*	*Dulul Graben*	49.29	2.66	13.90	12.80	0.20	6.10	10.64	2.69	0.60	0.37	-0.02	99.23	-	47.12	3.57	-	21.91	16.28	3.08	-	-	5.08	2.07	0.88
Upper Stratoids Series																											
AF20-14c	*11.47*	*41.68*	*Tendaho graben*	69.38	0.82	12.90	4.92	0.11	0.58	2.17	4.14	2.99	0.20	0.84	99.05	27.98	43.52	17.96	-	1.45	4.61	-	-	-	1.58	2.42	0.48
AF20-15	*11.47*	*41.68*	*Tendaho graben*	47.15	3.43	13.09	14.37	0.22	4.47	8.62	2.57	0.38	0.54	3.64	98.48	2.96	47.15	2.36	-	14.29	22.59	-	-	-	6.86	2.44	1.35
AF20-19*	*11.47*	*41.68*	*Tendaho graben*	49.32	3.27	13.42	13.77	0.21	4.54	8.77	3.17	0.95	0.48	-0.14	97.76	0.02	47.32	5.72	-	17.76	19.42	-	-	-	6.33	2.26	1.16
AF20-20	*11.47*	*41.68*	*Tendaho graben*	48.89	3.58	13.15	14.15	0.23	5.21	9.69	2.74	0.72	0.49	0.15	99.00	0.55	45.07	4.30	-	19.73	20.01	-	-	-	6.87	2.30	1.17
AF20-54	*11.62*	*40.91*	*Tendaho graben*	47.79	2.80	14.08	12.32	0.19	6.60	11.65	2.55	0.53	0.35	0.29	99.15	-	47.45	3.16	-	25.08	7.14	8.97	-	-	5.36	2.00	0.84
AF20-59	*11.61*	*40.91*	*Tendaho graben*	49.00	3.35	13.34	13.58	0.21	5.69	10.30	2.67	0.73	0.46	-0.27	99.05	-	45.08	4.34	-	21.57	18.44	0.89	-	-	6.38	2.20	1.09
AF20-04	*11.68*	*40.91*	*Tendaho graben*	50.06	2.65	13.52	12.34	0.20	4.76	9.29	2.88	0.68	0.40	0.23	97.01	2.61	47.79	4.15	-	18.52	18.71	-	-	-	5.20	2.05	0.98
AF20-09	*11.66*	*40.97*	*Tendaho graben*	51.33	3.15	13.06	13.23	0.25	3.63	8.06	3.36	1.40	1.29	0.24	98.99	3.45	45.32	8.36	-	12.90	18.69	-	-	-	6.04	2.15	3.09
AF20-12*	*11.66*	*40.98*	*Tendaho graben*	48.21	2.69	14.96	12.56	0.20	5.02	10.91	2.81	0.61	0.34	0.23	98.54	-	50.96	3.66	-	21.58	10.11	5.62	-	-	5.19	2.06	0.82
Z4*	*11.60*	*41.68*	*Tendaho graben*	48.75	3.34	13.36	14.77	0.23	4.78	9.26	2.99	0.96	0.52	0.00	98.96	-	45.89	5.72	-	18.91	16.00	3.46	-	-	6.39	2.40	1.24
Z137*	*11.60*	*41.68*	*Tendaho graben*	48.97	3.61	13.64	13.74	0.21	5.14	9.32	3.15	0.89	0.49	-0.14	99.02	-	47.42	5.29	-	18.95	14.13	3.91	-	-	6.90	2.23	1.17
AF20-67	*11.95*	*41.82*	*Dobi Graben*	47.60	3.07	13.97	12.66	0.20	6.25	11.45	2.75	0.59	0.43	-0.01	98.96	-	47.71	3.52	-	24.98	4.47	10.35	-	-	5.89	2.06	1.03
AF20-68	*11.83*	*41.89*	*Dobi Graben*	47.36	3.13	13.40	12.25	0.20	5.65	11.08	2.68	0.83	0.43	1.63	98.64	-	46.06	5.05	-	25.62	7.21	6.85	-	-	6.12	2.03	1.05
AF20-69a	*11.82*	*41.87*	*Dobi Graben*	64.44	1.34	13.45	6.01	0.18	1.23	3.03	4.44	0.83	0.34	1.46	98.95	18.50	46.49	18.34	-	4.32	6.95	-	-	-	2.60	1.98	0.82
AF20-34	*11.99*	*41.30*	*Serdo-Silsa cities*	52.31	2.77	13.00	12.98	0.27	3.32	7.29	3.64	1.51	1.32	0.26	98.68	3.97	46.10	9.05	-	11.04	19.22	-	-	-	5.33	2.12	3.17
AF20-71*	*12.20*	*41.19*	*Serdo-Silsa cities*	50.34	3.05	13.72	13.12	0.21	4.88	9.26	3.20	0.82	0.44	0.14	99.18	0.35	48.11	4.88	-	18.86	18.78	-	-	-	5.84	2.13	1.05
AF20-72	*12.20*	*41.19*	*Serdo-Silsa cities*	50.32	2.91	13.43	12.95	0.21	4.82	9.61	2.92	1.01	0.44	0.44	99.05	0.98	45.82	6.04	-	20.50	17.90	-	-	-	5.59	2.11	1.05
AF20-74	*12.08*	*41.25*	*Serdo-Silsa cities*	51.46	2.98	13.64	12.54	0.20	5.04	9.13	2.94	0.93	0.46	0.05	99.37	2.72	46.39	5.52	-	17.58	18.97	-	-	-	5.68	2.03	1.10
AF20-50	*12.26*	*41.15*	*Serdo-Silsa cities*	50.72	2.69	13.37	12.82	0.22	5.28	10.01	2.98	0.78	0.39	0.00	99.26	0.59	46.28	4.64	-	22.04	18.31	-	-	-	5.13	2.08	0.93
AF20-51	*12.37*	*41.16*	*Serdo-Silsa cities*	51.59	3.11	13.05	12.76	0.21	3.90	7.99	2.98	1.13	0.51	0.87	98.10	5.43	45.29	6.86	-	15.02	18.00	-	-	-	6.06	2.11	1.24
Central Afar Gulf Series																											
AF20-46	*12.27*	*41.15*	*Serdo-Silsa cities*	48.37	2.48	13.31	12.16	0.20	5.17	11.27	2.70	0.68	0.36	1.60	98.30	-	46.50	4.15	-	26.95	11.85	2.79	-	-	4.87	2.02	0.88
A238*	*11.81*	*41.32*	*Tendaho graben*	47.60	2.43	14.30	12.77	0.20	7.90	10.72	2.49	0.40	0.32	-0.12	99.01	-	48.07	2.38	-	20.23	9.65	12.18	-	-	4.65	2.07	0.76
H216*	*11.20*	*41.43*	*Tendaho graben*	47.44	2.32	14.38	12.28	0.19	8.38	10.70	2.65	0.48	0.40	-0.23	98.99	-	48.65	2.85	-	20.24	4.57	16.30	-	-	4.43	1.99	0.95
AF20-65	*12.14*	*42.03*	*EliDar city*	48.42	4.15	13.10	13.78	0.25	4.89	9.38	3.43	0.90	1.06	-0.55	98.81	-	46.92	5.34	-	18.35	12.35	4.39	-	-	7.91	2.23	2.52
AF20-66	*12.07*	*41.95*	*EliDar city*	46.42	3.21	13.97	12.55	0.23	4.69	11.52	3.16	0.71	0.90	2.05	99.41	-	48.70	4.30	0.59	25.16	-	10.73	-	-	6.26	2.07	2.19
AF20-29	*11.59*	*41.42*	*Tendaho graben*	53.24	2.02	14.55	9.64	0.17	5.20	8.76	2.94	1.12	0.33	1.13	99.10	4.79	49.00	6.75	-	15.23	17.94	-	-	-	3.91	1.58	0.80
AF20-22	*11.66*	*41.48*	*Tendaho graben*	51.48	1.60	15.75	9.14	0.16	6.29	9.42	2.87	1.00	0.23	0.07	98.01	0.54	52.45	6.03	-	15.13	20.71	-	-	-	3.10	1.50	0.56
H307*	*11.58*	*41.43*	*Tendaho graben*	48.00	2.98	14.06	13.74	0.22	5.88	9.95	2.84	0.60	0.53	0.16	98.96	-	48.37	3.58	-	18.53	13.56	6.74	-	-	5.72	2.24	1.27
AF20-25	*11.65*	*41.54*	*Tendaho graben*	48.74	2.89	14.47	12.38	0.22	5.84	10.77	2.69	0.55	0.55	0.29	99.38	-	48.91	3.27	-	20.07	16.47	2.43	-	-	5.52	2.01	1.31
Axial Series																											
AF20-31	*11.82*	*41.08*	*Tendaho graben*	47.76	2.37	14.86	11.90	0.20	6.86	11.41	2.48	0.43	0.41	-0.44	98.24	-	49.71	2.57	-	21.49	10.08	8.67	-	-	4.56	1.94	0.98
AF20-76	*11.81*	*41.02*	*Tendaho graben*	47.63	2.28	15.05	12.55	0.21	7.04	11.16	2.57	0.40	0.33	0.03	99.25	-	50.41	2.38	-	20.64	7.26	12.14	-	-	4.35	2.04	0.79
AF20-78	*11.81*	*41.02*	*Tendaho graben*	48.92	3.62	12.35	15.00	0.26	4.08	8.56	2.97	0.94	0.73	-0.14	97.30	1.91	43.75	5.69	-	17.37	19.99	-	-	-	7.05	2.48	1.77
AF20-08	*11.78*	*41.03*	*Tendaho graben*	48.37	2.80	14.44	13.71	0.22	5.41	11.09	2.69	0.39	0.37	-0.19	99.30	-	49.10	2.31	-	22.12	13.22	4.82	-	-	5.33	2.22	0.88

Sample	Trace elements ppm																
	Li	Be	V	Cr	Co	Ni	Cu	Zn	Ga	Rb	Sr	Y	Zr	Nb	Mo	Cs	Ba
Lower Stratoids Series																	
AF20-03	4.9	1.41	410	33	43	36	203	144	20.8	14.2	216	53	297	36	1.42	0.14	154
AF20-80*	10.7	1.95	196	21.0	27.9	13.6	29.9	149	21.9	20.1	275	60	311	42	1.75	0.30	237
AF20-60b	3.32	0.79	317	99	41	74	185	123	16.8	4.0	204	27.7	144	15.1	0.39	0.02	49
AF20-61*	4.9	1.45	229	46	30.8	69	78	70	18.4	63	278	25.7	152	16.3	1.58	0.85	468
AF20-62a*	5.7	1.24	185	39	28.4	61	66	62	15.8	44	222	21.2	124	14.2	1.28	0.57	346
H323*	4.0	1.46	<2	39	39	38	158	129	18.3	4.8	197	42	252	34	1.39	0.07	165
H332*	5.6	1.76	433	7.2	47	40	196	164	22.7	21.2	274	54	317	39	1.71	0.23	186
H436*	6.2	1.27	346	52	44	55	146	122	19.3	13.5	268	38	225	27.8	1.20	0.15	176
H449*	5.8	1.33	356	166	46	72	161	124	19.8	12.3	291	42	249	26.9	1.08	0.13	151
Upper Stratoids Series																	
AF20-14c	9.9	3.9	19.2	<8	4.4	1.17	26.7	137	23.0	68	150	85	528	68	4.3	0.50	521
AF20-15	8.5	2.13	381	10.0	43	32.4	155	177	22.5	5.1	295	81	293	41	1.31	0.05	157
AF20-19*	7.2	1.92	<2	13.1	44	38	148	148	23.0	12.5	303	48	339	45	2.08	0.09	208
AF20-20	4.4	1.58	415	31.8	46	51	208	143	22.1	15.7	319	43	282	41	1.74	0.15	210
AF20-54	4.9	1.11	341	216	49	103	168	120	21.1	7.2	331	30.1	193	28.5	0.82	0.03	124
AF20-59	5.1	1.51	409	76	47	67	188	140	22.6	14.9	319	39	259	37	1.30	0.13	174
AF20-04	4.8	1.43	377	46	41	27.7	103	129	21.1	15.5	379	37	232	27.2	1.12	0.15	931
AF20-09	7.9	2.21	202	<8	28.0	3.11	25.9	150	22.4	29.5	363	64	372	55	2.62	0.31	344
AF20-12*	5.0	1.26	359	25.8	44	46	170	137	19.4	10.2	362	32.3	200	28.4	1.31	0.11	266
Z4*	6.2	1.60	386	8.5	48	34	146	152	23.3	17.2	330	43	264	37	1.62	0.19	192
Z137*	7.2	1.71	387	31.3	42	47	181	143	20.8	16.3	306	40	273	40	2.46	0.16	170
AF20-67	5.0	1.26	393	147	46	81	175	119	19.8	12.1	353	34	240	37	1.44	0.11	192
AF20-68	7.2	1.37	386	108	44	70	173	131	20.0	17.1	354	36	250	38	1.46	0.28	241
AF20-69a	7.7	4.8	39	<8	6.6	2.61	14.4	121	24.2	78	204	85	875	113	5.5	0.77	600
AF20-34	9.5	2.56	131	<8	20.1	5.4	38	169	24.0	31.5	349	79	526	63	2.95	0.35	370
AF20-71*	6.0	1.41	391	51	41	24.4	59	129	20.3	14.6	374	40	257	31.5	1.67	0.17	244
AF20-72	3.6	1.43	388	52	41	23.5	58	128	20.8	16.9	390	42	274	34	1.95	0.18	444
AF20-74	5.1	1.34	382	50	37	13.9	29.8	125	20.5	15.4	384	39	248	29.2	1.80	0.14	285
AF20-50	5.7	1.20	401	19.5	41	16.4	47	120	19.6	13.2	314	36	207	23.2	1.81	0.14	224
AF20-51	12.9	1.64	361	9.5	32.1	4.7	25.4	137	21.5	23.4	373	45	302	35	2.39	0.25	484
Central Afar Gulf Series																	
AF20-46	5.2	1.11	368	54	40	24.0	63	110	18.3	11.1	313	35	196	22.5	1.25	0.13	197
A238*	4.8	0.89	340	301	52	148	133	113	17.5	5.6	341	30.4	150	18.0	0.70	0.06	134
H216*	4.9	1.04	319	345	53	168	106	115	18.3	5.6	307	31.8	195	25.7	0.99	0.05	136
AF20-65	6.9	1.39	340	12.8	38	12.5	43	141	20.3	14.3	458	50	278	45	1.41	0.05	300
AF20-66	6.3	1.18	309	30.7	37	26.7	83	116	19.9	6.7	411	46	224	39	1.13	0.01	268
AF20-29	7.4	1.77	263	122	37	82	128	102	19.5	29.6	272	37	228	28.3	1.30	0.36	291
AF20-22	6.9	1.20	225	51	41	91	95	75	17.6	23.3	301	25.0	156	24.8	1.48	0.22	230
H307*	7.3	1.60	452	110	50	70	166	147	22.6	11.4	326	47	272	34	1.33	0.12	185
AF20-25	6.9	1.30	344	99	42	51	120	119	19.4	10.6	310	42	262	36	1.24	0.09	219
Axial Series																	
AF20-31	6.2	1.02	343	283	48	97	130	116	19.4	7.8	318	35	177	23.6	0.40	0.13	163
AF20-76	5.9	1.01	391	270	50	98	132	119	19.4	6.3	539	32.2	162	21.5	0.73	0.03	138
AF20-78	7.5	2.14	387	<8	41	10.5	81	183	23.2	19.3	279	68	395	50	1.70	0.17	264
AF20-08	5.5	0.99	424	118	44	51	146	123	20.0	6.8	267	39	173	21.8	0.87	0.06	141
Detection Limit																	
WS-E	14.0	1.13	340	98	45	57	79	131	21.4	25.2	399	32.3	210	18.2	3.27	0.43	334
WSE Ref	13.5	1.10	336	97	45	54	66	113	21.6	25.8	407	31.8	204	17.9	3.5	0.47	335
WSE*	13.2	1.07	323	92	42	54	61	114	20.2	25.0	391	30.9	197	17.5	3.30	0.50	336
WSE Ref*	13.5	1.10	336	97	45	54	66	113	21.6	25.8	407	31.8	204	17.9	3.5	0.47	335

Sample	Trace elements ppm																				
	La	Ce	Pr	Nd	Sm	Eu	Gd	Tb	Dy	Ho	Er	Tm	Yb	Lu	Hf	Ta	W	Pb	Th	U	Sc
Lower Stratoids Series																					
AF20-03	28.9	67	8.8	39	9.3	2.90	10.5	1.64	9.7	1.97	5.5	0.76	4.5	0.66	7.4	2.23	0.41	<2	3.19	0.76	35
AF20-80*	38	86	11.3	49	11.7	3.6	12.8	2.03	12.0	2.31	6.4	0.89	5.4	0.78	8.1	2.70	0.48	3.17	4.7	1.24	29.0
AF20-60b	11.8	29.3	4.1	18.8	4.8	1.66	5.7	0.91	5.3	1.05	2.87	0.39	2.38	0.33	3.6	0.98	<0.2	<2	1.05	0.28	29.1
AF20-61*	26.6	49	5.5	19.9	4.1	1.18	4.3	0.70	4.2	0.86	2.50	0.37	2.35	0.37	4.0	1.41	0.53	6.3	8.4	2.29	18.0
AF20-62a*	22.0	42	4.6	17.6	3.7	1.10	3.9	0.64	3.9	0.78	2.26	0.33	2.09	0.31	3.4	1.21	0.45	5.1	6.7	1.78	20.0
H323*	24.9	58	7.6	32.9	7.9	2.43	9.0	1.39	8.0	1.61	4.5	0.64	3.7	0.54	6.1	2.12	0.32	2.04	2.42	0.68	36
H332*	30.4	69	9.2	40	9.5	2.91	10.9	1.67	9.9	1.92	5.3	0.72	4.4	0.68	7.9	2.45	0.39	2.67	3.4	0.83	34
H436*	23.6	54	7.0	30.3	7.1	2.23	7.8	1.26	7.5	1.46	4.0	0.56	3.4	0.50	5.7	1.74	0.27	2.01	2.51	0.58	36
H449*	22.9	52	7.0	30.4	7.4	2.32	8.4	1.29	7.6	1.49	4.1	0.57	3.4	0.52	6.1	1.68	0.23	2.08	2.64	0.61	36
Upper Stratoids Series																					
AF20-14c	75	162	19.5	76	16.5	3.9	16.6	2.73	15.9	3.18	9.1	1.33	7.9	1.16	14.1	4.5	1.15	4.7	12.0	2.87	7.9
AF20-15	69	150	20.7	88	18.5	5.3	19.5	2.81	15.7	3.02	8.0	1.14	6.4	0.96	7.2	2.63	0.36	<2	3.6	0.69	29.8
AF20-19*	36	80	10.3	44	9.8	3.07	10.7	1.63	9.4	1.82	5.0	0.70	4.1	0.59	8.0	2.84	0.46	2.59	3.9	1.01	32.0
AF20-20	31.3	70	9.0	39	9.1	2.92	9.5	1.43	8.2	1.62	4.4	0.61	3.4	0.51	6.7	2.57	0.42	<2	3.25	0.78	31.0
AF20-54	20.5	47	6.2	27.1	6.3	2.17	7.0	1.08	6.0	1.16	3.10	0.42	2.47	0.34	4.7	1.86	0.23	<2	2.02	0.51	33
AF20-59	27.3	63	8.3	36	8.2	2.72	9.1	1.37	7.8	1.49	4.1	0.56	3.29	0.46	6.3	2.44	0.36	<2	2.83	0.76	33
AF20-04	24.7	57	7.4	32.4	7.4	2.38	8.0	1.24	7.2	1.36	3.8	0.53	3.26	0.46	5.6	1.72	0.30	5.2	2.43	0.61	30.1
AF20-09	52	119	15.5	67	14.9	4.8	15.8	2.24	12.5	2.42	6.5	0.88	4.9	0.74	9.1	3.6	0.65	<2	5.2	1.35	21.0
AF20-12*	21.2	48	6.4	27.1	6.3	2.05	6.9	1.04	6.0	1.13	3.14	0.43	2.59	0.39	4.8	1.74	0.25	3.4	1.97	0.50	35
Z4*	29.9	67	8.6	37	8.5	2.79	9.3	1.43	8.3	1.57	4.2	0.58	3.6	0.51	6.3	2.31	0.38	2.12	3.23	0.77	33
Z137*	27.9	62	8.2	35	7.9	2.54	8.6	1.31	7.6	1.41	3.9	0.52	3.19	0.48	6.4	2.42	0.38	2.03	3.15	0.78	34
AF20-67	27.7	63	7.9	34	7.7	2.50	7.9	1.16	6.7	1.30	3.5	0.48	2.73	0.41	5.7	2.26	0.36	<2	2.86	0.71	36
AF20-68	29.0	66	8.5	36	8.1	2.55	8.1	1.25	7.0	1.36	3.6	0.52	3.02	0.45	6.1	2.39	0.33	<2	2.98	0.71	30.8
AF20-69a	87	188	22.9	91	18.6	4.8	17.7	2.84	16.3	3.27	9.4	1.35	8.4	1.19	20.8	7.1	1.51	4.3	13.3	3.6	12.2
AF20-34	59	137	18.2	78	17.4	5.3	18.1	2.74	15.6	3.04	8.1	1.16	6.7	1.02	12.2	4.0	0.67	2.78	5.1	1.35	22.5
AF20-71*	25.6	58	7.7	33	7.7	2.43	8.2	1.24	7.3	1.39	3.9	0.53	3.17	0.48	6.1	1.91	0.34	2.53	2.53	0.61	36
AF20-72	28.7	67	8.5	37	8.4	2.74	8.9	1.36	8.0	1.57	4.3	0.60	3.3	0.51	6.5	2.08	0.43	<2	2.78	0.77	35
AF20-74	26.3	60	7.9	35	8.0	2.62	8.4	1.27	7.3	1.46	4.0	0.55	3.14	0.48	6.0	1.78	0.39	<2	2.31	0.62	32.0
AF20-50	21.4	50	6.7	29.5	6.9	2.29	7.4	1.18	6.9	1.39	3.9	0.56	3.22	0.49	5.1	1.46	0.25	<2	1.79	0.52	32.7
AF20-51	31.7	72	9.6	41	9.3	2.88	9.8	1.49	8.5	1.69	4.7	0.66	3.8	0.59	7.3	2.18	0.40	<2	3.14	0.89	28.2
Central Afar Gulf Series																					
AF20-46	19.9	47	6.3	27.8	6.6	2.16	7.3	1.15	6.7	1.33	3.7	0.54	3.08	0.47	4.9	1.42	0.24	<2	1.74	0.56	35
A238*	13.8	34	4.7	21.9	5.4	1.95	6.3	1.00	5.9	1.15	3.17	0.43	2.67	0.39	3.7	1.14	0.14	1.37	0.88	0.23	34
H216*	19.3	45	6.0	26.4	6.2	2.06	6.7	1.04	6.2	1.20	3.30	0.45	2.71	0.40	4.5	1.53	0.17	1.37	1.15	0.32	33
AF20-65	37	85	11.5	51	11.6	4.0	12.2	1.75	9.8	1.91	5.1	0.68	3.9	0.59	6.4	2.84	0.32	<2	2.47	0.60	31.1
AF20-66	34	77	10.6	47	10.8	3.7	11.1	1.69	9.3	1.78	4.7	0.64	3.7	0.55	5.5	2.57	0.34	<2	2.69	0.51	28.4
AF20-29	27.1	59	7.4	31.1	6.9	2.14	7.4	1.16	6.8	1.33	3.8	0.54	3.4	0.48	5.6	1.95	0.44	<2	4.5	1.26	23.3
AF20-22	23.9	50	5.9	23.6	5.0	1.61	5.1	0.79	4.6	0.90	2.56	0.37	2.23	0.34	3.9	1.63	0.41	<2	3.9	0.97	22.9
H307*	25.6	60	8.0	35	8.0	2.58	9.1	1.39	8.2	1.59	4.5	0.62	3.9	0.59	6.3	1.99	0.22	2.21	2.00	0.46	36
AF20-25	27.9	63	8.2	36	8.2	2.75	9.0	1.34	7.8	1.58	4.4	0.60	3.5	0.52	6.1	2.21	0.30	<2	2.24	0.61	34
Axial Series																					
AF20-31	18.0	44	5.9	27.0	6.4	2.26	7.3	1.15	6.5	1.29	3.7	0.51	3.09	0.44	4.2	1.49	<0.2	<2	1.08	0.31	35
AF20-76	16.7	39	5.3	23.4	5.5	1.98	6.5	1.01	5.9	1.19	3.4	0.47	2.90	0.41	3.8	1.33	<0.2	<2	1.17	0.32	36
AF20-78	39	91	12.2	54	12.5	3.9	13.7	2.16	12.7	2.51	7.2	1.00	6.2	0.90	9.3	3.15	0.37	<2	3.06	0.82	35
AF20-08	17.5	41	5.7	25.4	6.4	2.21	7.3	1.19	7.1	1.42	4.0	0.58	3.5	0.52	4.4	1.36	<0.2	<2	1.21	0.30	35
Detection Limit																					
WS-E	27.0	61	8.0	34	8.9	2.29	7.7	1.15	6.3	1.20	3.24	0.43	2.58	0.35	5.2	1.14	0.45	8.7	3.02	0.63	25.7
WSE Ref	26.6	60	7.7	32.8	8.8	2.20	7.2	1.08	6.1	1.18	3.07	0.42	2.51	0.36	5.2	1.12	0.50	12.3	2.99	0.62	27.6
WSE*	26.1	57	7.5	31.6	8.3	2.10	7.3	1.08	6.0	1.12	3.03	0.40	2.39	0.36	5.0	1.04	0.42	13.0	2.98	0.59	-
WSE Ref*	26.6	60	7.7	32.8	8.8	2.20	7.2	1.08	6.1	1.18	3.07	0.42	2.51	0.36	5.2	1.12	0.50	12.3	2.99	0.62	-

			Major elements wt.%												Trace elements ppm							
Sample	Lat	Long	SiO_2	TiO_2	Al_2O_3	$FeO_{tot.}$	MnO	MgO	CaO	Na_2O	K_2O	P_2O_5	LOI	Tot.	Nb	Zr	Y	Sr	Rb	Ba	La	Ce
Z1	*11.60*	*41.68*	52.30	2.46	14.88	11.21	0.26	3.70	7.25	4.05	1.21	1.78	-	99.10	-	-	-	-	-	-	-	-
C380	*12.52*	*41.23*	53.12	2.34	12.56	13.17	0.20	3.22	6.83	3.50	1.65	1.20	0.46	97.79	-	-	-	-	-	-	-	-
Z142	*11.60*	*41.68*	55.49	1.88	14.60	10.47	0.30	2.63	6.29	4.23	1.53	1.25	-	98.67	-	-	-	-	-	-	-	-
B458	-	-	55.89	2.03	15.95	6.04	0.27	6.94	4.41	2.16	2.21	0.53	0.08	96.43	-	-	-	-	-	-	-	-
Z144	*11.60*	*41.68*	56.00	1.87	14.63	10.38	0.27	2.45	6.16	4.21	1.54	1.21	-	98.72	-	-	-	-	-	-	-	-
C300	*12.72*	*40.95*	57.74	2.85	10.39	13.11	0.16	4.91	8.73	3.45	1.00	0.42	0.33	102.76	-	-	-	-	-	-	-	-
G441	*12.22*	*40.95*	59.23	1.74	12.33	8.54	0.18	2.25	5.20	4.80	2.45	0.31	0.59	97.03	-	-	-	-	-	-	-	-
C388	*12.54*	*41.09*	59.42	1.50	12.56	8.93	0.12	2.25	4.93	4.85	3.00	0.44	0.54	98.00	-	-	-	-	-	-	-	-
G442	*12.24*	*40.95*	60.41	1.80	11.46	9.51	0.17	2.17	5.23	3.80	2.40	0.29	0.30	97.24	-	-	-	-	-	-	-	-
Z140	*11.60*	*41.68*	60.91	1.26	14.74	8.55	0.21	1.74	4.70	4.16	1.99	0.62	-	98.88	-	-	-	-	-	-	-	-
C303	*12.76*	*41.00*	62.07	1.14	14.56	7.09	0.19	1.25	3.64	4.90	3.10	0.41	0.20	98.35	-	-	-	-	-	-	-	-
C396	-	-	62.47	1.02	14.85	5.31	0.09	1.12	2.68	4.80	4.00	0.29	0.33	96.63	-	-	-	-	-	-	-	-
C419	*12.70*	*41.61*	64.48	0.73	11.84	7.68	0.14	0.64	2.46	5.15	3.10	0.12	1.15	96.34	-	-	-	-	-	-	-	-
HM16	-	-	64.68	1.37	12.62	5.97	0.06	1.43	3.64	5.05	3.24	0.37	0.10	98.43	-	-	-	-	-	-	-	-
C350	*12.50*	*41.19*	64.80	0.75	13.10	5.46	0.13	0.80	2.68	3.90	4.40	0.28	1.61	96.30	-	-	-	-	-	-	-	-
C429	*12.71*	*41.40*	65.49	0.30	13.07	3.78	0.10	0.72	3.36	5.00	4.30	0.08	0.31	96.20	-	-	-	-	-	-	-	-
C442	*12.38*	*41.15*	66.65	0.80	13.08	4.12	0.13	0.80	2.35	4.10	4.00	0.20	0.63	96.23	-	-	-	-	-	-	-	-
C407	*12.90*	*41.63*	67.07	0.39	13.16	4.49	0.14	0.19	2.08	3.88	4.22	0.04	-	95.66	-	-	-	-	-	-	-	-
C438	*12.36*	*41.16*	67.29	0.37	12.54	5.48	0.10	0.40	1.73	5.00	3.75	0.06	2.32	96.72	-	-	-	-	-	-	-	-
S58	*12.06*	*40.51*	71.29	0.41	12.72	3.59	0.06	0.31	1.54	2.97	4.84	0.11	1.77	97.84	27.9	427	61	127	82	932	57	123
G528	*12.44*	*40.27*	74.75	0.07	12.34	2.09	0.02	0.32	0.50	3.35	4.65	0.04	0.73	98.13	-	-	-	-	-	-	-	-
C295	*12.84*	*41.00*	69.89	0.25	13.86	2.21	0.07	0.48	2.07	4.90	4.05	0.03	1.21	97.81	-	-	-	-	-	-	-	-
C298	*12.85*	*41.00*	70.54	0.23	13.24	2.97	0.03	0.40	1.73	4.85	4.00	0.03	0.60	98.02	-	-	-	-	-	-	-	-
C314	*12.75*	*41.08*	74.52	0.22	12.15	3.03	0.07	0.07	0.92	4.51	3.54	0.02	0.62	99.05	116	712	103	113	90	743	102	237
C322	*12.65*	*41.05*	70.10	0.35	12.17	4.26	0.12	0.48	2.18	4.65	3.75	0.09	0.91	98.15	-	-	-	-	-	-	-	-
C372	*12.48*	*41.21*	69.58	0.40	12.27	4.56	0.08	0.24	1.45	4.70	4.10	-	0.97	97.38	-	-	-	-	-	-	-	-
G479	*12.47*	*41.19*	74.41	0.16	12.56	2.31	0.06	0.03	0.72	4.68	4.21	0.01	0.58	99.15	96	427	104	46	81	908	100	217
C330	*12.64*	*41.06*	73.71	0.09	11.61	1.83	0.02	0.24	0.67	3.85	4.70	-	2.25	96.72	-	-	-	-	-	-	-	-
C432	-	-	75.70	0.16	11.80	1.50	0.02	0.20	0.44	4.40	4.40	-	0.10	98.62	-	-	-	-	-	-	-	-
C338	*12.56*	*41.10*	73.96	0.18	12.73	1.69	0.02	0.20	0.67	4.70	4.80	0.15	0.60	99.10	-	-	-	-	-	-	-	-
C336	*12.49*	*41.09*	74.09	0.07	12.28	1.78	0.02	0.24	0.72	4.90	5.00	0.03	0.60	99.13	-	-	-	-	-	-	-	-
G527	*12.60*	*40.54*	74.37	0.17	12.04	2.49	0.06	0.01	0.34	5.05	4.46	-	0.72	98.99	122	768	124	1.40	143	61	103	225
C340	*12.38*	*41.07*	73.89	0.13	11.87	2.00	0.04	0.32	0.89	4.90	4.70	0.03	0.47	98.77	-	-	-	-	-	-	-	-
S14	*12.37*	*40.40*	70.97	0.33	11.42	5.59	0.19	0.10	0.59	4.72	4.57	0.03	0.87	98.51	222	1234	109	19.7	145	115	154	309
C424	*12.58*	*41.51*	70.05	0.32	11.02	4.46	0.13	0.44	1.23	5.00	3.90	-	1.94	96.55	-	-	-	-	-	-	-	-
S22	*12.40*	*40.37*	70.94	0.33	11.03	5.83	0.48	0.20	0.65	4.68	4.60	0.01	1.01	98.75	206	1162	113	15.3	125	44	158	326
K94	*12.37*	*41.68*	69.81	0.62	11.17	5.35	0.32	0.35	0.79	5.17	4.69	0.05	1.09	98.32	274	1701	106	20.1	126	169	182	395
S17	*12.41*	*40.41*	70.03	0.46	10.57	7.06	0.26	0.07	0.57	5.01	4.49	0.02	0.68	98.54	243	1243	108	16.7	121	52	168	261
G511	*12.38*	*40.61*	72.98	0.26	10.78	3.87	0.05	0.36	0.39	5.35	4.40	-	0.29	98.44	-	-	-	-	-	-	-	-
G541	*12.26*	*40.46*	74.11	0.45	10.20	3.76	0.04	0.20	0.39	5.30	4.40	-	0.98	98.85	-	-	-	-	-	-	-	-
S24	*12.42*	*40.38*	73.08	0.21	9.08	6.67	0.19	0.04	0.32	4.64	4.27	-	0.76	98.50	304	1643	128	13.5	169	39	202	44
S15	*12.39*	*40.40*	69.07	0.47	10.37	7.20	0.26	0.03	0.39	5.96	4.43	0.01	1.00	98.19	248	1259	138	8.4	136	77	163	393
G447	*12.35*	*40.72*	73.74	0.24	9.06	5.88	0.13	0.23	0.19	5.65	4.22	0.01	0.41	99.35	159	1408	174	7.5	183	66	159	350
G448	*12.34*	*40.72*	73.65	0.25	9.01	5.89	0.13	0.05	0.23	5.70	4.19	0.01	0.23	99.11	157	1382	171	9.3	180	75	154	338
S36	*12.36*	*40.37*	72.10	0.31	9.23	6.61	0.18	0.01	0.28	6.36	4.18	0.01	0.45	99.27	191	915	112	0.50	124	24.3	147	308
G540	*12.35*	*40.36*	71.15	0.35	8.47	7.57	0.26	0.02	0.34	6.51	4.20	0.01	0.27	98.88	260	1357	143	2.20	160	39	197	409

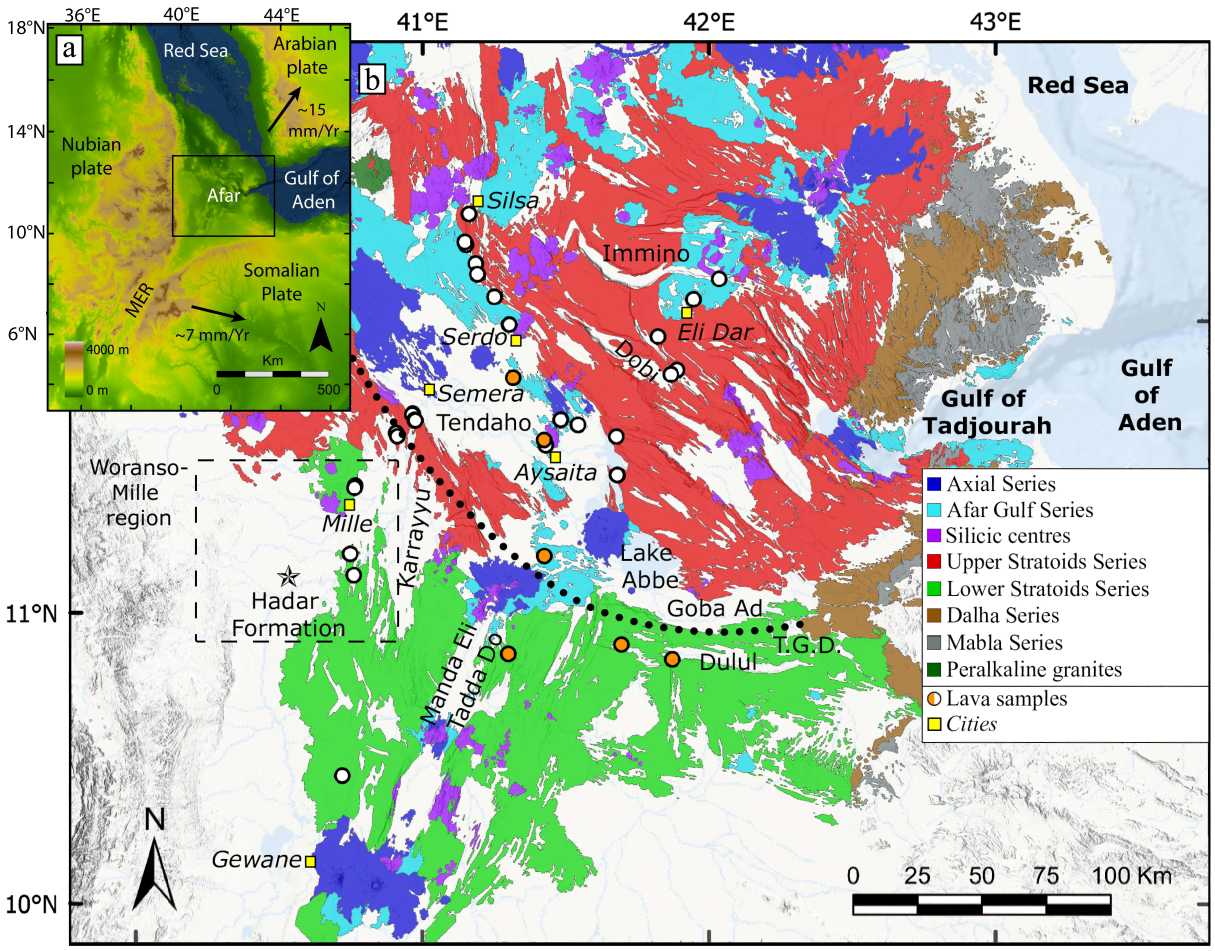

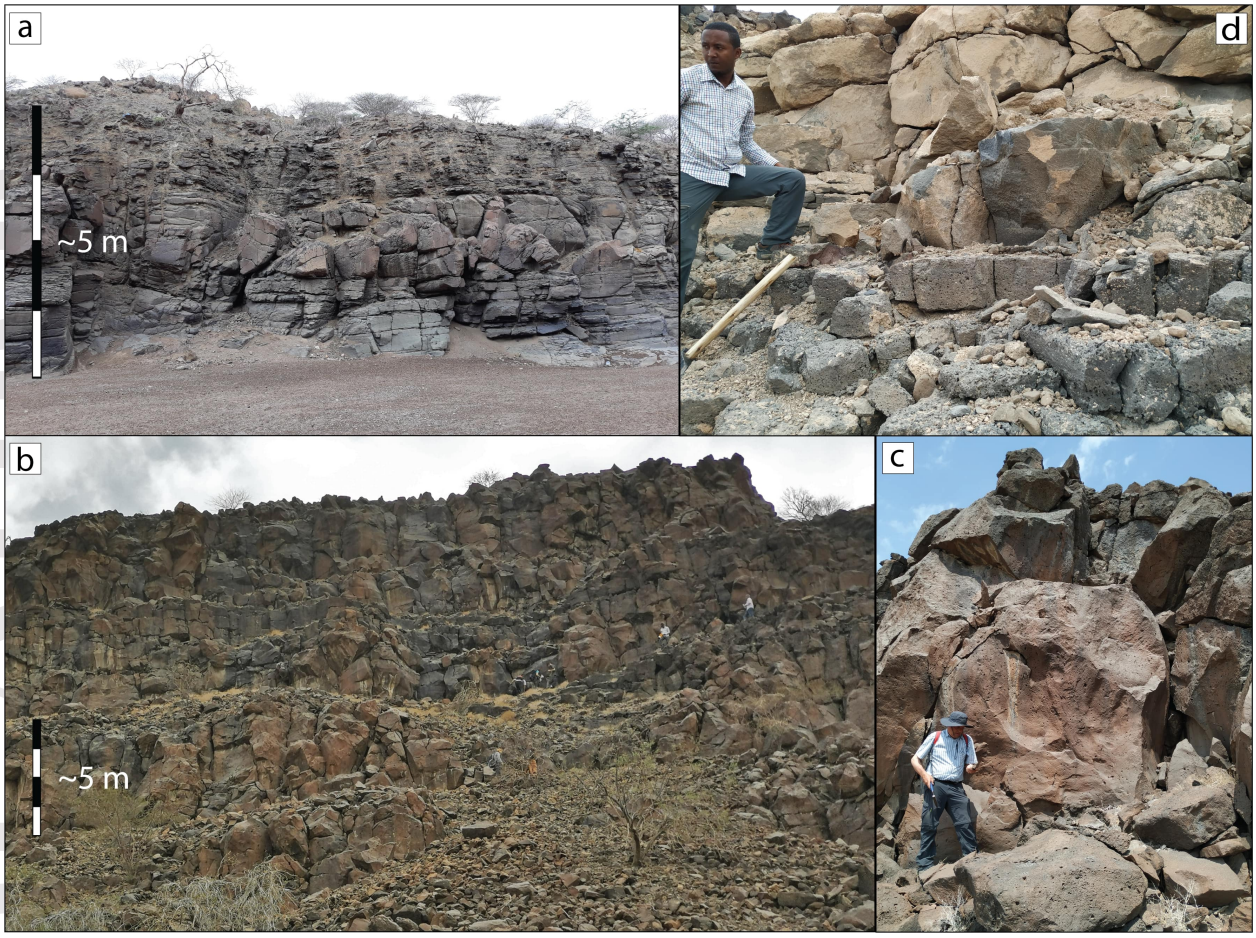

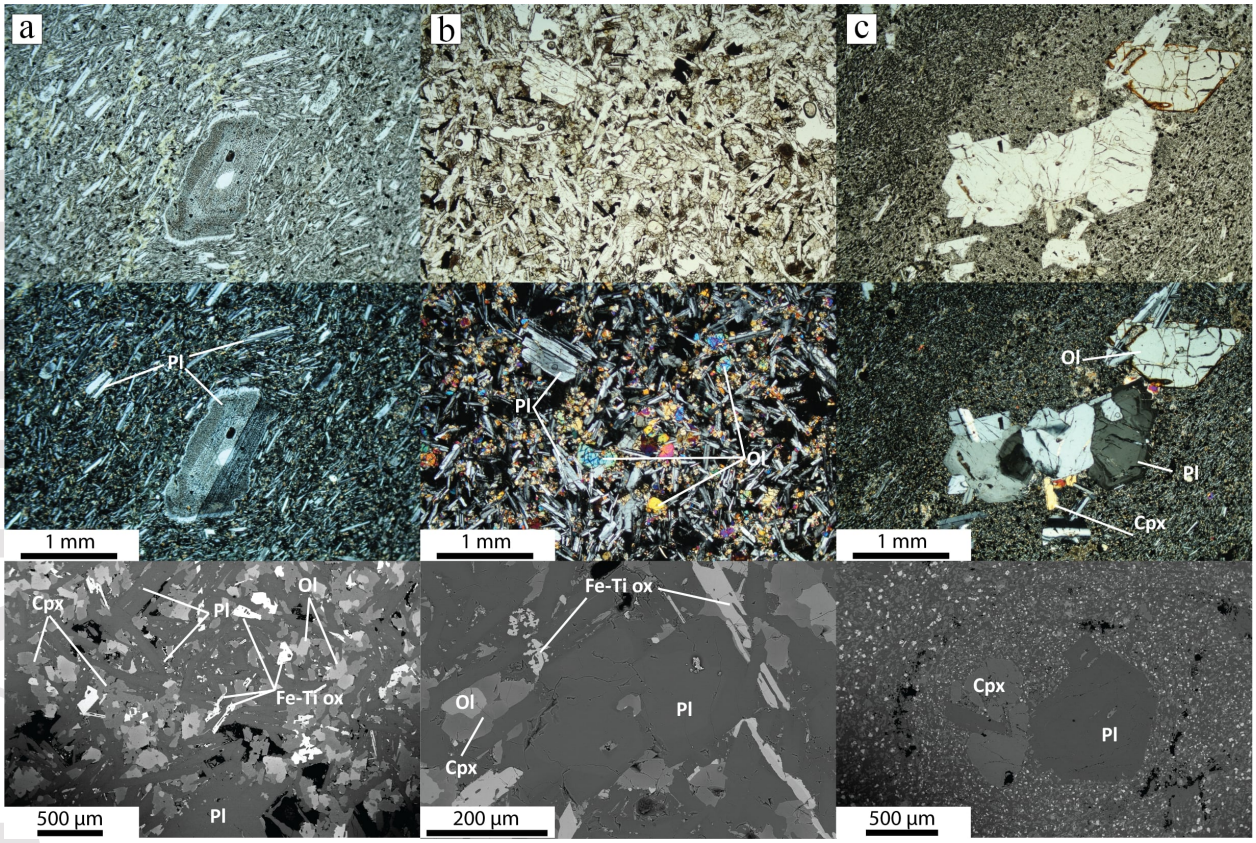

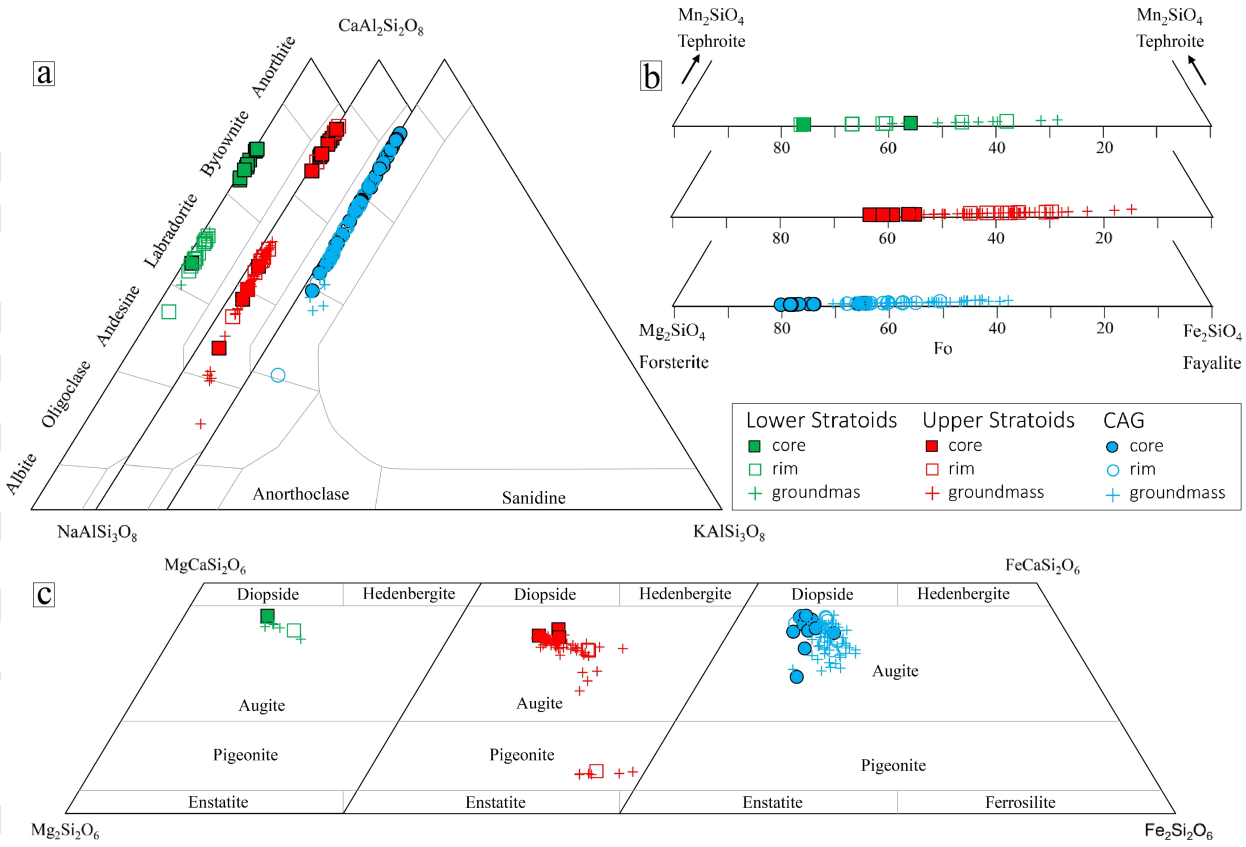

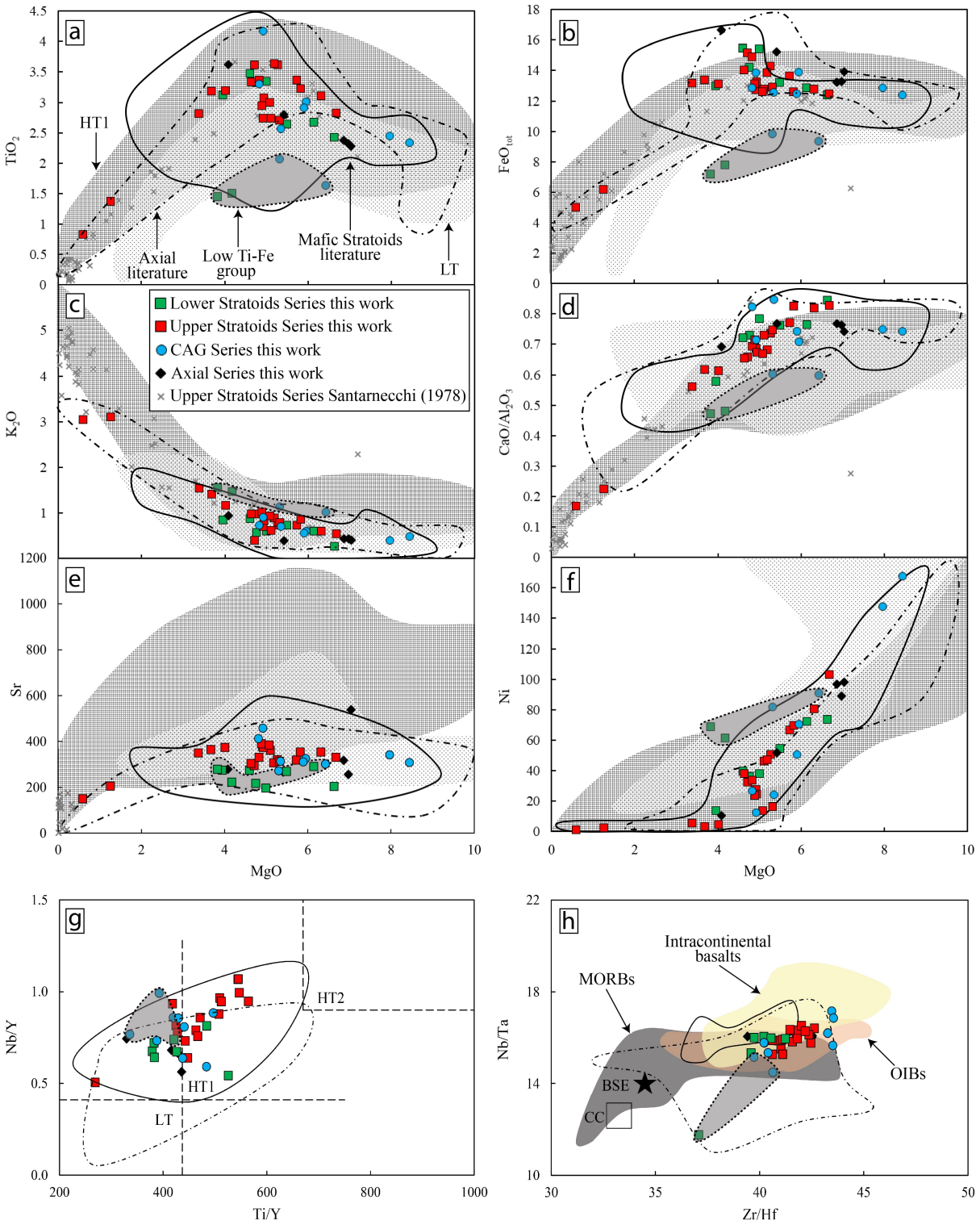

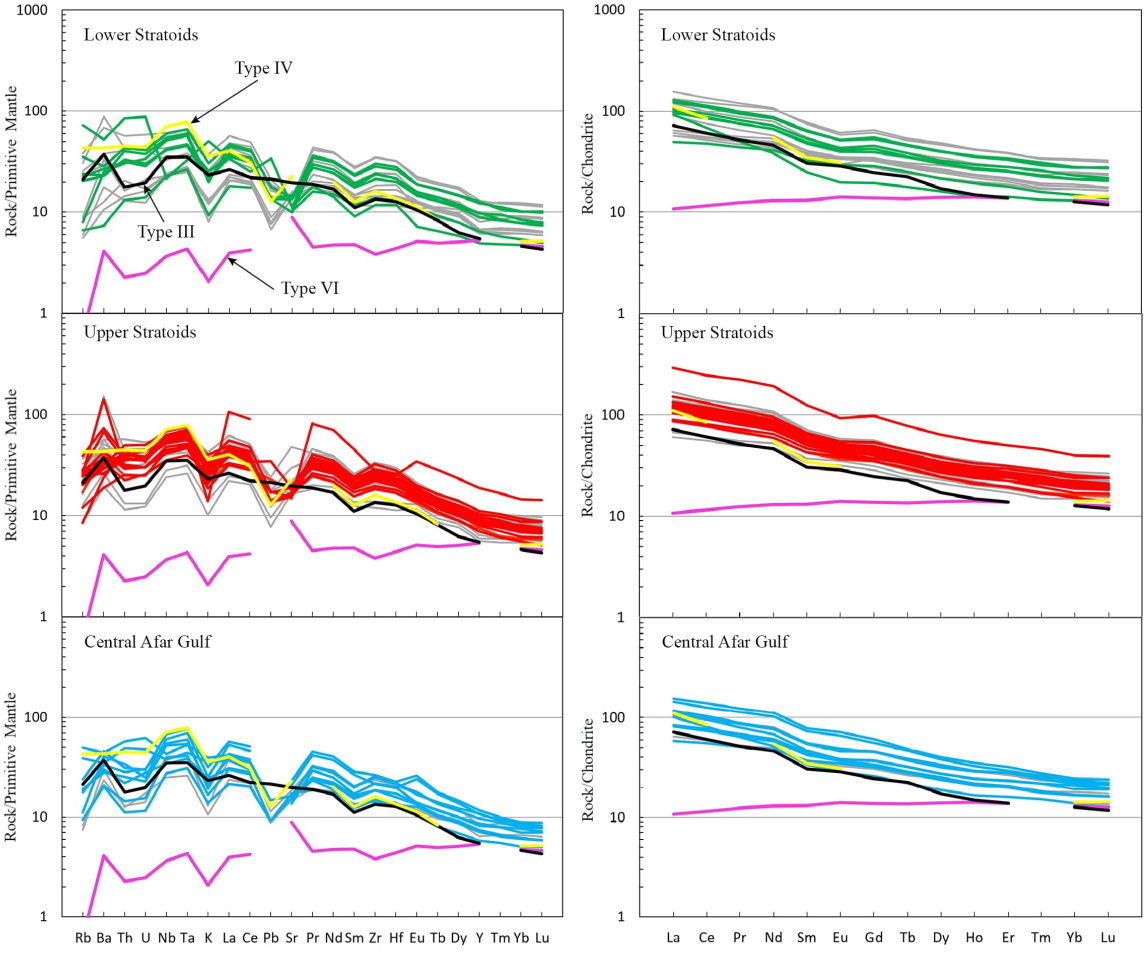

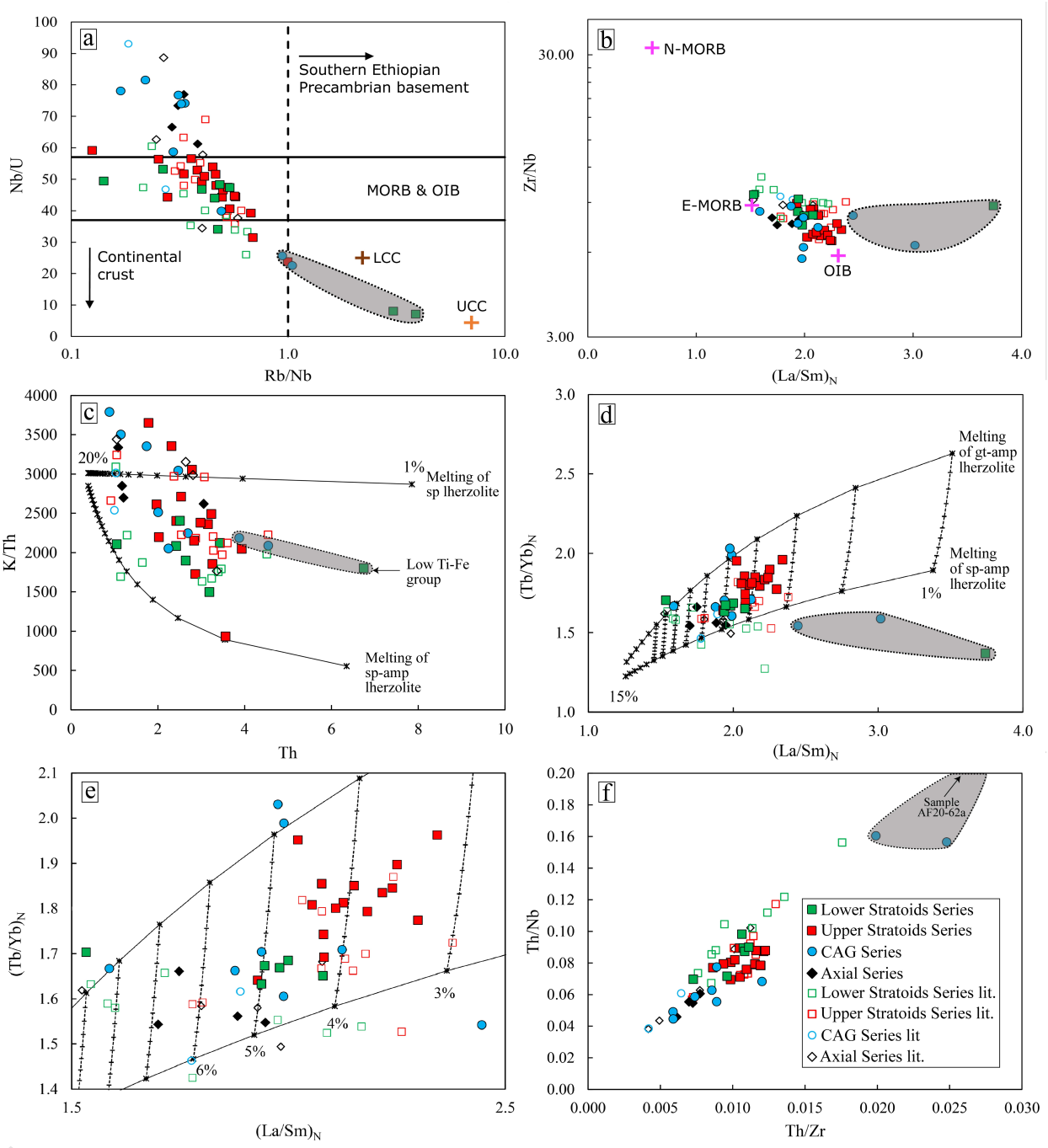

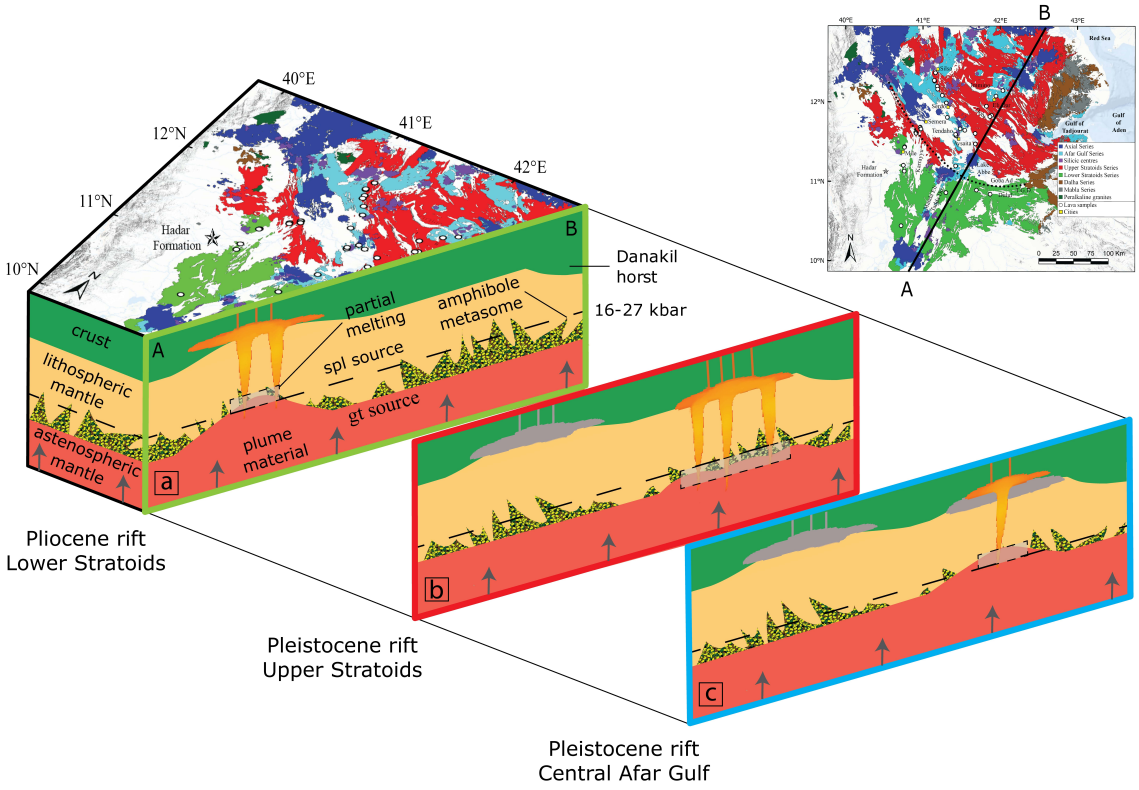

AGU PUBLICATIONS

Constraints on the magma source and rift evolution from geochemistry of the Stratoids flood basalts (Afar, Ethiopia)

G. Tortelli[1,2], A. Gioncada[1], C. Pagli[1], E. Braschi[3], E. F. Gebru[4,5], D. Keir[2,6]

[1] Dipartimento di Scienze della Terra, Università di Pisa, Via Santa Maria, 53, 56126 Pisa, Italy

[2] Dipartimento di Scienze della Terra, Università degli Studi di Firenze, Via G. La Pira, 4, 50121 Florence, Italy

[3] CNR, IGG, sezione di Firenze, Via G. La Pira, 4, 50121 Firenze, Italy

[4] Department of Geosciences, University of Fribourg, Chemin du Musée 6, 1700 Fribourg, Switzerland

[5] School of Earth Sciences, Addis Ababa University, P. O. Box, 1176, Addis Ababa, Ethiopia

[6] School of Ocean and Earth Science, University of Southampton, European Way, SO14 3ZH, Southampton, U.K.

Corresponding author: Gianmaria Tortelli (gianmaria.tortelli@unifi.it)

Contents of this file

Additional Supporting Information (files uploaded separately)

Tables S1 to S3

Introduction

This Supplement presents four figures of major and trace elements and geochemical modeling with captions.

Three excel files contain:

- the petrographic description,

- major and trace elements analysis of our new samples collected during the 2020 campaign and of the Santarnecchi (1978) samples,

- the EPMA microanalytical data.

The captions of the excel spreadsheets are reported also in this supplement file.

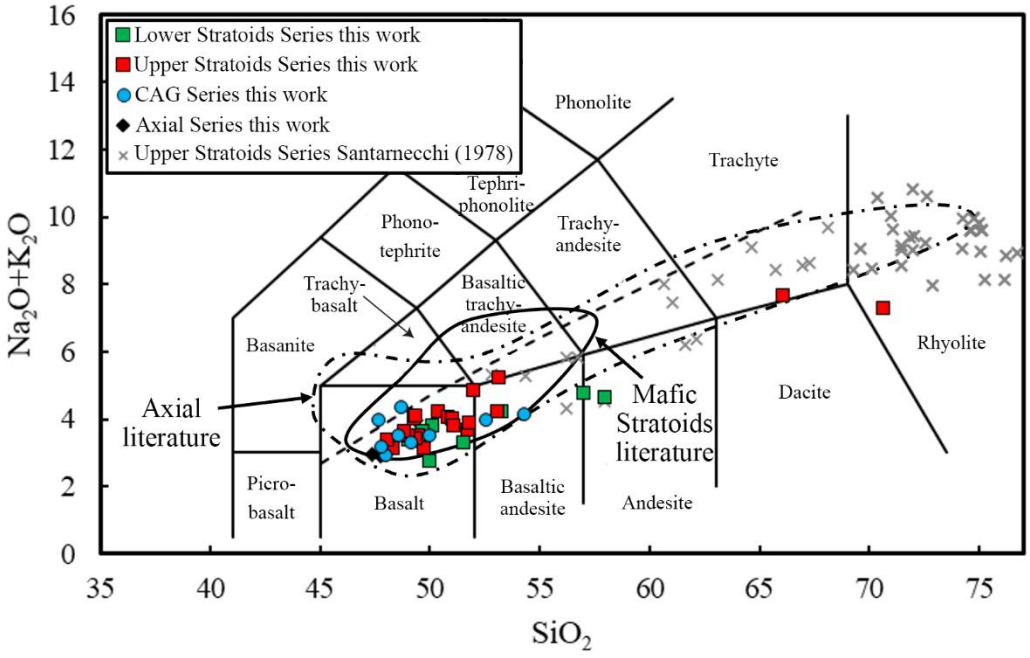

Figure S1. TAS (Total Alkali vs Silica, wt%) classification diagram for Lower Stratoids, Upper Stratoids, CAG and Axial Series. Data recalculated to 100% on a water-free basis. Total iron as FeO_{tot} = $FeO+Fe_2O_3*0.8998$. The dashed line marks the limit between subalkaline-alkaline fields (Irvine and Baragar, 1971). Data of silicic central volcanoes intercalated in the upper part of the Upper Stratoids Series are from Santarnecchi (1978) and reported in Table S3. Stratoids Series literature data of Central and Southern Afar (solid line) are from Barberi and Santacroce (1980); Deniel et al. (1994); Feyissa et al. (2019). Axial literature data of Manda Hararo and Manda Inakir (dashed line) are from Barrat et al. (2003); Deniel et al. (1994); Feyissa et al. (2019).

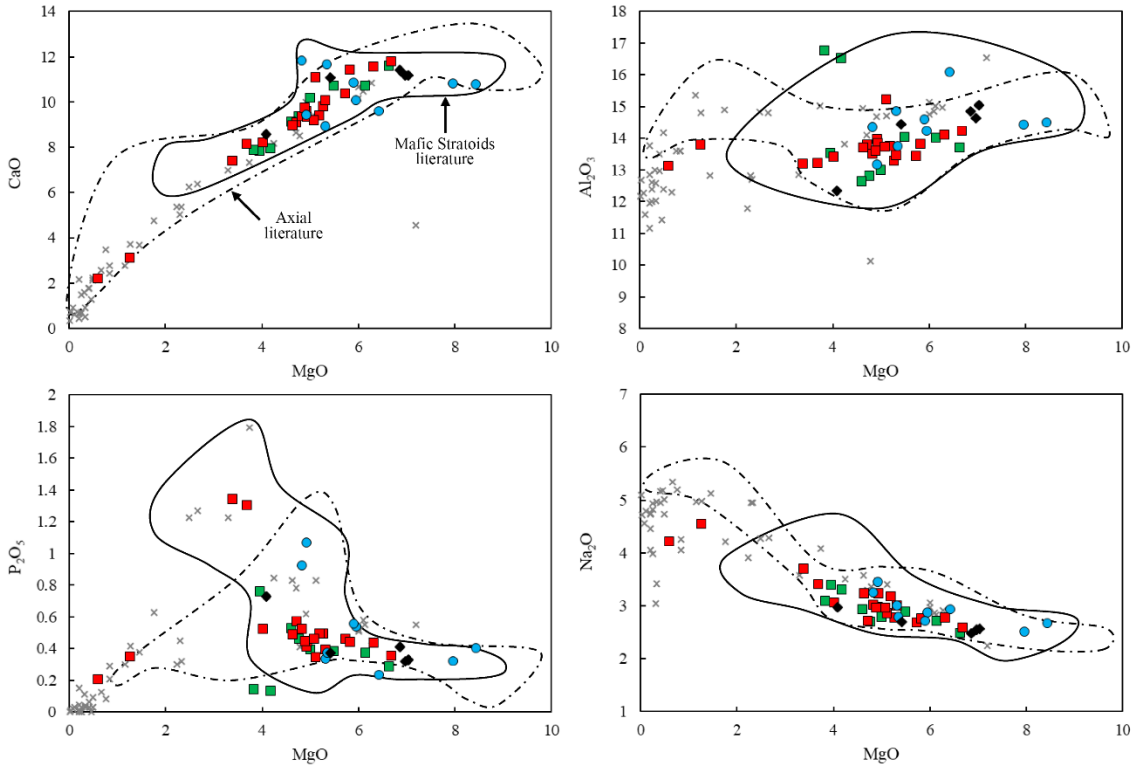

Figure S2. Variations diagrams (wt%) for Lower Stratoids, Upper Stratoids, CAG and Axial Series. Legend, literature data and references as in Figure S1.

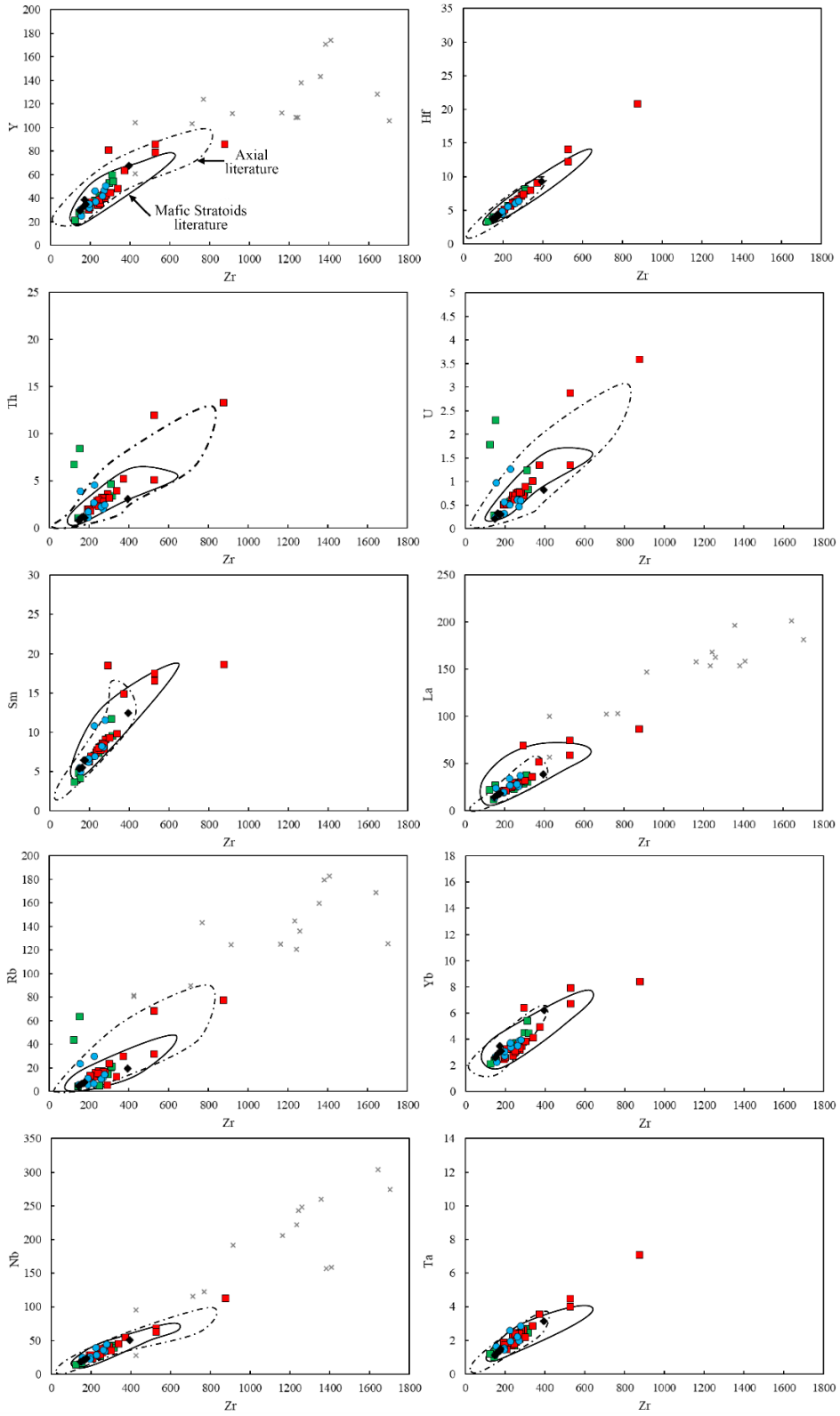

Figure S3. Trace elements (ppm) binary diagram for Lower Stratoids, Upper Stratoids, CAG and Axial Series. Legend, literature data and references as in Figure S1. Note that the Axial literature field has different extent because not all the references have a full trace element suite.

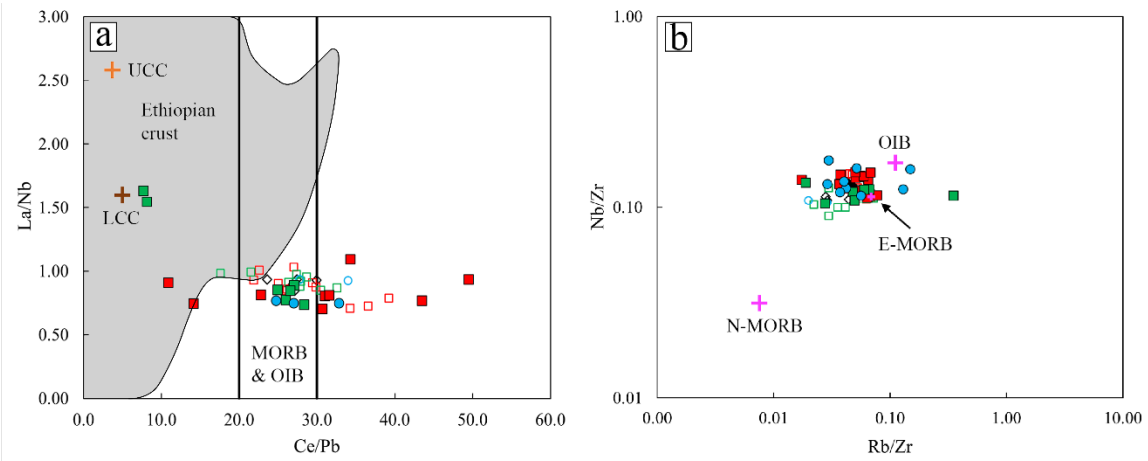

Figure S4. (a) Trace elements indicators for crustal contamination. MORB and OIB field from Hofmann et al. (1986). Ethiopian crust field is from Kebede et al. (1999); Sifeta et al. (2005); Tadesse and Allen (2005); Yihunie et al. (2006). UCC and LCC are respectively the upper continental crust and the lower continental crust (Rudnick and Gao, 2003). (b) Incompatible trace elements ratios for mantle source investigation. OIB, N-MORB and E-MORB values from Sun and McDonough (1989).

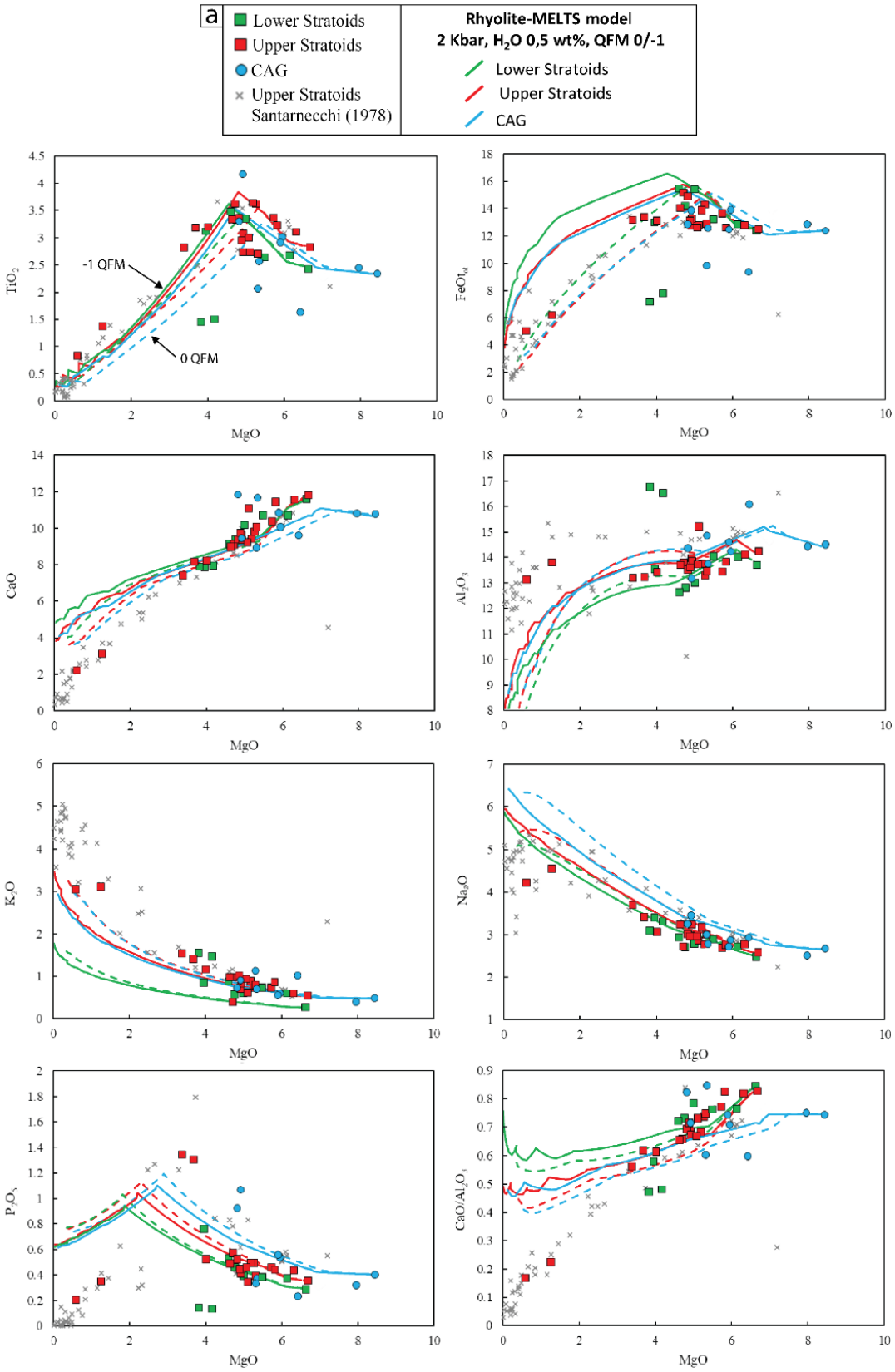

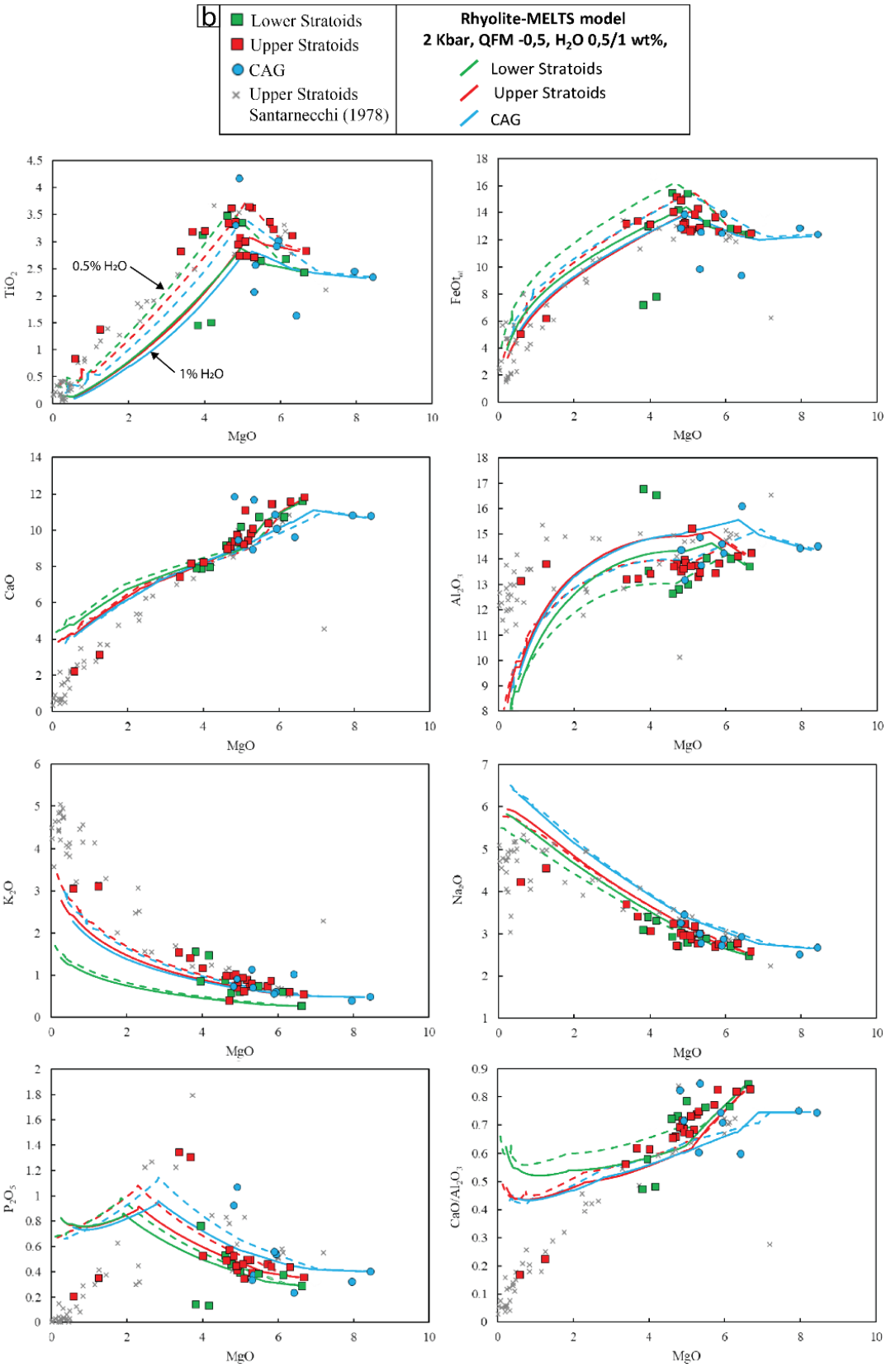

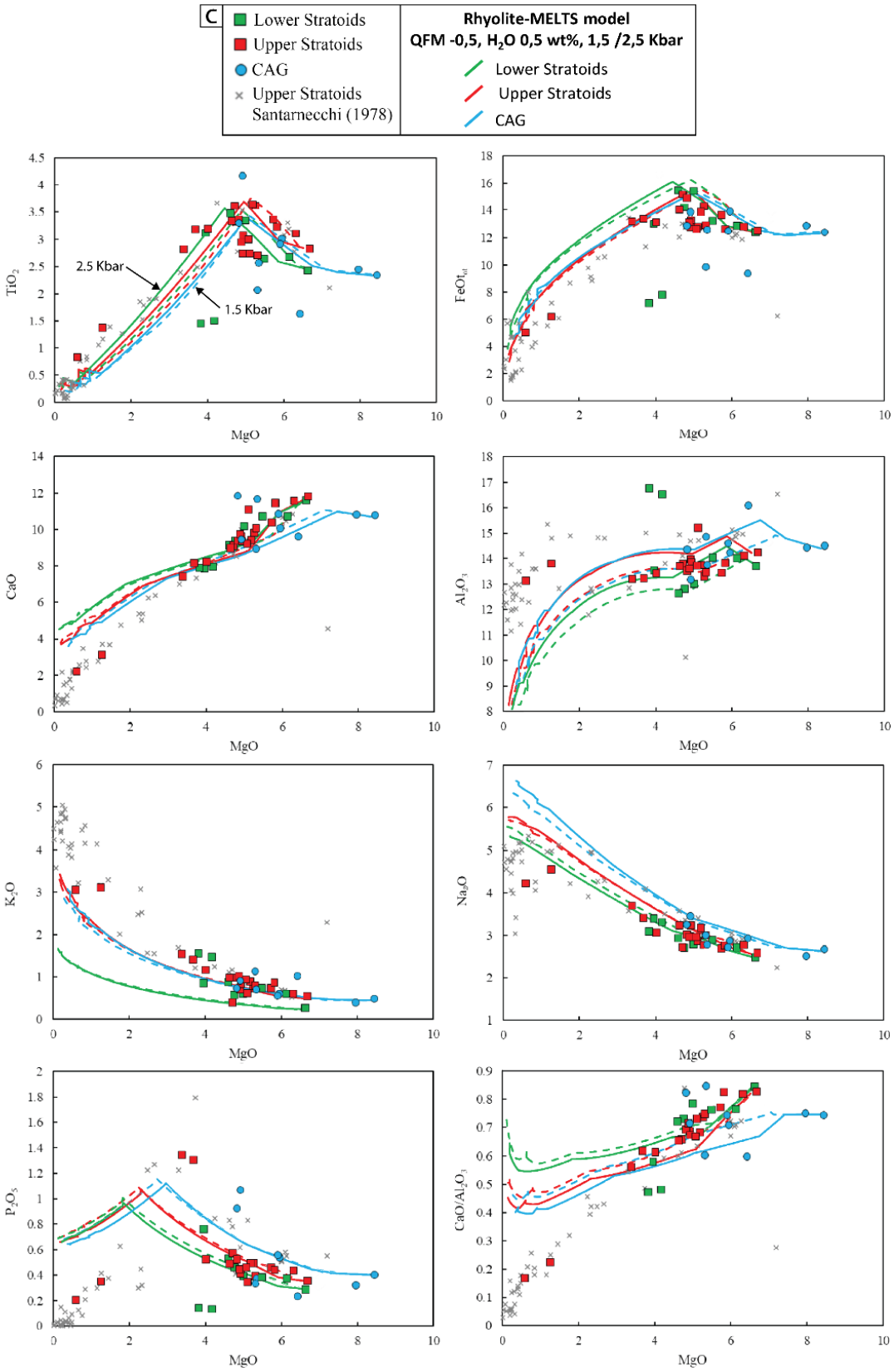

Figure S5. Modelled liquid line of descent for Lower Stratoids, Upper Stratoids and CAG Series major elements (wt%) by means of rhyolite-MELTS, (Asimow et al., 2004; Ghiorso and Sack, 1995). (a) Model with fixed pressure and water content and variable oxygen fugacity from QFM (dashed line) to QFM-1 (solid line). (b) Model with fixed pressure and oxygen fugacity and variable water content from 0.5 wt% (dashed line) to 1 wt% (solid line). (c) Model with fixed oxygen fugacity and water and variable pressure from 1.5 kbar (dashed line) to 2.5 kbar (solid line). Data of silicic central volcanoes whose products are interlayered in the upper part of the Upper Stratoids Series are from Santarnecchi (1978) and reported in Table S3.

Table S1. Petrographic and mineralogical analysis of the studied Lower Stratoids, Upper Stratoids and CAG Series samples. Pl, plagioclase; Cpx, clinopyroxene; Ol olivine; Ilm, ilmenite; Mag, magnetite; Ap, apatite; opq, opaque minerals.

Note. Number in brackets refer to samples AF20-12. Sulfide accessories have been observed in samples AF20-04 and AF20-19.

Table S2. Electron Probe Microanalysis. Point and profile analysis.

Note. Fe-Ti oxides end-members following Spencer and Lindsley (1981). Microanalysis were performed using the Electron Probe MicroAnalyzer (EPMA) JEOL JXA8230 device of the joined CNR-IGG-DST laboratory at the Department of Earth Sciences of Florence.

Table S3. CIPW norm and major and trace elements analysis of the Lower Stratoids, Upper Stratoids, CAG and Axial Series samples. Data of silicic central volcanoes whose products are interlayered in the upper part of the Upper Stratoids Series are from Santarnecchi (1978).

Note. * Second batch of analysis and relative reference material. For the second batch Sc has been analysed by means of ICP-OES. The analyses of Santarnecchi (1978) have been made by means of X-Ray Fluorescence.

Table 1. Summary table of the main petrographic and chemical characteristics of the Lower Stratoid, Upper Stratoid and CAG Series. The complete datasets are presented in Table S1 and Table S3.

Petrography																							
Series	Mafic samples								Silicic samples														
	N° of samples	mean vol% ph	mean vol% mph						N° of samples			mean vol% ph											
Lower Stratoid	12	1.8	7.3						0			-											
Upper Stratoid	25	2.5	5.8						5			20											
CAG	11	9.6	0.7						0			-											
NORM and major element chemistry																							
	N° of samples	NORM	MgO wt%			TiO_2 wt%			Tot. alk. wt%														
			min	mean	max	min	mean	max	min	mean	max												
Lower Stratoid	9	Mainly Qz norm	3.75	4.85	6.47	1.42	2.61	3.41	2.68	3.68	4.66												
Upper Stratoid	20	Mainly Qz norm	0.58	4.54	6.60	0.82	2.89	3.61	2.95	4.04	7.13												
CAG	9	Mainly Hy-Ol norm	4.69	6.03	8.38	1.60	2.68	4.15	2.89	3.58	4.33												
MgO > 4 wt% trace element chemistry																							
	N° of samples	Sr ppm				Nb ppm			Th ppm			Nb/Ta											
			min	mean	max	min	mean	max	min	mean	max	min	mean	max									
Lower Stratoid	7		197	239	291	14.24	27.53	39.29	1.05	3.14	6.74	11.76	15.29	16.05									
Upper Stratoid	15		295	341	390	23.20	34.46	44.78	1.79	2.78	3.93	15.28	15.96	16.52									
CAG	9		272	338	458	17.99	30.35	44.51	0.88	2.40	4.54	14.49	15.82	17.15									
MgO > 4 wt% trace element chemistry																							
	N° of samples	Ti/Y				Nb/U			Rb/Nb			Ce/Pb *											
			min	mean	max	min	mean	max	min	mean	max	min	mean	max									
Lower Stratoid	7		369	420	512	8.01	42.39	53.10	0.14	0.76	3.06	8.18	22.83	28.38									
Upper Stratoid	15		255	468	558	44.25	50.32	59.14	0.12	0.41	0.57	10.94	23.54	31.61									
CAG	9		329	418	493	22.52	58.97	81.54	0.17	0.46	1.04	24.79	28.23	32.84									

Note. *Due to Pb being below the detection limit, Ce/Pb values are the means of 5 Lower Stratoid samples, 6 Upper Stratoid samples and 3 CAG samples.